Analysis of Spine Plasticity in CA1 Hippocampal Pyramidal Neurons employing Live Cell Nanoscopic Imaging

Dissertation
zur Erlangung des Grades eines
Doktors der Naturwissenschaften

an der Fakultät für Biologie
der Ludwig–Maximilians–Universität
München,

vorgelegt von
Marcus T. Knopp,
Diplom Physiker,
aus Oelsnitz im Vogtland.

Martinsried, 25. März 2014

Die vorliegende Arbeit wurde zwischen September 2009 und März 2014 am Max-Planck-Institut für Neurobiologie, Abteilung Schaltkreise - Synapsen - Plastizität, in Martinsried bei München angefertigt.

Erstgutachter: Prof. Dr. Tobias Bonhoeffer
Zweitgutachter: Prof. Dr. Rainer Uhl
Tag der mündlichen Prüfung: 22. Juli 2014

Für meinen Großvater Erhard,

der mich nie gekannt und doch seinen Beitrag zur vorliegenden Arbeit geleistet hat, denn er besaß offenbar nicht nur entsprechende Gene, sondern auch ausreichend Duldsamkeit gegenüber den Wünschen und Zielen seines Erstgeborenen.

Zusammenfassung

In der Großhirnrinde von Säugetieren befindet sich die Mehrheit erregender Synapsen auf Dornfortsätzen, kleinen dendritischen Ausbuchtungen, die in Größe und Form stark variieren. Die Auslösung aktivitätsabhängiger synaptischer Langzeitplastizität geht mit strukturellen Veränderungen dendritischer Dornen einher. Da das beugungsbegrenzte Auflösungsvermögen konventioneller Lichtmikroskope nicht ausreicht um die Morphologie der Dornen verlässlich zu untersuchen, stellte die Elektronenmikroskopie bisher das wichtigste bildgebende Verfahren zur Erforschung von struktureller Plastizität dar, blieb dabei jedoch auf die Betrachtung fixierter Gewebeproben beschränkt. Die Anwendung hochauflösender Laser-Raster-Mikroskopie mit Stimulierter-Emissions-Auslöschung hat es mir möglich gemacht, die Dynamik dendritischer Dornenmorphologie in lebenden Zellen zu studieren. Die N-Methyl-D-Aspartat-Rezeptor-abhängige Langzeitpotenzierung von Pyramidenzellen der *Cornu-Ammonis* Region 1 des Hippocampus bildete dabei den Mechanismus, welcher plastische Veränderungen hervorrief. Nach Potenzierung exzitatorischer Synapsen durch die lokale Ultraviolett-Photolyse von *caged*-Glutamat wurde ein starker, vorrübergehender Anstieg des Anteils dendritischer Dornen mit sichelförmigen Köpfen und ein leichter, anhaltender Zuwachs an pilzförmigen Dornfortsätzen über einen Zeitraum von 50 Minuten beobachtet. Meine Untersuchungen ergänzen frühere Studien zur Wechselbeziehung zwischen synaptischer Potenzierung und struktureller Plastizität dendritischer Dornen und korrespondieren mit dem aktuellen Kenntnisstand der zu Grunde liegenden molekularen Mechanismen.

Abstract

The majority of excitatory synapses in the cortex of mammalian brains is situated on dendritic spines, small protrusions, heterogeneous in size and shape. The induction of activity-dependent long-term synaptic plasticity has been associated with changes in the ultrastructure of spines, particularly in size, head shape and neck width. Since the dimensions of dendritic spines are at the border of the diffraction-limited resolving power of conventional light microscopes, until recently, electron microscopy on fixed tissue constituted the primary method for investigations on spine morphology. I have employed live cell stimulated emission depletion imaging to analyse spine motility and structural transitions in response to n-methyl-d-aspartate receptor dependent long-term potentiation over time at super-resolution in *Cornu Ammonis* area 1 pyramidal neurons of the hippocampus. Local induction of long-term potentiation via ultraviolet photolysis of caged glutamate facilitated a strong transient increase in the proportion of spines with curved heads and a subtle persistent growth in the amount of mushroom spines over a time course of 50 minutes. My findings reinforce previous investigations on the relation of synaptic potentiation and spine motility, and are in good agreement with the current knowledge of the molecular mechanisms underlying long-term plasticity.

Contents

List of Figures

List of Tables

List of Technical Terms and Symbols

2D two dimensional / two dimensions
2PE two-photon-excitation
3D three dimensional / three dimensions

ACSF artificial cerebro-spinal fluid
AMPA α-amino-3-hydroxy-5-methyl-4-isoxazolepropionic acid
AStEx anti-Stokes excitation

BFP back focal plane

CA1 *Cornu Ammonis* area 1
CA3 *Cornu Ammonis* area 3
CAM cell adhesion molecule
CASIM channelrhodopsin assisted synapse identity mapping
CCD charged coupled device
cLTP chemical long-term potentiation
CNS central nervous system

DAQ data acquisition
DIV days *in-vitro*
DNA deoxyribonucleic acid

EC entorhinal cortex
ECM extracellular matrix
EM electron microscopy
ER epoxy resin

FCS fluorescence correlation spectroscopy
FOV field of view

FWHM full width at half maximum

GFP green fluorescent protein

IR infrared

LCD liquid-crystal display
LED light-emitting diode
LSM laser scanning microscope
LTD long-term depression
LTP long-term potentiation

MIP maximum intensity projection

N.A. numerical aperture
NIR near infrared
NIRB near infrared branding
NMDA n-methyl-d-aspartate

OPO optical parametrical oscillator

PALM photoactivated localization microscopy
PC personal computer
PCIe peripheral component interconnect express
PSD post-synaptic density
PSD-95 post-synaptic density protein 95
PSF point spread function

RESOLFT reversible switchable optical fluorescence transition
RICS raster image correlation spectroscopy
RNA ribonucleic acid
ROI region of interest

S.E.M. standard error of the mean
SCE single-cell electroporation
shRNA short hairpin RNA
SLR spine learning rule
SSIM saturated structured illumination microscopy
STED stimulated emission depletion

TCSPC time-correlated single photon counting
TEM transmission electron microscope
Ti:Sa titanium-sapphire
TIFF tagged image file format
TTL transistor-transistor-logic

USB universal serial bus
UV ultraviolet

YFP yellow fluorescent protein

Preamble

It's a popular fact that 90 % of the brain is not used and, like most popular facts, it is wrong. Not even the most stupid Creator would go to the trouble of making the human head carry around several pounds of unnecessary grey goo if its only real purpose was, e.g., to serve as a delicacy for certain remote tribesmen in unexplored valleys. It is used. One of its functions is to make the miraculous seem ordinary, and turn the unusual into the usual. [...] It is very efficient, and can make people experience boredom in the middle of marvels.

— Terry Pratchett, Small Gods (Discworld), 1992

Chapter 1

Introduction

The Neuron Doctrine[1]**.** Brains can be characterized as complex networks of countless fibers, that are interconnected to exchange information in terms of electrical or chemical signals. The principal anatomical units of brains are neurons [Waldeyer, 1891], ramified cells that are polarized into receiver and transmitter parts emanating from their somata, so called dendrites and axons (cp. Fig.1.2.A and the reviews by Braitenberg [2007]; Llinas [2008]). Signal transduction between neurons is located at specialized contact sites, the synapses. Remarkably, neural networks are by no means static entities. Instead, interconnections have proven to be plastic, which means tunable by learning (see for example review by Pascual-Leone et al. [2005]).

1.1 The Hippocampus

As reviewed by Buzsaki [2011], a critical role during declarative learning and memory consolidation is constituted by the hippocampus, a central element of the limbic system[2]. It is part of the forebrain, located in the medial temporal lobe, and in rodents consists of

[1] The organizational and functional principle of the nervous system based on neuro-anatomical work of Camillo Golgi and Santiago Ramón y Cajal, who both were awarded the nobel prize in 1906 "in recognition of their work on the structure of the nervous system" [Nobel Media AB, 2013]. Its historical development was for instance reviewed by Jones [1994].

[2] Structures that line the edge of the cerebral cortex of mammals. They include the hippocampus, cingulate cortex, olfactory cortex, and amygdala.

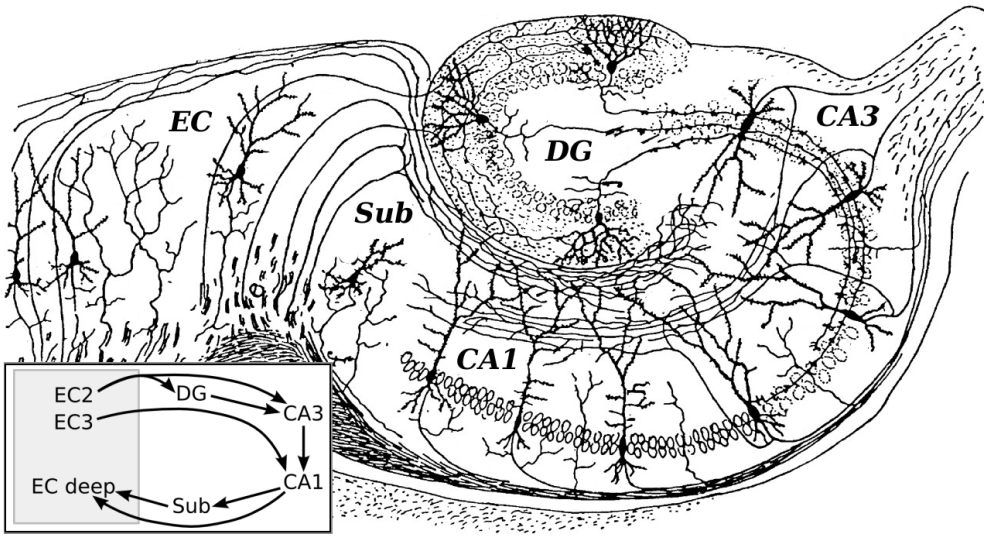

Figure 1.1: Modified Drawing of the Basic Neural Circuitry of the Rodent Hippocampus. CA1: *Cornu Ammonis* area 1, CA3: *Cornu Ammonis* area 3, DG: dentate gyrus, EC: entorhinal cortex, Sub: *Subiculum*. By Santiago Ramón y Cajal, Histologie du Système Nerveux de l'Homme et des Vertebrétés, Vols. 1 and 2. A. Maloine, Paris, 1911 [Cajal, 1952].

ventral and dorsal portions, both of which are composed similarly but seem to be parts of different neural circuits [Moser and Moser, 1998]. The hippocampus as a whole is shaped like a curved tube, which has been occasionally compared to a seahorse[3]. Fig.1.1 shows a schematic transverse sectional drawing of its anatomy as found in rodent brains, though the general layout holds for all mammalian species. It can be identified as a region, where cortex narrows to a single, densely packed layer of pyramidal neurons, which curl into a tight U shape, the *Cornu Ammonis* areas. They are embedded into a backward-facing, strongly flexed, V-shaped cortex, the dentate gyrus (cp. review by Amaral and Lavenex [2006]). Neighbouring and part of the parahippocampal gyrus, the entorhinal cortex (EC) is anatomically connected to the hippocampus in an alternating pattern of multi-synaptic feed-forward loops. According to Buzsaki [2011], the advantage of this type of organization might be, that neuronal representations can be iteratively segregated and integrated in successive layers: Information from the cerebral cortex in the entorhinal-hippocampal system is passed on mainly unidirectionally, with signals propagating through a series of tightly packed cell layers. Granule cells of the dentate gyrus constitute the main input to the hippocampus, receiving signals from the upper layers of the EC via the perforant path. They send their axons, called mossy fibers, to the pyramidal cells of the *Cornu Ammonis*

[3]Hence the name from the Greek *hippos* meaning "horse" and *kampos* meaning "sea monster".

areas. *Cornu Ammonis* area 3 (CA3) axons extend to *Cornu Ammonis* area 1 (CA1) along the so called Schaffer collaterals, supposedly the most extensive recurrent system in the brain [Buzsaki, 2011]. To complete a reciprocal circuit, CA1 pyramidal neurons send axons to the subiculum and sparsely back into the deep layers of the EC. Each entorhinal-hippocampal cell layer contains additional intrinsic circuitry and extensive longitudinal connections.

The hippocampal formation has become a primary object of neuroscientific investigation after Scoville and Milner published a case study on Henry Gustav Molaison[4]. To treat his epilepsy, the hippocampi of both hemispheres were surgically removed from this patient's brain. After that, he suffered from severe memory deficits [Scoville and Milner, 1957], which indicated an essential hippocampal involvement in episodic learning and memory. Later O'Keefe and Dostrovsky [1971] discovered so called "place cells", hippocampal neurons that are activated selectively when a mammal moves through a particular location in space. This lead to the proposal of the hippocampus to resemble the spatial memory of the brain.

The principal excitatory pathways of the hippocampus are organized in a lamellar fashion. Entorhinal activity is therefore projected through the hippocampal formation along a slice or lamella of tissue, oriented normally to the alvear surface and perpendicular to the long axis of the hippocampus [Andersen et al., 1971]. This organization enables the cultivation of tissue explants for several weeks [Gähwiler et al., 2001]. In large parts they retain their *in-vivo* structure and develop with the same time course as *in-situ* [Muller et al., 1993]. Additionally, neural connections and expression profiles of synaptic proteins are similar to those found in acute slices [De Simoni et al., 2003; Buckby et al., 2004], but organotypic hippocampal explants stay widely unaffected by tissue degradation associated with acute preparations. They are also easily amenable to cellular staining methods with synthetic dyes, antibodies or genetic markers. Alongside its relatively simple circuitry, these features have made the hippocampus a well-suited *in-vitro* model system, not only to scrutinize neural wiring, but also for long-term manipulations and imaging studies to investigate learning and memory formation in mammalian brains.

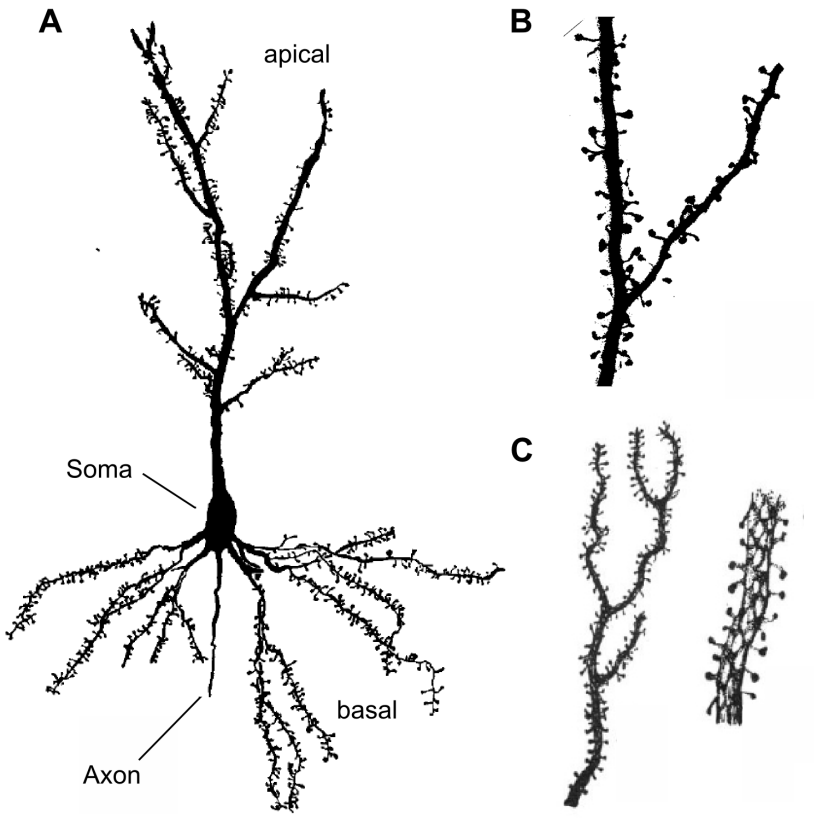

Figure 1.2: Dendritic Spines on Different Types of Neurons. *A* Modified camera lucida drawing of the dendritic tree of a rat cerebral cortex pyramidal cell. Reprinted by permission from John Wiley & Sons: The American Journal of Anatomy [Peters and Kaiserman-Abramof, 1970]. *B* High magnification view of the main apical dendrite of a hippocampal pyramidal cell from a binary segmented fluorescence image. *C* Low (left) and high (right) magnification views of a cerebellar Purkinje cell drawn by Santiago Ramón y Cajal, Textura del sistema nervioso del hombre y de los vertebrados (Primera Edicion), Madrid, 1899 [Cajal, 1899].

1.2 Dendritic Spines

The dendritic trees of many neurons in the central nervous system (CNS) are covered with small protrusions, heterogeneous in size and shape. They were named "espinas", i.e. *spines*, by the Spanish neuroscientist Santiago Ramón y Cajal, who first described them in 1888 [Yuste, 2002]. Spines are found in many species and are exceptionally abundant in brains of vertebrates. Since they constitute major structural elements of the majority of principal neurons in most areas of the CNS, they are considered essential for neural

[4]Usually referred to as "patient H.M."

processing [Yuste, 2010]. Indeed, they have proven to mediate most ($> 90\,\%$) excitatory inputs to a cell [Gray, 1959]. Besides, practically all spines are regarded to possess an excitatory synapse at their tip [Colonnier, 1968; Arellano et al., 2007]. On the other hand, spines are absent, or present at much lower densities, on some classes of neurons like inhibitory interneurons [Yuste, 2010].

Fig.1.2 illustrates two examples of spiny nerve cells: pyramidal neurons, so named for the shape of their cell bodies, and Purkinje cells of the cerebellum. From the apex of a pyramidal neuron a long dendritic trunk, the main apical dendrite, emanates, giving rise to a number of lateral dendritic branches (cp. Fig.1.2.A). From the base of the soma a second bundle of dendrites emerges, as well as the cell's axon. At higher magnification dendritic spines become clearly visible (cp. Fig.1.2.B). Cajal already acknowledged the appearance of dendritic spines investigating silver-impregnated histological tissue sections using Golgi's staining method (cp. Fig.1.2.C). Moreover, he already noticed their diversity of shapes, postulated that spines were the primary points of synaptic contact between nerve cells and involved in learning and memory [Bourne and Harris, 2001; Tashiro and Yuste, 2003].

Structural characteristics of spines could be closely connected to the function of synapses, leading to the claim, that dendritic spines serve as basic functional units of neuronal integration [Yuste and Denk, 1995]: 1) Spine necks enable the compartmentalization of second messengers like calcium and are therefore linked to their localization in the spine heads [Majewska et al., 2000a,b]. 2) The narrowing in spine necks poses a small resistive barrier causing a time delay in charge transfer of a few hundred milliseconds. This seems to be sufficient to provide a transient amplification of voltage at the synapse and, hence, facilitate the opening of voltage-dependent channels in the spine head [Bourne and Harris, 2001; Grunditz et al., 2008]. 3) Dendrites with spines can synapse with neurons $1-3\,\mu$m away, thereby increasing the density of possible connections. Besides, the shape of dendritic spines allows efficient convolution and interdigitation of dendrite, axon and spine membranes. For that, the presence of spines is thought to submit an increase in synaptic density without increasing the overall volume of the brain [Bourne and Harris, 2001; Yuste, 2010].

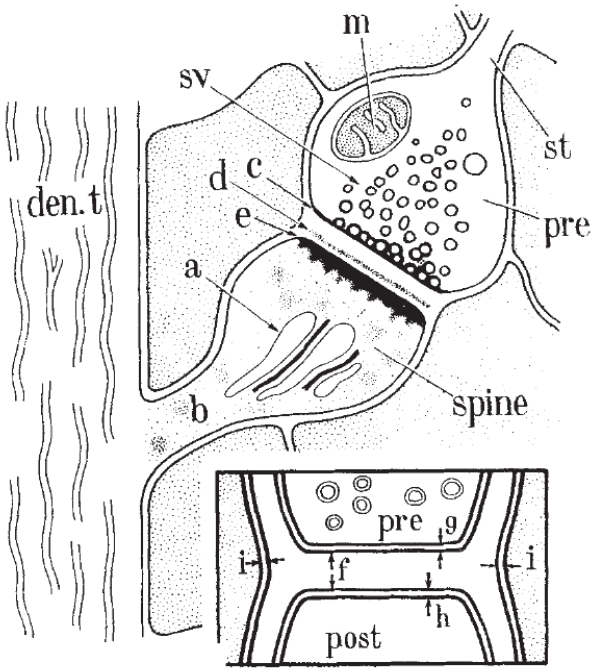

Figure 1.3: Diagram of a Synaptic Contact on a Dendritic Spine, observed with the electron microscope after osmium tetroxide fixation. The strippled regions represent neuronal and glial processes of the neuropil. a: spine apparatus, b: stalk of the spine, c: pre-synaptic membrane, d: extracellular electron-dense thickening, den.t: dendritic shaft, e: post-synaptic density, m: mitochondrion, st: stalk of the bouton, sv: synaptic vesicles. *Inset* The opposed regions of the pre- and post-synaptic membranes seen after potassium permanganate fixation. The membranes (i) are of neighbouring processes of the neuropil. f: synaptic cleft, g: pre-synaptic membrane, h: post-synaptic membrane. Reprinted by permission from Macmillan Publishers Ltd: Nature [Gray, 1959].

1.2.1 Synapses

Each neuron connects to several thousand other neurons via synapses. Gray [1959] undoubtedly confirmed that dendritic spines are actual sites of these connections[5]. He used electron microscopy (EM), which facilitated direct visualization of the contacts, and revealed a cleft separating the pre-synaptic axon from the post-synaptic dendrite (cp. Fig.1.3) [Harris and Weinberg, 2012]. He identified two main classes of synaptic contacts: asymmetric excitatory (type I), and symmetric inhibitory (type II). Type I synapses contain spherical vesicles in the pre-synaptic compartment and are characterized by an electron-dense protein band, the post-synaptic density (PSD), located $35 - 50\,\text{nm}$ into the cyto-

[5]It should be noted, that this is referring to synapses in the mammalian brain, as for example found in rodent hippocampus, cerebral cortex, and cerebellum.

plasm beneath the post-synaptic plasma membrane [Gulley and Reese, 1981; Landis and Reese, 1983]. The PSD houses a whole "signalling machinery" [Kennedy, 2000] including glutamate receptors[6], ion channels, cell adhesion molecules and signaling enzymes, as well as membrane trafficking, cytoskeletal and scaffolding proteins (see reviews by Ziff [1997]; Tashiro and Yuste [2003]; Kim and Sheng [2009]; Harris and Weinberg [2012]). It is opposed by a thin electron-dense pre-synaptic density, the active zone, where neurotransmitters are released into the synaptic cleft by synaptic vesicle exocytosis [Südhof, 2004; Südhof and Rizo, 2011]. In contrast, type II synapses, mainly recipient to *γ-amino-butyric acid* (GABA) [Roberts, 2007], typically do have thin pre- and post-synaptic densities of similar width and vesicles in the pre-synaptic compartment appear ellipsoid or egg-shaped under EM.

As pointed out earlier, excitatory synapses are mainly found on dendrites and dendritic spines. In contrast, inhibitory synapses concentrate on the cell soma and axonal initial segment, but do also sparsely distribute along dendritic shafts of certain neuronal cell types. Together with astrocytic[7] processes, dendrites and axons form a fine mesh, the neuropil, where most of the synaptic interactions occur [Harris and Weinberg, 2012]. In the *stratum radiatum* of CA1, axons pervading the neuropil develop bulges that contain neurotransmitter-filled vesicles and sometimes mitochondria, the so called pre-synaptic boutons. The large majority ($\approx 75\,\%$) of these boutons make a single synaptic contact, about one fifth form multiple synapses, and a small proportion ($\approx 4\,\%$) lack a post-synaptic partner [Shepherd and Harris, 1998; Sorra et al., 2006].

Interestingly, the synaptic cleft, an approximately 20 nm wide gap in the apposition between the pre- and post-synaptic partners, is not an empty space. It seems to be packed with electron-dense material, that appears to contain extracellular matrix proteins, as well as specialized synaptic proteins [Lučić et al., 2005; Zuber et al., 2005; Dityatev et al., 2010].

Complementing the chemical synapses described above, electrical synapses enable rapid signal transfer between nerve cells [Hinrichsen, 1970; Baker and Llinás, 1971]. In contrast to chemical synapses, here pre- and post-synaptic cell membranes are closer together and physically connected by gap junctions, special pores allowing passive flow of ionic current [Brightman and Reese, 1969]. Changes in pre-synaptic membrane potential therefore induce respective voltage changes in the downstream cell. Gap junctions are present throughout the whole CNS . Extensive investigations considered electrical synapses between

[6] The most common excitatory neurotransmitter is glutamate.

[7] Astrocytes are a subtype of glia, non-neuronal cells, that supposedly maintain and protect neurons.

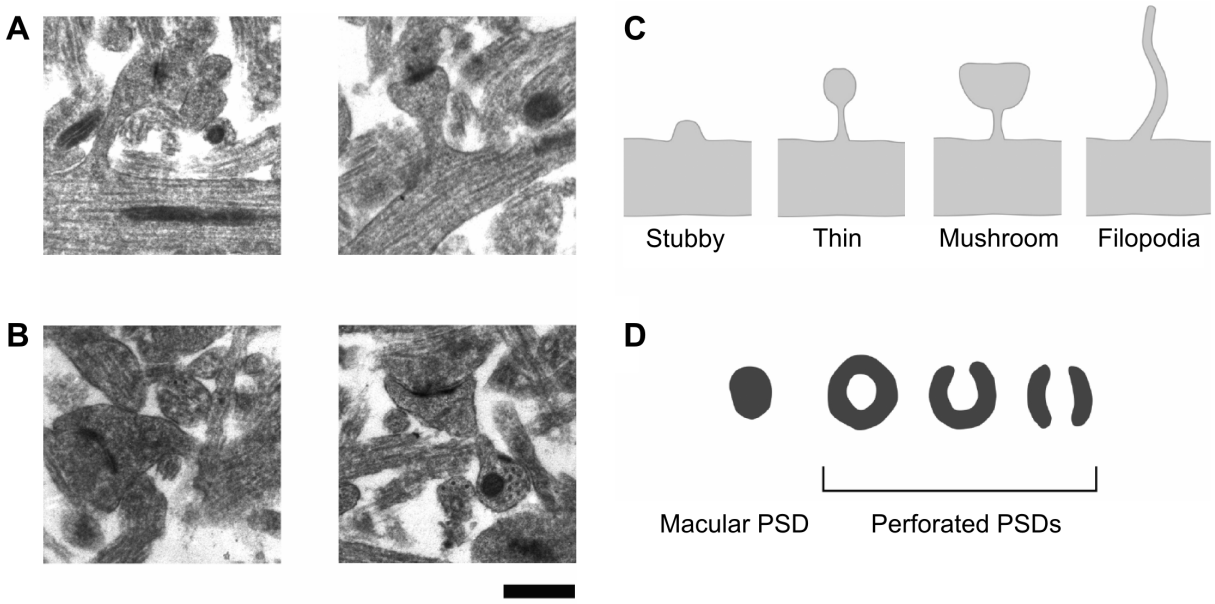

Figure 1.4: Ultrastructure of Dendritic Spines. Electron micrographs of dendritic spines in hippocampal slice culture. *A* Thin spines with macular PSDs. *B* Mushroom spines with perforated PSDs. *C* Modified schematic drawing of spine morphologies in categories, as described by Peters and Kaiserman-Abramof (1970). *D* Modified schematic drawing of macular and perforated PSDs. Scale bar: 500 nm. Reprinted by permission from Juan F. Madrid (editor): Histology and Histopathology [Tashiro and Yuste, 2003].

excitatory projections of the inferior olivary nucleus and between inhibitory interneurons of the neocortex, hippocampus, and thalamus, as reviewed by Connors and Long [2004].

1.2.2 Spine Morphology

The ultrastructure of dendritic spines comes at a great diversity of morphological characteristics, that are abnormal in many mental and neurological disorders [Kasai et al., 2010]. In the past excessive efforts were made, especially employing EM, to classify them accordingly [Bourne and Harris, 2001], although recent investigations suggest no clear affirmation of distinct subtypes [Arellano et al., 2007]. Generally spoken, spines emerge from dendritic shafts and can be divided into a spine neck / stalk and a spine head containing the synapse (cp. Fig.1.3) [Nimchinsky et al., 2002]. Under EM, they come out as small protrusions ranging more than 100-fold in length (typically less than $2-3\,\mu$m, from shaft to tip) having a bulbous head (diameter: $0.5-1.5\,\mu$m) and a narrow neck (diameter: $< 0.5\,\mu$m) [Tashiro and Yuste, 2003]. Figs.1.4.A and B show examples of electron micrographs of dendritic spines in organotypic slice culture. Sometimes, dendritic spines are found to have more

than one head. Such *branched* spines can connect to the same pre-synaptic axon or to different axons, though they do not necessarily have a pre-synaptic partner at all [Bourne and Harris, 2001].

Interestingly, the actual ultrastructure of spine heads might not be reflected correctly by traditional EM. It has been argued, that tissue fixation could alter their shape and bulbous heads are a mere artifact of this treatment, since investigations on live tissue showed concave cup-shaped spine heads with lamellipodia, so called spinules, surrounding the pre-synaptic terminal [Fischer et al., 1998; Dunaevsky et al., 1999; Lendvai et al., 2000; Nägerl et al., 2008]. These finger-like protrusions were shown to be rich of actin and undergo plastic structural changes in response to the activation of ionotropic, as well as metabotropic receptors of principal neurons [Fischer et al., 2000; Roelandse et al., 2003; Richards et al., 2005; Schätzle et al., 2011].

Despite the distributions of morphological spine variables being highly skewed[8] [Nimchinsky et al., 2002; Yuste, 2010; Harris and Weinberg, 2012], a traditional idea of four main subtypes has evolved, greatly influenced by Peters and Kaiserman-Abramof [1970] (cp. Fig.1.4.C): *thin* spines are most common and have a thin, long neck and a small (bulbous) head [Tashiro and Yuste, 2003], *mushroom* spines possess a large head and are typically found in mature samples [Yuste, 2010], *stubby* spines lack an obvious stalk and are strikingly noticeable during postnatal development [Jones and Powell, 1969; Peters and Kaiserman-Abramof, 1970; Harris et al., 1992], *filopodia*, finally, are developmentally transient, elongated arborizations without a clear head-compartment, that lack a PSD [Fiala et al., 1998; Kasai et al., 2010]. Regarding synaptic constituents, the majority of thin spines has a disk-like, macular PSD, whereas more than 80 % of mushroom spines have more complex, perforated (non-macular) ones (cp. Fig.1.4.D) [Harris et al., 1992]. Larger spines contain more structural components (receptors, smooth endoplasmatic reticulum, endosomes, polyribosomes) and show more astroglial contacts [Yuste, 2010].

Quantitative studies of spine morphology revealed strong correlations between certain structural / synaptic elements. PSD thickness is not only sensitive to alterations of its constituent proteins' organization [Hu et al., 1998; Otmakhov et al., 2004b; Tao-Cheng, 2007], but also the PSD surface area correlates very well with spine head volume and the total number of (docked) synaptic vesicles, which relates to their release probability, and therefore, synaptic strength [Harris and Stevens, 1988; Lisman and Harris, 1993; Harris and Sultan, 1995; Schikorski and Stevens, 2001; Arellano et al., 2007; Meyer, 2013]. Also,

[8] They are unimodal, but certainly not normal, with long tails and great variability between different brain regions.

the number of post-synaptic receptors is tied in the areas of the PSD and active zone and could be associated with the current injected at a synapse [Nusser and Somogyi, 1997; Nusser et al., 1998; Matsuzaki et al., 2001, 2004; Holderith et al., 2012].

1.2.3 Synaptic Plasticity

From time immemorial, one of the most intriguing questions of neuroscience has been, how learning and memory are implemented and maintained in the brain. Based on Hebb's learning rule[9] from 1949, long-lasting experience-dependent changes in the efficacy of synaptic transmission have long been believed to pose the underlying mechanism and are generically embraced by the conception of long-term synaptic plasticity [Lüscher and Malenka, 2012]. Two of the most prominent forms of activity-dependent long-term changes are long-term potentiation (LTP) [Bliss and Lomo, 1973] and its potential counterpart long-term depression (LTD) [Levy and Steward, 1979], leading to a persistent increase or decrease in synaptic strength, respectively. Both being widespread phenomena, expressed at a large part of excitatory synapses in the mammalian brain, several forms of LTP and LTD exist on the basis of the particular molecular mechanisms required to elicit and maintain the synaptic change [Malenka and Bear, 2004; Castillo, 2012]. Notably, several protocols have been discovered to potentiate or depress synapses by purely pharmacological means. Therefore referred to as chemical long-term potentiation (cLTP) [Aniksztejn and Ben-Ari, 1991; Otmakhov et al., 2004a; Fujii et al., 2004] and chemical) [Palmer et al., 1997; Nicoll et al., 1998; Santschi et al., 1999] in the literature, they affect different extra- and intracellular systems. N-methyl-d-aspartate (NMDA) receptor dependent LTP / LTD, occuring between CA3 and CA1 pyramidal neurons of the hippocampus, remain the most extensively studied and therefore prototypic forms of synaptic plasticity [Malenka and Bear, 2004]. Other forms of experience- / activity-dependent plasticity are for example reviewed by Alvarez and Sabatini [2007]; Nelson and Turrigiano [2008]; Holtmaat and Svoboda [2009]. At the Schaffer collaterals, the loci of induction and expression of changes are situated in the post-synaptic neurons, pyramidal cells, whose excitatory synapses are characterized by the presence of two ionotropic glutamate receptors: α-amino-3-hydroxy-5-methyl-4-isoxazole-propionic acid (AMPA) and NMDA receptors. AMPARs drive strong and rapid synaptic signalling, having a high conductance for sodium in the glutamate bound conformation,

[9] "When an axon of cell A is near enough to excite a cell B and repeatedly or persistently takes part in firing it, some growth process or metabolic change takes place in one or both cells such that A's efficiency, as one of the cells firing B, is increased." [Hebb, 1949]

whereas NMDARs activate more slowly and are additionally permeable to calcium (see reviews by Bliss and Collingridge [1993]; Lüscher and Malenka [2012]). LTP and LTD are induced by specific patterns of pre- and post-synaptic activity [Malenka and Nicoll, 1993]: while weak calcium influx activates phosphatases leading to LTD, strong calcium influx activates kinases triggering LTP. The conductance for calcium ions depends on the strength of post-synaptic depolarization due to magnesium ions entering the pores of NMDA receptors, blocking the passage for all other ions at resting potential [Collingridge et al., 1988]. Under physiological conditions this has been shown to occur during spike timing dependent plasticity (STDP), when pre-synaptic action potential firing precedes post-synaptic back-propagating spiking within a window of several tens of milliseconds [Dan and Poo, 2006]. Through that mechanism, NMDARs play the role of molecular coincidence detectors [Lüscher and Malenka, 2012].

Diverse morphological correlates of long-term synaptic plasticity have been observed in the past, particularly with regard to structural alterations in dendritic spine size, shape and number. Comprehensive reviews of a large body of literature dealing with this fascinating subject were prepared for example by Bonhoeffer and Yuste [2002]; Bourne and Harris [2007]; Harms and Dunaevsky [2007]; Kasai et al. [2010]; Bosch and Hayashi [2011]. They are briefly summarized below, focusing on spine plasticity associated with LTP in pyramidal cells of the neocortex and hippocampus. The induction of LTD by either chemical or electrical stimulation usually induces shrinkage or loss of dendritic spines [Bosch and Hayashi, 2011]. Investigations of structural spine plasticity can be categorized according to their methodical approaches — EM and light microscopy:

Electron Microscopic Studies. Van Harreveld and Fifkova [1975]; Fifková and Van Harreveld [1977]; Fifková and Anderson [1981] reported larger spines with wider but shorter necks on stimulated compared to unstimulated pathways. Desmond and Levy [1983, 1986a,b, 1988] found an increase in the proportion of cup-shaped and an accompanying decrease in bulbous spines after stimulation. Also, concave spines showed larger PSD surface areas and lengths. These observations were supported by Calverley and Jones [1990]; Harris et al. [1992]; Toni et al. [2001]; Popov et al. [2004]; Stewart et al. [2005], who detected increases in the number of perforated PSDs after LTP induction. A strong effect of increased spine density after LTP was reported by Andersen and Soleng [1998]. Complementary findings cover a stimulus related increase in the number of branched spines and multiple-synapse boutons [Trommald et al., 1996; Toni et al., 1999; Fiala et al., 2002], as well as the formation of spinules [Richards et al., 2005; Tao-Cheng et al., 2009] and a

gain of spines containing polyribosomes after potentiation [Ostroff et al., 2002]. Although structural changes of spines during synaptic plasticity are strongly backed by all these investigations, contradictory findings were also published, e.g. by Lee et al. [1979, 1980]; Chang and Greenough [1984]; Geinisman et al. [1991]; Sorra et al. [1998]. Discrepancies could be ascribed to variations in the brain regions studied, in tissue preparation (cultured vs. acute brain slices), in stereological details and to the methodical approach itself, since EM investigations rely on statistical evaluation of dead tissue, where small changes could be "buried within noise" [Yuste and Bonhoeffer, 2001].

Light Microscopic Studies. Initial time-lapse experiments linking LTP to morphological spine plasticity were performed by Hosokawa et al. [1995], who observed increases in spine length and changes in spine orientation in response to a pharmacological stimulus. LTP associated outgrowth of new spines was detected by Maletic-Savatic et al. [1999] and by Engert and Bonhoeffer [1999]. Drastic enlargement of spines was observed by Matsuzaki et al. [2004] in response to a potentiating photolysis of caged glutamate. Further investigations, employing electric stimuli [Okamoto et al., 2004], or glutamate uncaging paired with opto-genetically induced post-synaptic depolarization [Zhang et al., 2008], supported those findings. Kopec et al. [2006] were able to show similar increases in spine volume using a cLTP protocol, that resulted in a transfer of additional AMPA receptors into the spine heads. Additionally local glutamate uncaging induced the formation of new spines [Kwon and Sabatini, 2011]. Changes towards wider spine necks in response to classic cLTP were reported by Urban et al. [2011].

Taken together, a general idea of LTP converting "learning spines" into "memory spines" evolved [Bourne and Harris, 2007]. The transition is supposed to be accompanied by morphological changes that resemble the cellular correlate of memory consolidation. The most probable mechanism driving structural spine plasticity involves the regulation of the actin cytoskeleton, as reviewed by Bosch and Hayashi [2011] or Kasai et al. [2010]. However, according to Bourne and Harris [2007]; Harms and Dunaevsky [2007] several questions remain open. For example: Which structural changes are specific to particular classes of synapses? Is structural plasticity in the mature brain fundamentally different from developmental transitions? How long do structural changes last? Motility can be correlated with alterations in network organization and biochemical compartmentalization, but does induction of synaptic plasticity itself cause changes in motility? It is also unclear, if spine movement alone substantially alters synaptic transmission. A number of studies are in

support of structural plasticity being dissociated from functional plasticity [Lang et al., 2004; Zhou et al., 2004; Yang et al., 2008; Gu et al., 2010]. Therefore, it is yet to be shown that spines are sites that are specifically acted upon during learning and memory formation.

1.3 Super-Resolution Imaging

Dimensions of dendritic spines are right at the border of the diffraction-limited resolving power of conventional light microscopes [Yuste, 2010]. Therefore, the advent of super-resolution microscopy opened a completely new perspective to structural and functional investigations on spines, as it did to cellular biology in general. Before the scope of the present investigation is outlined, state-of-the-art nanoscopic technologies will be briefly introduced, laying the focus on far-field fluorescence imaging. Being of less importance for live cell investigations, near-field optical microscopy (NOM) [Pohl et al., 1984], for example reviewed by Novotny [2007] will be left out, as well as methods expanding the aperture solid angle of the imaging lens like 4Pi microscopy [Cremer and Cremer, 1978; Hell et al., 1994]. Furthermore, a summary of fluorescence nanoscopy applications to neuroscience is provided, and the method of choice for my analysis, stimulated emission depletion (STED) imaging, delineated.

1.3.1 Overview

About one century had passed after the discovery of the resolution barrier[10] for light microscopes by Verdet [1869]; Abbe [1873] and Rayleigh [1903], stating that objects closer than a distance $d \approx \lambda/(2 \cdot n \cdot sin(\alpha))$ can not be distinguished, since their images are fused by the diffraction of light to a single blur[11] (cp. Fig.1.5), when suggestions came up, that this barrier can be broken [Hell and Wichmann, 1994]. Today it is clear, that diffraction still limits the resolution obtained with any lens-based optical system apart from certain exceptions. One of them is fluorescence imaging. There is a heated discussion going on in the field, about who initially came up with the ground breaking concepts to bring super-resolution microscopy to life. Fortunately, it is not within the scope of the present thesis,

[10] Also *Abbe limit*, *Rayleigh criterion* or *angular resolution limit*.

[11] λ denotes the wavelength of illumination and $n \cdot sin(\alpha)$ denotes the numerical aperture (N.A.) of the imaging lens, where n corresponds to the refractive index of the medium in which the lens is working and α to half of the lens' opening angle.

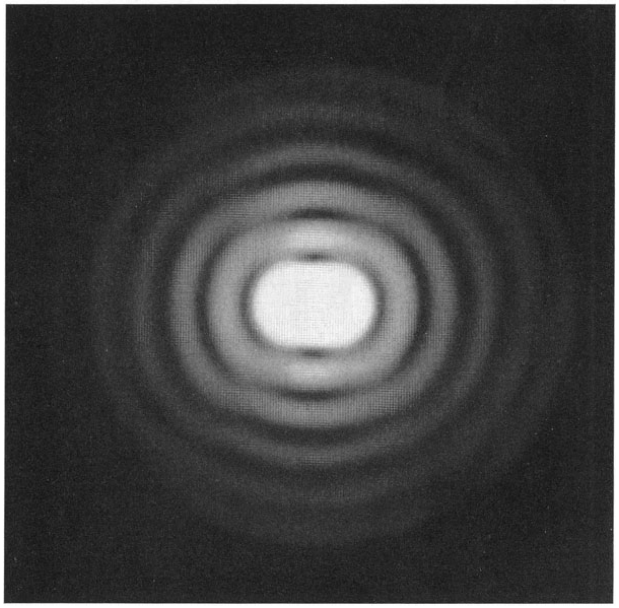

Figure 1.5: Diffraction Pattern of Two Incoherent Light Sources. The separation of the point sources corresponds right to the resolution limit. Reprinted with kind permission from Springer Science+Business Media B.V.: M. Cagnet, M. Françon, J. C. Thrierr, Atlas of optical phenomena (Springer, Berlin, Heidelberg, 1962) [Cagnet et al., 1962].

to resolve this issue. I follow Hell [2009] for the most part surveying the various modalities of fluorescence nanoscopy, primarily, because his classification seemed consistently compelling to me[12]. Besides, his lab published the first real super-resolved images [Klar and Hell, 1999].

As pointed out by Lemmer et al. [2008], to overcome the limiting character of diffraction in fluorescence microscopy, neighbouring structures, i.e. emitters closer than the Abbe limit of approximately 200 nm, if labelled with different spectral signatures, can optically be isolated with spectrally selective detection schemes and can be discerned via high precision location determinations. When thinking of spectral signatures as different excitation / emission spectra (i.e. colors) of the fluorophores, their separation seems rather unproblematic and has been predicted to attain 1/30 of the Rayleigh criterion [Burns et al., 1985]. However, that approach required a way to selectively label neighbouring structures in a sample with distinct markers of different color. Isolating single coloured fluorophores either needs alternative signatures, like fluorescence lifetimes, photoluminescence, or random la-

[12]Further reading: Elaborate reviews with a focus on applications to (neuro-)biology were published for example by Patterson et al. [2010]; Toomre and Bewersdorf [2010]; Cremer et al. [2011]; Tønnesen and Nägerl [2012]; Requejo-Isidro [2013], just to name a few. Some of them approach the subject differently in parts.

belling schemes [Lemmer et al., 2008; Cremer et al., 2011]. A paradigm change to the time domain of the data acquisition, finally, poses the underlying concept of nearly all current far-field nanoscopy implementations, that is to switch fluorescent signals of neighbouring structures on and off, so that they are detected consecutively [Hell, 2009]. Tab.1.1 summarizes the most prominent super-resolution fluorescence techniques. They can be subdivided in two classes [Hell, 2009]:

1. Methods based on targeted fluorescence switching (STED, GSD, SPEM/SSIM and RESOLFT).

2. Methods based on stochastic fluorescence switching (PALM, STORM, dSTORM, GSDIM).

The second group could be complemented by Single-Molecule High-Resolution Imaging with Photobleaching (SHRImP) [Gordon et al., 2004], Photobleaching Microscopy with Non-Linear Processing (PiMP) [Munck et al., 2012] and Super-Resolution Optical Fluctuation Imaging (SOFI) [Dertinger et al., 2009]; other authors tend to pool all pointillist (see below) super-resolution approaches under the common term Localization Microscopy, thereby also covering the concepts of Spectral Position Determination Microscopy (SPDM) [Lemmer et al., 2008; Gunkel et al., 2009; Cremer et al., 2011].

Table 1.1: Glossary of Far-Field Fluorescence Nanoscopy Techniques. In part reprinted by permission from Macmillan Publishers Ltd: Nature Methods [Hell, 2009].

Technique	Description	References
STED: stimulated emission depletion microscopy	A non-diffraction-limited form of scanning far-field fluorescence microscopy. Typically, fluorescence excitation created by a focused beam of excitation light is narrowed down in space by simultaneously applying a second spot of light for molecular de-excitation featuring a central zero (for example, a doughnut). The role of the de-excitation (STED) beam is to effectively confine molecules to the ground state, thus, effectively switching off the ability of the dye to fluoresce. De-excitation occurs within the nanosecond lifetime of the fluorescent state. Because no de-excitation occurs at the central zero, the excited state is established only in the region close to the zero.	[Hell and Wichmann, 1994; Klar et al., 2000; Willig et al., 2006; Schmidt et al., 2008]

Table 1.1 – continued from previous page

Technique	Description	References
GSD: ground state depletion microscopy	Analogous to STED microscopy. The area in which molecules can reside in the fluorescent state is narrowed down in space by transiently switching the dyes to a metastable dark state — specifically, the triplet state. The use of a dark state of micro- to millisecond lifetime reduces the intensity required for the molecular switch in comparison to STED. The concept of switching fluorophores between long-lived bright and dark states has successively been extended to switching by *cis–trans* isomerization and other optically induced molecular bistabilities in the concept called RESOLFT.	[Hell and Kroug, 1995; Hell, 2002; Bretschneider et al., 2007]
SPEM/SSIM: saturated pattern excitation microscopy or saturated structured illumination microscopy	A wide-field recording, highly parallelized scanning microscopy in which the molecules are strongly excited to the fluorescent state, depleting the ground state (that is, switched from the ground state to the fluorescent state) outside the line-shaped zeros produced by a standing wave interference pattern. To cover the field of view, the pattern is scanned across the specimen by phase-shifting the maxima of the interference pattern and reading out the fluorescence imaged onto a camera for each scanning step. Because resolution is improved only perpendicular to the line-shaped zeros, the pattern is tilted several times to cover all directions in the focal plane. Mathematical analysis of the data renders super-resolved images. Even scanning a single line-zero would give super-resolution, but the use of an array of lines parallelizes the process over a large area.	[Heintzmann et al., 2002; Gustafsson, 2005]
RESOLFT: reversible saturable/switchable optically linear fluorescence transition	A generalization of STED and GSD microscopy for molecular switching, including switching of reversibly activatable proteins and organic fluorophores. Switching can be regarded as a perfect saturable transition from one state to the other. The terminology 'saturated transition' is used in conjunction with molecular ensembles to also account for the fact that in an ensemble the population of the two states may equilibrate to fractions — say, 90% in the *Off* state and 10% in the *On* state.	[Hell, 2003; Hell et al., 2003; Hell, 2004; Hell et al., 2004, 2006]

Table 1.1 – continued from previous page

Technique	Description	References
(F)PALM, STORM: (fluorescence) photoactivation localization microscopy, stochastic optical reconstruction microscopy	Switches individual molecules stochastically and sparsely on by light-induced activation and then off, to detect a bunch of m photons from a single molecule on a camera, emitted while the molecules are in the *On* state. Calculating the centroid of the diffraction blob produced by each molecule and registering the coordinates of each molecule produces an image consisting of individual molecule positions. STORM has been initiated with pairs of photochromic cyanine dyes with one of them used as an activation (switch-on) facilitator.	[Betzig et al., 2006; Hess et al., 2006; Rust et al., 2006; Bates et al., 2007; Shroff et al., 2007; Huang et al., 2008; Juette et al., 2008; Shroff et al., 2008]
dSTORM: direct STORM	A simplified version of STORM that refrains from using a special dye for activation.	[Heilemann et al., 2008]
GSDIM: ground state depletion followed by individual molecule return	Switches off by depleting the molecular ground state and shelving the dye molecules in their triplet state, as in GSD. However, unlike GSD, it uses a stochastic readout, as in PALM, STORM, FPALM and dSTORM. It differs from these stochastic methods in that the dye molecule is not optically activated but is automatically switched on after its spontaneous return from the dark (triplet) state to its singlet state.	[Fölling et al., 2008; Steinhauer et al., 2008]

In targeted fluorescence switching, detection also happens in a targeted manner. In fact it works like any laser scanning microscope, where images are acquired point-by-point or line-by-line, and the coordinates and intensities of photon-emission are rendered to a raster image of the sample. To achieve super-resolution the scanning spot / line is usually reduced in size by switching off the fluorescence signal in its periphery [Hell and Wichmann, 1994]. Stochastic fluorescence switching, on the contrary, relies on parallel detection schemes with cameras catching the whole field of view (FOV) at once. Here a subset of fluorophores are switched on randomly in space and their coordinates determined with sub-wavelength accuracy through centroid calculation, provided that they are more than a Rayleigh distance apart [Bobroff, 1986; Betzig, 1995]. Subsequent registration of fluorophore coordinates enables to reconstruct the corresponding relative positions. To finally form an image at super-resolution a superposition of these pointillist maps is rendered. An exception to the general picture just drawn is made by SPEM/SSIM [Heintzmann et al., 2002; Gustafsson,

2005], since it provides resolution improvement in a targeted manner, but allows for parallel detection from many sample coordinates at once. It also spatially confines the *Off* state of a chromophore, proving that molecular switching has no preferred direction (on→off or off→on) to yield super-resolved images.

Whether a targeted or a stochastic switching approach is chosen, greatly affects the implementation of an actual fluorescence nanoscope. Systems for stochastic switching are generally considered easier and faster to built up than targeted switching designs. On the other hand, the former rely on sophisticated data processing, whereas the latter delivers immediately interpretable images. Implementations therefore vary in imaging speed and detection efficiency. According to Hell [2009], however, the most relevant practical difference between the two strategies is the economy of the switching: in the stochastic mode a fluorophore has to undergo a switching cycle only once to be registered, whereas in targeted implementations the molecules are perforce switched on and off repeatedly. Time lapse imaging aside, this puts hard constraints on the molecular mechanisms utilized for the switching, as the number of switching cycles in most current chromophores (fluorescent proteins or synthetic dyes) is limited.

That said, another defining feature of current fluorescence nanoscopes comes to the fore — the switching mechanism utilized to achieve optical isolation of neighbouring structures. Exemplifying saturated transitions, Hell [2009] denotes why:

> "The shared molecular [switching] mechanism leads to common aspects in many of these concepts, and these can be readily understood by looking into the basics of an incoherently driven optical transition. If a molecule can be transferred from one state to the other by light, the probability that the molecule remains in the first state decreases exponentially with the beam intensity I used; that is, it varies as $exp(-I/I_s)$. The "saturation intensity" I_s is a characteristic of the transition used, scaling inversely with the lifetimes of the two states. Applying intensities I to a molecule that exceed I_s makes it $> 63\%$ probable that one of the photons brings about the switch; $I > 5I_s$ makes it almost certain ($> 99\%$). The longer the lifetime of the initial state, the more time we have to impinge upon it with a photon, and the longer the lifetime of the final state, the more durable the switch becomes. The lifetimes of the states can vary by orders of magnitude, and so does I_s."

In other words, the photo-physics of a fluorophore determines the light exposure necessary to induce a particular optical transition with respect to intensity and timing. Hence, the

switching process of choice not only affects the amount of energy delivered to a sample, but also the frame rates of image acquisition — both crucial parameters for time lapse studies of live biological specimens. Moreover, it restricts the variety of fluorescent markers to be used, potential sample environments and the possibilities of multi-color imaging.
Finally, all current super-resolution techniques share a common concept of non-linearity, which comes yet into play at contrasting points with respect to the route taken to discern neighbouring structures. Targeted modalities are based upon an exponential dependence on the illumination intensity applied, when switching respective chromophores on / off, to spatially *constrain* the coordinates of fluorescence [Schönle et al., 2007]. In stochastic modes this is avoided, but they feature a non-linear dependence on the number of simultaneously detected photons to *register* respective coordinates of fluorescence [Hell et al., 1995]. Thus, the non-linear character of nanoscopy becomes manifest either at photon absorption or emission, interestingly enough, affecting the photon representation intrinsic to the emergent images, which is linear in targeted super-resolution approaches, but non-linear in stochastic modes [Hell, 2009].

1.3.2 STED Nanoscopy: A Role Model of the Targeted Switching Concept

Once stimulated emission[13] was proposed to pose a viable mechanism to circumvent the diffraction barrier in laser scanning microscopy [Hell and Wichmann, 1994], it took nearly a decade until Klar et al. [2000] furnished their ground breaking proof of principle. After that, many studies followed elaborating STED nanoscopy to become a readily usable imaging modality for the life sciences [Müller et al., 2012]. Its basic working principle is depicted in Figs.1.6 and 1.7, referring to the implementation used for the current study with respect to the laser pair employed, which was optimal for green fluorescent protein (GFP) and / or yellow fluorescent protein (YFP) to serve as molecular switches.

In STED imaging, the *On / Off* states of a fluorescent probe are formed by its ground state and first excited singlet state (cp. Fig.1.6.A). An incident photon of the excitation source switches the chromophore to its fluorescent *On* state, if its energy is sufficient to overcome the gap between S_0 and S_1^*, the photon itself being absorbed in the process. If left to its fate without further interference the excited molecule will return to the ground state spontaneously emitting a Stokes- / red-shifted photon of lower energy. Via stimulated

[13] Also induced emission; a quantum-chemical transition well known from laser physics.

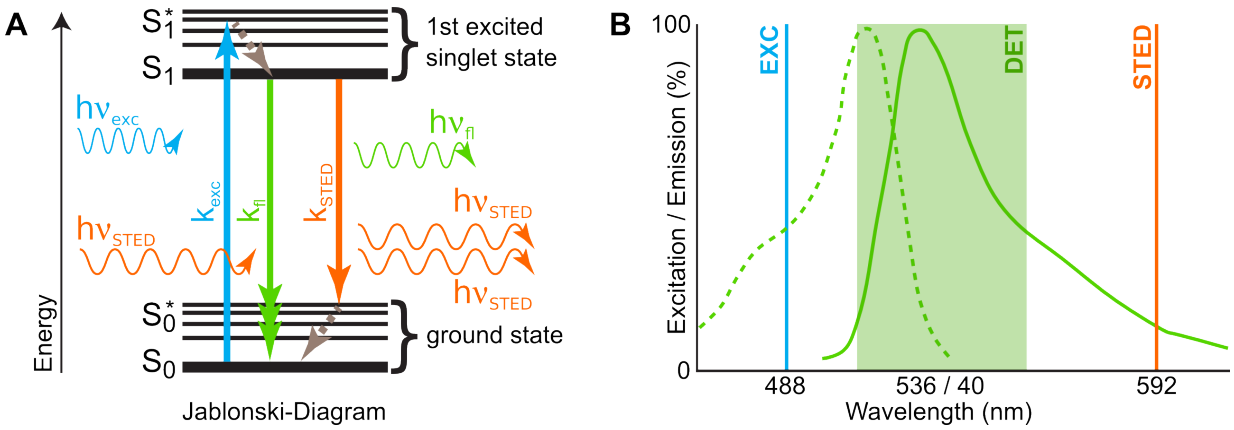

Figure 1.6: Principle of Stimulated Emission. *A* Jablonksi diagram of the molecular states used in STED nanoscopy. k_{exc} denotes the photophysical transition from the ground state S_0 to the first excited state S_1^* after the absorption of an excitation photon, k_{STED} denotes the stimulated transition from S_1 back to S_0^*, and k_{fl} denotes the spontaneous transition from S_1 to S_0. The dashed arrows symbolize internal conversions. Adapted from Naredi-Rainer [2014]. *B* The wavelength of the STED beam lies at the right edge of the YFP emission spectrum, where YFP excitation is negligible. Adapted from Nägerl and Bonhoeffer [2010].

emission, a photon of energy fitting the gap between S_1 and S_0^* can *quench* the excited fluorophore back to its ground state. So, with a second light source one is able to switch off fluorescence emission. Energy and momentum are conserved during stimulated quenching by the emission of a photon matching the wavelength, phase, polarization and direction of the photon inducing the molecular transition [Lakowicz, 2006].

Determinant for imaging, due to internal conversion processes the off-switching light is also Stokes-shifted with respect to the excitation light, such that the former can be tuned to have no overlap with the excitation spectrum of the dye (cp. Fig.1.6.B) and can be excluded from detection with spectral filtering. Both, the on- and off-switching beams, are then concentrically superimposed in the focal plane, where the off-switching point spread function (PSF) is given a toroidal shape with an intensity zero at its center. This is achieved by patterning the phase of incident wavefronts across the entrance pupil of the objective lens in its back focal plane (BFP). Several ways to create hole-centered PSFs to break the diffraction-limit have been investigated. The most common STED nanoscope designs employ various phase plates [Klar et al., 2001; Wildanger et al., 2009] or spatial light modulators [Willig et al., 2006; Auksorius et al., 2008]. Eventually, that way the volume of fluorescence emission is spatially confined to the intensity zero of the off-switching PSF and a specimen scanned by a significantly smaller spot (cp. Fig.1.7.A, upper panel).

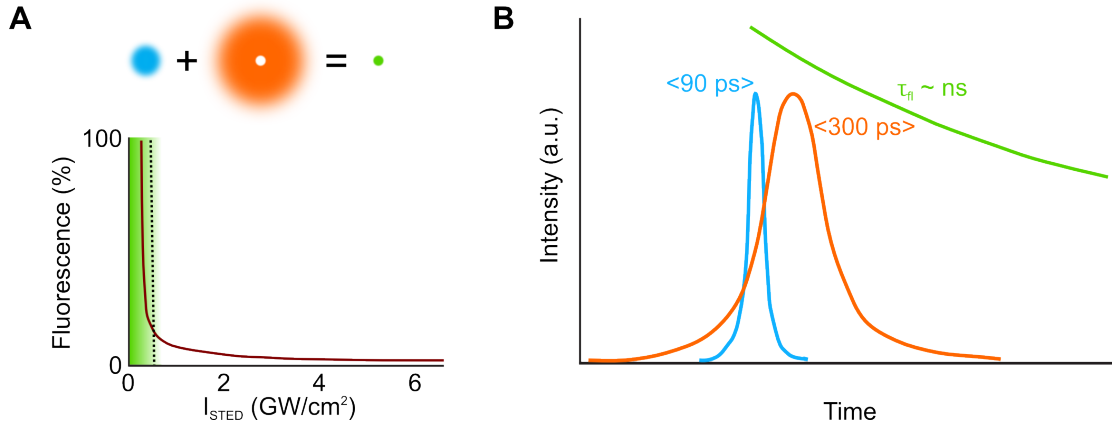

Figure 1.7: Principle of STED Nanoscopy. *A* Upper panel: Superposition of the diffraction-limited spot of the excitation laser (blue) and the doughnut of the STED laser (orange) dramatically reduces the size of the fluorescence spot (green). Lower panel: Non-linear relationship between the intensity of the STED beam (I_{STED}) and the suppression of the fluorescence. The dotted line indicates the STED power that effectively switches off the fluorescence. *B* Temporal relationship between excitation and STED pulses. The fluorescence lifetime (τ_{fl}) of YFP is $\approx$ 3 ns. Adapted from Nägerl and Bonhoeffer [2010].

The resulting raster image is therefore resolved in much greater detail by purely physical means. Notably, the angular resolution limit is not violated, since both the excitation and de-excitation PSFs still fully comply with diffraction.

To ensure efficient quenching within the desired region of the off-switching PSF, stimulated emission rates have to be favourable compared to spontaneous photon emission, i.e. the excited state S_1 has to be depleted[14]. On that condition Westphal and Hell [2005] estimated the attainable resolution to the following:

$$d \approx \frac{\lambda}{2 \cdot n \cdot sin(\alpha) \cdot \sqrt{1 + a \cdot \xi}}. \tag{1.1}$$

This equation is basically an extension of Abbe's formula (cp. Sec.1.3.1), where $\xi = I_{STED}/I_{sat}$ defines the saturation level of the de-excitation. The constant a denotes for the steepness of the intensity zero and depends on the particular phase filter used to create the hole-centered PSF [Harke et al., 2008]. I_{STED} is the maximum of the intensity distribution of the de-excitation light and I_{sat} is the effective saturation intensity of the fluorophore, which can be defined as the de-excitation intensity at which the population of the excited *On* state is reduced by 63 % (cp. Fig.1.7.A, lower panel). For $I_{STED} = 0$, Eq.1.1 gives

[14] Hence the term *Stimulated Emission Depletion*.

the diffraction limit, whereas for $I_{STED} \gg I_{sat}$, the *On* state is sharply confined. As the square root of I_{STED}/I_{sat} increases, d decreases and is therefore theoretically not limited anymore.

Though mathematically not fully stringent, one can understand the dependence of the resolution on the intensity of the de-excitation light in Eq.1.1 by contemplating the probability to find a dye molecule in state S_i as given by its occupation number N_i in the following differential equation:

$$\frac{dN_1}{dt} = -k_{off}N_1 + k_{on}N_0 = -\frac{dN_0}{dt}, \tag{1.2}$$

where k_i denote the transition rates for on- / off-switching. More detailed deductions can be found in Hell and Wichmann [1994]; Klar [2001]; Hell [2003, 2004]. The total decay rate is provided by the rate constant of spontaneous fluorescence emission $k_{fl} = 1/\tau_{fl}$ and the rate constant of stimulated emission:

$$k_{off} = k_{fl} + \sigma_{STED} \cdot I_{STED}, \tag{1.3}$$

where σ_{STED} denotes for the optical cross-section of the stimulated transition $S_1 \rightarrow S_0$. Assuming N_1^0 chromophores in state S_1 at time t_0 after a well defined excitation *pulse*, the population in state S_1 at time $t > t_0$ is given by a simple decay curve:

$$N_1(t) = N_1^0 \cdot exp(-k_{off} \cdot t). \tag{1.4}$$

Hence, application of a de-excitation pulse of duration τ_{STED} will lead to an occupation number of

$$N_1(\tau_{STED}) = N_1^0 \cdot exp(-k_{fl} \cdot \tau_{STED}) \cdot exp(-\sigma_{STED} \cdot I_{STED} \cdot \tau_{STED}). \tag{1.5}$$

Compared to the situation without stimulated emission ($I_{STED} = 0$), the amount of exited molecules N_1, i.e. the fluorescence signal, is reduced by

$$\eta = exp(-\sigma_{STED} \cdot I_{STED}). \tag{1.6}$$

η is called the STED suppression coefficient, as it describes the amount of fluorescence inhibition[15]. To fully deplete the outer rim of a fluorescence volume, induced emission rates have to exceed spontaneous emission dramatically in the corresponding region, i.e.

[15] For numerical simulations of the suppression coefficient see Klar [2001].

$k_{off} \approx \sigma_{STED} \cdot I_{STED}$. A function of the de-excitation intensity, η is accessible by experiments and can vary under real conditions. For real fluorescent molecules Eq.1.6 is a good approximation if vibrational relaxation is short compared to the duration of a de-excitation pulse, and if fluorescence is not prevented by further processes like photobleaching [Dyba, 2004]. Experimental depletion curves were for example published in Klar et al. [2000, 2001]; Dyba and Hell [2003]; Westphal et al. [2003]. Considering a standard dye, typical cross-sections for the stimulated transition are in the order of $\sigma_{STED} \approx 10^{-16}\,\mathrm{cm}^2$ [Kastrup and Hell, 2004], which leads to values of $I_{sat} \propto (\tau_{STED} \cdot \sigma_{STED})^{-1}$ in the order of several $\mathrm{MW/cm}^2$ [Hell, 2009].

My investigation employed pulsed excitation and depletion light sources (cp. Fig.1.7.B). For such implementations, the pulse width of the STED beam has to be in a range of a few hundred picoseconds[16]. Additionally, de- / excitation pulses need to be synchronized in time, such that excited molecules are allowed to relax to the vibrational ground state of S_1 before a STED pulse arrives. Implementations with cw-lasers were also reported to work for STED nanoscopy [Willig et al., 2007], and could be combined with time-gated detection schemes to increase the efficiency of targeted switching / readout [Moffitt et al., 2011; Vicidomini et al., 2011, 2013].

1.3.3 Applications to Neuroscience

Operating at much smaller wavelengths than light microscopy, until recently, EM constituted the primary method to investigate the ultrastructure and functional domains of synaptic constituents. Since it is not suited for the examination of live tissue, the dynamics of synaptic compartments remained mostly unexplored [Requejo-Isidro, 2013]. The advantage of super-resolution light microscopy has gained impact on neurobiology, tackling questions on neuronal protein function and dendritic spine motility.

Photoactivated localization microscopy (PALM) was utilized to investigate the nanoscale dynamics of the actin-cytoskeleton [Tatavarty et al., 2009; Frost et al., 2010; Izeddin et al., 2011; Tatavarty et al., 2012] and to follow post-synaptic AMPA receptor trafficking [Hoze et al., 2012] in live dissociated cultured neurons with photo-switchable tdEos and Dronpa fusion proteins. Dani et al. [2010] adopted multi-color three dimensional / three dimensions (3D) STORM to assess the distribution of 10 protein components of the pre-synaptic active zone and PSD in cryosections of fixed mouse brains labelled with fluorescently marked

[16] Dependent on the laser source, this is usually achieved by dispersion of fs-pulses, which have a broad spectral range, in stretches of glass.

antibodies. Reversible switchable optical fluorescence transition (RESOLFT) imaging of a Lifeact[17]-Dronpa fusion construct has been applied to examine the cytoskeletal structure of living neurons in organotypic slice cultures [Testa et al., 2012].
Over the years, STED nanoscopy has become increasingly popular with neuroscientists. Its applications cover several variants of sample preparations. Fixed tissue studies were performed to investigate the *Drosophila* active zone protein Bruchpilot [Kittel et al., 2006], as well as synaptic vesicle fusion and exocytosis [Willig et al., 2006; Opazo et al., 2010]. Hoopmann et al. [2010]; Kamin et al. [2010]; Dean et al. [2012] and Westphal et al. [2008] used time lapse and video-rate STED imaging to further study the latter in live primary neuronal cultures immunostained with synthetic dyes. Hippocampal organotypic slice cultures marked with cytosolic fluorescent proteins or Lifeact fusions served as a model system to study spine motility at the nanoscale in response to cLTP [Nägerl et al., 2008; Urban et al., 2011]. To facilitate nanoscopy in acute brain slices Ding et al. [2009] and Takasaki et al. [2013] combined two-photon-excitation (2PE) with one-photon de-excitation using Alexa Fluor-594 as their cellular marker. This was complemented by dual-color imaging, discerning microglial and neuronal cells labelled with cytosolic GFP and YFP, respectively, in a transgenic mouse line at super-resolution [Bethge et al., 2013]. Finally, even time lapse *in-vivo* STED imaging has been demonstrated, examining YFP expressing neurons in layer 1 of the cerebral cortex of anaesthetized transgenic mice for up to half an hour [Berning et al., 2012; Willig et al., 2014].

1.4 Objectives

In the backdrop of its potential relevance for learning and memory, morphological spine plasticity was within the central scope of the current thesis. Focusing on the major benefits of super-resolution light microscopy – nearly non-invasive, time-lapse suitability, sub-100 nm resolution – dendritic spine morphing was attempted to be analysed in response to the induction of synaptic potentiation in live tissue. I decided on organotypic hippocampal slice cultures to constitute an appropriate *in-vitro* model system, and the induction of NMDAR dependent LTP in CA1 pyramidal neurons to constitute an eligible plasticity paradigm. The objectives of my project, then, comprised of three major steps:

1. Implementation and characterization of a confocal STED-laser scanning microscope (LSM), designed for the imaging of green fluorescent probes and adapted to the

[17] An actin-binding peptide [Riedl et al., 2008]

standards of neurobiological research. A crucial point concerned the penetration depth of the imaging optics in organotypic slice preparations.

2. Integration of local light stimulation by means of ultraviolet (UV) flash photolysis of caged glutamate, as it presented a non-invasive, reliable and specific way to induce LTP in spines.

3. Investigation of morphological spine plasticity in longitudinal experimental sessions at Schaffer collateral synapses over at least one hour *in-vitro*. To exclude imaging related artefacts, appropriate control experiments had to be conducted.

With this I aimed at an examination of the current understanding of spine (sub-) structure and its dynamics:

1. I investigated the persistence of morphological transitions in live cells.

2. I scrutinized to what extent synaptic potentiation perturbs the baseline motility of dendritic spines.

3. I related my findings to actual assessments on the molecular mechanisms driving structural plasticity.

Finally, with the experience gained on STED nanoscopy, I intended to evaluate its aptitude for neurobiological live-cell studies, in particular in combination with local light stimulation.

Chapter 2

Experimental Methods

2.1 Organotypic Slice Cultures

Organotypic slice cultures facilitate the investigation of single regions of the CNS *in-vitro* under nearly physiological conditions. They develop thin cellular structures organized very similar to those found in the intact brain and can be maintained in culture for relatively long periods of time of up to several weeks [Gähwiler, 1988; Gähwiler et al., 2001; Muller et al., 2001].

2.1.1 Preparation of Membrane Cultures

According to the protocol introduced by Stoppini et al. [1991] transverse hippocampal explants were cultivated. The method obviates the need for a roller drum (cp. Sec.2.1.2). Instead explants reside on a membrane at the interface between medium and air.
Tissue slices were prepared under laminar flow either from wild-type (C57BL/6) or transgenic (Thy1-GFP-M and Thy1-YFP-H [Feng et al., 2000]) mice bred at the MPI of Neurobiology at postnatal day 5 to 7. Mice were sacrificed by decapitation, skin and skull were removed. Hippocampi were resected in Preparation Medium before they were cut into 350 μm thick transverse slices with a McIlwain Tissue Chopper. The explants were then incubated at 4 °C for half an hour and afterwards transferred one by one onto pieces of membrane cut to size (pore size: 0.4 μm, Biopore Membranes). Three slices on membrane snippets each were placed onto cell culture inserts (pore size: 0.4 μm, diameter: 30 mm,

height: 2 mm, Millicell Cell Culture Inserts) and incubated at 35 °C with a 5 % CO_2 enriched atmosphere in 6-well Tissue Culture Test Plates. Half of the Membrane Culture Medium, i.e. 500 µL per well, was exchanged twice a week and slices kept in culture for up to 20 days. Before further investigated with STED imaging, slices were screened for labeling density, fluorescence brightness and integrity of tissue on grounds of morphological criteria with a commercial stereo microscope (SteREO LumarV.12).

2.1.2 Preparation of Roller Tube Cultures

Gähwiler [1981] introduced a protocol to culture brain explants in a slightly different fashion than described above. With his method tissue slices are embedded in chicken plasma on a glass substrate and put upstanding into a closed culture tube filled with enough medium to submerge half the culture on substrate. For incubation the tube resides in a roller drum, rotating at specific speed and angle to repeatedly expose the cultured slices to air and growing medium, respectively.

Transverse hippocampal slices were prepared under laminar flow either from wild-type (C57BL/6) or transgenic (Thy1-GFP-M and Thy1-YFP-H [Feng et al., 2000]) mice bred at the MPI of Neurobiology at postnatal day 5 to 7. As for the membrane cultures described above, mice pups were decapitated, skin and skull removed, hippocampi resected in Preparation Medium and cut into 350 µm thick transverse slices with a McIlwain Tissue Chopper. Next, explants were incubated at 4 °C for 30 − 60 min, before they were transferred one by one to a drop of 10 µL Chicken Plasma Solution either on a glass cover slip (No. 1.5H) or on a glass bottom dish (diameter: 35 mm, glass diameter: 14 mm, P35GC-1.0-14-C). To induce coagulation of the plasma 10 µL Thrombin Working Solution were added. After a resting time of approximately half an hour coverslips were placed in a roller incubator tube (Nunc Cell Culture Tubes) containing 750 µL of Roller Tube Culture Medium, pre-warmed to 35 °C. 1.5 mL of pre-warmed Roller Tube Culture Medium were added to explants in glass bottom dishes. Both preparations were incubated at 35 °C for 3 to 4 days, before 10 µL (20 µL for glass bottom dishes) of Mitotic Inhibitor Solution were added to each slice. After another 16 − 24 h two thirds of the medium were exchanged with fresh Roller Tube Culture Medium, which was then repeated once a week (every 10 days for glass bottom dishes). In total, slices were kept in culture for up to 100 days to be used for imaging. Before further studied with the STED-LSM, slices were screened for labeling density, fluorescence brightness and health of tissue on grounds of morphological criteria with a commercial stereo microscope (SteREO LumarV.12).

Table 2.1: DNA Constructs Used Throughout the Work at Hand. Sequences are given in Appx.C.

Construct	Promoter	Resistance	Source
pCI-hSyn-tdimer2RFP	Synapsin	Ampicillin	Dr. Tobias Rose Synapses - Circuits - Plasticity MPI of Neurobiology Martinsried, Germany
pCI-Neo-PSD-95::EGFP	CMV	Ampicillin	Prof. Dr. Valentin Stein Physiology Department 2 University of Bonn Bonn, Germany
pCI-hSyn-PSD-95::EGFP	Synapsin	Ampicillin	Claudia Huber Synapses - Circuits - Plasticity MPI of Neurobiology Martinsried, Germany
pSCA-Lifeact::EYFP	CMV	Ampicillin	Dr. Roland Wedlich-Söldner Cellular Dynamics and Patterning MPI of Biochemistry Martinsried, Germany

2.1.3 Generation of Plasmid DNA

pCI-hSyn-PSD-95::EGFP for single-cell electroporation (SCE) mediated gene transfection of pyramidal neurons in CA1 was designed, generated, and amplified using standard molecular biology techniques. Deoxyribonucleic acid (DNA) constructs used are listed in Tab.2.1. Briefly, a pCI-hSyn expression vector backbone was obtained from a pCI-hSyn-tdimer2RFP plasmid, removing the transgene by digestion with XhoI and NotI restriction enzymes. The backbone was isolated by gel-extraction following gel-electrophoresis (QIAquick Gel Extraction Kit). The PSD-95::EGFP transgene was isolated from a pCI-Neo-PSD-95::EGFP vector using the same restriction reaction as for the pCI-hSyn backbone, followed by gel-electrophoresis and -extraction. All restriction digestions were carried out at 37 °C for 2 to 3 hours. Ligation reactions were performed for 3 hours with T4 ligase at 23 °C, mixing the backbone and insert in a 1:7 molar ratio. Ligation products were transformed to competent *Escherichia coli* DH5α by heat shock and transformants were grown overnight on Luria-Bertani medium agar plates at 37 °C. Colonies carrying the plasmid were selected based on their resistance to ampicillin and amplified. Target plasmid DNA was purified from liquid cultures of identified colonies (QIAGEN Plasmid Plus Midi Kit) and verified via test

restriction.

2.1.4 Transfection via Single-Cell Electroporation

Targeted SCE provides efficient means to manipulate gene expression of identified subsets of mammalian neurons within intact tissue [Judkewitz et al., 2009]. Increasing the electrical conductivity and permeability of its plasma membrane by an externally applied electric field, a neuron can be loaded with synthetic dyes, molecular markers or coding DNA [Haas et al., 2001; Rae and Levis, 2002; Rathenberg et al., 2003; Nevian and Helmchen, 2007; Wang et al., 2010]. To overexpress fluorescently marked post-synaptic density protein 95 (PSD-95) in CA1 pyramidal cells, I followed the protocol of Judkewitz et al. [2009]. In brief, cultured hippocampal explants of wild-type mice were transferred to a custom built setup after 7 to 10 days *in-vitro* (DIV) and immersed in HEPES-buffered ACSF at room temperature ($22 \pm 1\,^{\circ}\mathrm{C}$) under sterile conditions. The setup comprised the following hardware: a motorized stage was mounted to a Axioskop2 research microscope, equipped with a long distance imaging lens (LUMPlanFL, 60x/0.9 W); the stage hosted a micro-manipulator (Unit MRE/MLE Mini-25) to carry a micro-electrode pipette; to measure pipette resistances and apply voltage pulses I employed a commercial electroporation system (Axoporator 800A). Micro-electrodes were pulled from glass capillaries (GC150F-10) with a vertical puller (PC-10) to have a resistance of approximately $10\,\mathrm{M\Omega}$ and were back-filled with cooled, sterile filtered Electroporation Solution. 3 to 5 pyramidal neurons in CA1 per slice were targeted under visual control and electroporated with $12\,\mathrm{V}$ pulses of $5\,\mathrm{ms}$ duration at $50\,\mathrm{Hz}$ for $1\,\mathrm{s}$, positioning the mico-electrode in a loose patch configuration ($20 - 30\,\mathrm{M\Omega}$) at the soma of a cell. Slices were transferred back to the incubator for 5 to 7 days to allow for expression of the transgenes. Before further investigated with STED imaging, slices were screened for fluorescence brightness and integrity of marked cells on grounds of morphological criteria with a commercial stereo microscope (SteREO LumarV.12).

2.1.5 Transfection via Viral Injection

To label the cytoskeleton of hippocampal pyramidal neurons Lifeact, an actin-binding peptide derived from yeast [Riedl et al., 2008], fused to enhanced YFP was used. Labelling fine-veined structures, cytoskeletal markers are ideal candidates for super-resolution imaging. Moreover, Lifeact is likely to be a less invasive probe than labels grounded on the

overexpression of fusion constructs. Additionally, the fluorescence signal of a Lifeact fusion protein is less prone to photobleaching due to the reversible binding kinetics of the probe [Urban et al., 2011]. It has been utilized for neurobiological studies in diverse preparations including dissociated neuronal cultures, organotypic slice cultures and transgenic animals [Riedl et al., 2008; Swanger et al., 2011; Urban et al., 2011; Kerr and Blanpied, 2012; Testa et al., 2012; Chmyrov et al., 2013; Lauterbach et al., 2013].
For transfection, a modified Semliki Forest virus [Ehrengruber et al., 1999] containing a pSCA-Lifeact::EYFP vector plasmid (courtesy of Claudia Huber), was injected into hippocampal slice cultures of wild-type mice, immersed in HEPES-buffered ACSF at room temperature, after 7 to 30 DIV. Micro-electrodes (resistance: $4-6\,\mathrm{M\Omega}$), pulled from glass capillaries (TW150F-4) with a vertical puller (PC-10), were first backfilled with virus particles dissolved in distilled water (titer: 10^{-16}). Under visual control pipettes, connected to a pressure injector (TooheySpritzer), were guided to CA1 at the setup described in Sec.2.1.4. Four to ten pressure pulses (duration: 100 ms, pressure: 138 kPa) were applied to deliver the necessary amount of virus containing solution into the tissue to generate sparse cellular labelling. Transfected slices were then incubated overnight for at least 16 h, before they were screened for fluorescence brightness and imaged the following day.

2.1.6 Handling During Experimental Sessions

Chemical LTP. Experiments were conducted on cultured slices of transgenic animals (traditional roller tube cultures) after 14 to 96 DIV at room temperature ($22 \pm 1\,^{\circ}\mathrm{C}$) in artificial cerebro-spinal fluid (ACSF). Tissue slices on coverslips were taken out of their roller incubator tubes and pasted into a custom made experimental chamber with duplication silicone (Picodent Twinsil). They were immersed in ACSF for cLTP with a perfusion system, connected to the chamber with magnetic mounts, that was driven by a peristaltic pump (Minipuls 3). Slices rested in ACSF for 20 min, while STED images were taken at 10 min intervals. Then LTP was induced by means of chemical stimulation adding 25 mM of TEA (Tetraethylammonium, Et_4N^+) to the bath for 5 min. Subsequent imaging went on for up to an hour.

Imaging of PSD-95. Super-resolution images were taken from cultured slices (membrane cultures), transfected with pCI-hSyn-PSD95::EGFP and pCI-hSyn-tdimer2RFP via SCE (cp. Sec.2.1.4), after 12 to 17 DIV at room temperature ($22 \pm 1\,^{\circ}\mathrm{C}$) in ACSF. The red volume marker was mainly used not to unnecessarily bleach the PSD label, when checking

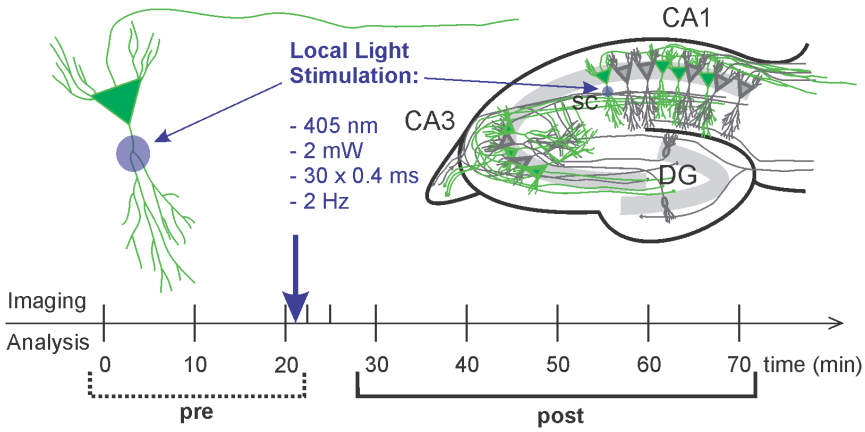

Figure 2.1: Experimental Paradigm for Glutamate Uncaging. Images were taken at 10 min intervals and immediately after the induction of LTP to confirm plastic changes. A light stimulus was directed to the center of the FOV at the first or second branchpoint of the main apical dendrite of a GFP positive CA1 hippocampal pyramidal cell.

the efficiency of the transfection and searching respective cells at minimal light exposure in the green fluorescence channel. A slice on membrane snippet was transferred to a custom made experimental chamber with a glass bottom (coverslip No. 1.5H), immersed in pH-buffered saline (HEPES-buffered ACSF) turned bottom up[1] and held down by a nylon mesh attached to a small ring of platinum wire. By this means the distance of the tissue to the imaging optics was minimized. The objective lens (cp. Sec.2.3.5) was additionally equipped with a mechanical correction collar to adjust for spherical aberrations, and therefore to optimize the penetration depth of the STED-LSM as demonstrated by Urban et al. [2011]. Imaging sessions lasted about $10 - 15$ min after the explants climatized to the new environment for approximately 10 min.

Glutamate Uncaging (see Sec.2.2). Experiments were carried out on cultured slices of transgenic mice pups (membrane cultures) after 7 to 20 DIV at room temperature ($22 \pm 1\,^{\circ}\mathrm{C}$) in ACSF, saturated with humidified carbogen to stabilize pH and oxygenate the solution. An explant on a membrane snippet was transferred to a custom made experimental chamber as described above for the imaging of PSD-95, with the exception that specimens were immersed in ACSF for Glutamate Uncaging. Solution was applied via a closed perfusion system of 10 mL holding capacity, connected to the chamber with magnetic mounts, that was driven by a peristaltic pump (Minipuls 3). ACSF for Glutamate Uncaging contained no magnesium and a low concentration of D-serine to activate

[1] The membrane was facing upward and the tissue downward.

NMDA driven calcium channels by the removal of their Mg^{2+} block, tetrodotoxin (TTX) was added to prevent spontaneous activity of the slices and Trolox to reduce potential effects of phototoxicity. In the cases where caged glutamate was added to the ACSF, its concentration was set to 2 mM. Experimental sessions lasted no longer than 90 min including an acclimation phase for the cultures of about 10 min. The time course of trials is given in Fig.2.1.

2.2 Glutamate Uncaging

2.2.1 Methodological Conception

In several studies the photolysis of caged glutamate has been shown to serve as an efficient approach to locally induce synaptic plasticity [Callaway and Katz, 1993; Kandler et al., 1998; Matsuzaki et al., 2004; Richards et al., 2005; Kwon and Sabatini, 2011; Meyer, 2013]. Both, an immediate and selective enlargement, as well as an enhancement of synaptic strength of stimulated spines have been reported (see Sec.1.2.3). When exposed to UV light MNI-caged-L-glutamate (4-Methoxy-7-nitroindolinyl-caged-L-glutamate or MNI-glutamate) rapidly and efficiently releases the neurotransmitter glutamate, that can then bind to AMPA and NMDA receptors. Tight focusing of the incident light beam and sequential pulsing of the light source allows for spatial confinement and finely graduated titration of the stimulus. Hence, glutamate uncaging unites the advantages of other plasticity induction paradigms: 1) being a light-driven process it is less invasive than electrical stimulation with an electrode impaling the tissue, but maintains a comparable locality, 2) bath application of the caged compound preserves the simplicity and low time exposure of cLTP protocols. In combination with 2PE, glutamate uncaging has been proven to be suited for the stimulation of single synapses, confining the photolysis-reaction to a defined focal volume of a few femtoliters [Denk, 1994].

2.2.2 Setup for Local Light-Stimulation

Even though the ideal wavelength for the uncaging of glutamate lies in the UV part of the visible spectrum ($300 - 380$ nm), in the past MNI-glutamate was successfully photolyzed at longer wavelengths, particularly at 405 nm [Trigo et al., 2009]. At that wavelength the light absorption of the caged compound is sufficiently low to allow for deeper penetration of the preparation. The reduced photolysis performance can be compensated by using

higher light intensities or higher cage concentrations, and was reported to be still better than with 2PE. Additionally, the use of near UV light puts less constraints onto the optics to be employed with respect to their transmittance.
At the setup adopted throughout this study, 405 nm light from a fiber coupled solid state laser (OXX-405-100-LBX-ZIR) was collimated and guided through the side port of an upright micro-inspection lens system (Optem Zoom 70XL) to an objective lens (LUMPlanFL, 60x/0.9 W) positioned par-focally to the imaging optics of the LSM. The collimated beam diameter was set to overfill the back aperture of the lens and the average light power in the BFP to 2 mW. The laser was externally triggered at its analog input by a Master-8-cp pulse generator to provide a stimulus of 30 pulses of 4 ms duration at 0.5 Hz. The effective reach of action of the uncaging spot was estimated to $13.2 \pm 0.4\,\mu$m from examining its effect on dendritic spines during glutamate uncaging experimental sessions.

2.3 Laser Scanning Microscope

The layout of the custom built STED - LSM used throughout the current study, geared to image live GFP- or YFP-labeled cells, essentially followed Willig and Nägerl [2012]. Its components are described in detail below. It was situated in a temperature-controlled laboratory space on vibration damped optic tables (ST Series). Variations in temperature were limited to $\pm 0.5\,^{\circ}$C and relative humidity stood below 50 %. A diagram of its optical layout is shown in Fig.2.2.

2.3.1 Excitation Source

To excite fluorescence in a specimen, a pulsed diode laser was used (Pico TA). It generates pulsed laser light of up to 4 mW average power at a fixed wavelength of 488 nm, at a repetition rate of up to 80 MHz and a pulse width of 90 ps. Its controller (PDL 800-B) was externally transistor-transistor-logic (TTL)-triggered by an optical constant fraction discriminator (OCF-401) measuring the repetition frequency of the depletion light. The OCF-output signal was electronically delayed by a custom-made circuit board (DELAY) to synchronize the pulse patterns of both the excitation and depletion light sources in time with 10 ps accuracy. The excitation light was coupled into a 2 m long polarization maintaining single mode fiber (PMC-460Si-3.0-NA012-3-APC-200-P) in a free space arrangement via two dielectric mirrors and a custom made fiber port coupler, after it passed through an electro-optic modulator (M350-80) tuning its intensity.

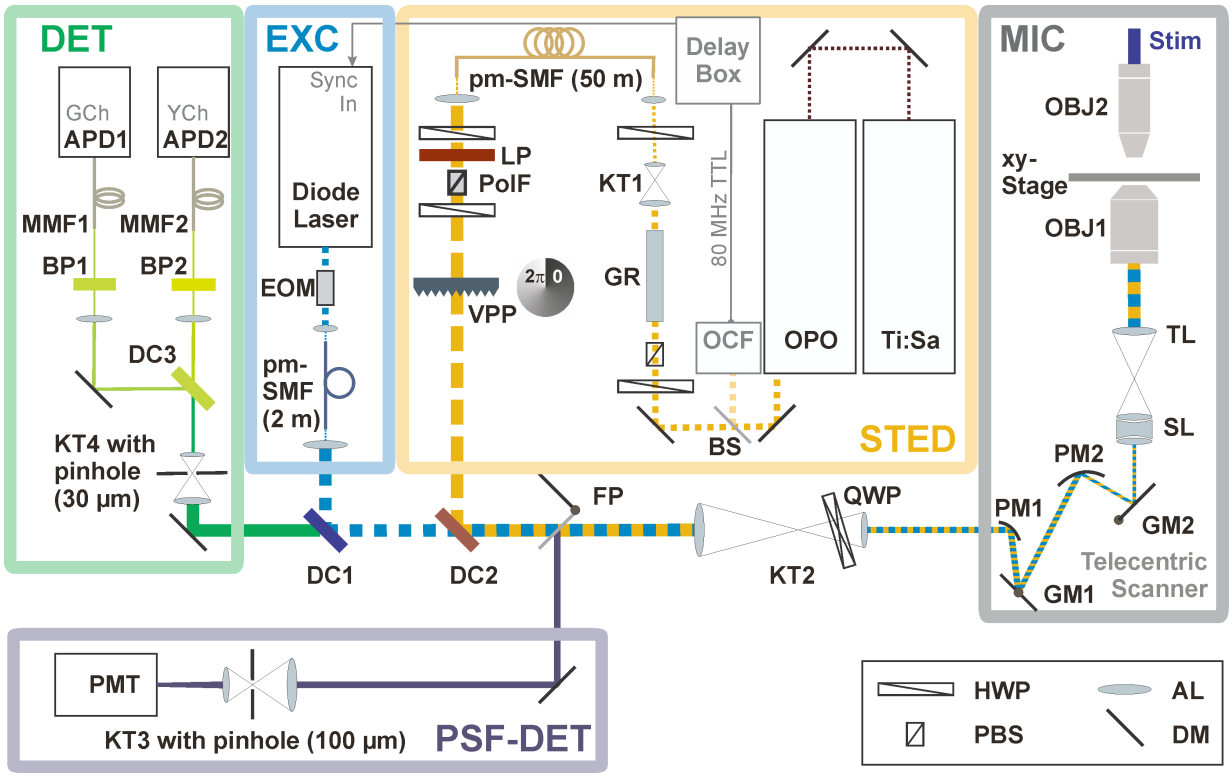

Figure 2.2: Optical Layout of the STED-LSM. A detailed description can be found in the text. AL: achromatic lens, APD: avalanche photo diode, BP: band pass filter, BS: beam splitter, DC: dichroic mirror, DM: dielectric mirror, EOM: electro-optic modulator, FP: flipable pellicle beam splitter, GM: galvo mirror, GR: glass rod, HWP: half wave plate, KT: kepler type telescope, LP: long pass filter, MMF: multi-mode optic fiber, OBJ: objective lens, OCF: optical constant fraction discriminator, OPO: optical parametrical oscillator, PBS: polarizing beam splitter, PolF: linear polarizer, PM: parabolic mirror, pm-SMF: polarization maintaining single-mode optic fiber, PMT: channel photomultiplier, QWP: quarter wave plate, SL: scan lens, Ti:Sa: titanium-sapphire laser, TL: tube lens, VPP: vortex phase plate.

2.3.2 Depletion Source

A pulsed titanium-sapphire (Ti:Sa) laser (MaiTai HP) pumping an optical parametrical oscillator (OPO) (OPO Advanced) served as a coherent light source for the induction of stimulated light emission in a fluorescently labeled specimen. The laser emits light pulses $150-300$ fs wide at a repetition rate of 80 MHz. The wavelength of the pump laser light was tuned to 795 nm at an average output power of about 2.8 W. The OPO was set up in the so called Ring Version to intracavity frequency double the wavelength of the pump laser, i.e. the near infrared (NIR) light of the Ti:Sa was "shifted" to the visible spectral range (592 nm). This nonlinear process comes at a power loss of $70-80$ %, therefore the output

of the OPO averaged to about 700 mW. A combination of a Glan-type polarizer (GL5-A) and an optical retarder (AHWP05M-600) was used to adjust intensity, before the light was coupled into a 50 m long polarization maintaining single mode fiber[2] (PMJ-3U3A-633-4/125-3-50-1-HP) in order to disperse the pulse widths to $300 - 500$ ps. Pre-stretching the pulses in a glass rod (SF6 glass) by a factor of about 10 to 20 helped minimizing potential damage to the fiber through absorption of high energy light.

2.3.3 Beam Combination and Telecentric Scanner

Both laser beams were collimated at the fiber outputs with $f = 60$ mm achromatic lenses to overfill the back aperture of the objective lense (cp. Sec.2.3.5) having a diameter of 8.25 mm. The excitation light was then straightly directed to a dichroic long pass mirror (500 DCXR, DC1 in Fig.2.2), whereas the depletion light passed through a long pass clearing filter (561 LP Edge Basic), a combination of linear polarizer and achromatic retarders (CM1-PBS251, AHWP05M-600 and RAC 3.2.15) to set its polarization, and a spiral phase plate (VPP-1) before it was directed to a dichroic short pass (z 590 sprdc, DC2 in Fig.2.2). The VPP-1 introduces a certain phase shift, a so called screw dislocation or phase singularity, in incident wave fronts that results in a toroidal PSF when focused at a large angle or by a high N.A., respectively [Keller, 2006]. To create toroidal PSFs with central holes of ideally zero intensity the depletion light must at best be circularly polarized, which was achieved by placing an achromatic quarter wave plate (AQWP05M-600) carefully oriented and tilted into the beam path after the dichroic mirrors. By that, the distance an incident light wave travelled through the retarder, i.e. the effective crystal thickness, could precisely be adjusted.

The aforementioned telescope basically served two purposes. First, it relayed the BFP of the imaging lens, such that a mirror on a piezoelectric mount (AG-M100N) as part of the STED beam path (not shown in Fig.2.2) could be positioned into a conjugate Fourier plane; that way it was conveniently possible to overlay both the excitation and depletion PSFs by only changing the incidence angle of the depletion beam at the objective lens' back aperture without introducing an x/y-shift in its BFP. Second, it counterbalanced the magnifying effect of the scan-telescope (SL and TL in Fig.2.2), which widened the beam diameters by factor of 4; since the telecentric scanner (Yanus IV) via two parabolic mirrors resembled a 2:1 Keplerian telescope, the relay lenses were chosen to follow a ratio of 2:1 of

[2]This was done in the same way as for the excitation light utilizing a custom made fiber port coupler in a free space arrangement.

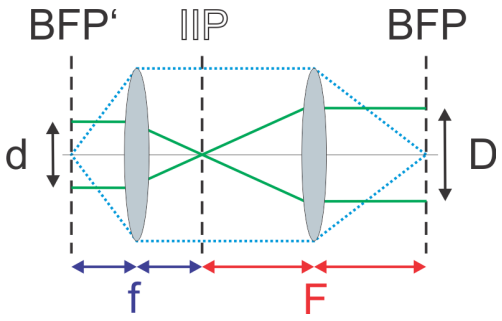

Figure 2.3: 4f-Arrangement. Two convex lenses of a Keplerian telescope, separated a distance that corresponds to the sum of their focal lengths, relay an optic plane by a span two times the sum of their focal lengths along the optical axis. A collimated beam entering the system exits collimated with altered diameter (solid line), a point source is imaged onto a single point (dotted line). BFP: back focal plane, IIP: intermediate image plane.

their focal distances, as well. At system construction great care had to be taken to set up the scan-head and scan-telescope in a so called "4f-arrangement" (cp. Fig.2.3), meaning to settle the second galvo mirror (GM2 in Fig.2.2) into a conjugate Fourier plane, to be able to properly relay the BFP to the piezo mirror.

2.3.4 Confocal Detection Unit

Fluorescent light from a specimen was collected with the same objective lens the illuminating beams had passed (HCX PL APO CS 63x/1.30 GLYC). It was de-scanned backward progressing along the excitation beam path and spectrally filtered by dichroics (DC2 and DC1 in Fig.2.2). Confocal detection was achieved by placing a pinhole of 30 μm in diameter at a conjugate image plane[3]. The light then passed another dichroic mirror (zt 514 RDC, cp. DC3 in Fig.2.2) before it was spectrally cleared by bandpass filters (525/50 BrightLine HC and 536/40 BrightLine HC, cp. BP1 and BP2 in Fig.2.2) and directed to fiber-coupled single-photon counting detectors (SPCM-AQRH-13-FC). Separation of the detected signal had two main advantages: 1) it granted the option of two-color imaging at a single excitation wavelength via spectral imaging and linear unmixing, as reviewed by Zimmermann et al. [2003] and introduced for STED microscopy by Tønnesen et al. [2011], 2) when used with monochrome specimens it boosted the signal by way of enhanced photon counting statistics.

To measure the PSFs of the excitation and depletion beams, fixated gold nanoparticles (diameter: 150 nm) were scanned and the back-scattered light detected with a channel

[3]The pinhole size was chosen to correspond to approximately 0.7 Airy units.

photomultiplier (MD-963). For that a 50:50 pellicle beam splitter (BP145B1) could be swung into the beam path when required. A large pinhole (size: 100 μm), siting in a conjugate image plane, reduced the contribution of out of focus light to the PSF-measurement.

2.3.5 Setup for Live Cell Imaging and Electrophysiology

Mainly on grounds of convenience a commercial inverted research microscope (DMI6000 B) was used as a "front end" for the LSM. Optical coupling was performed via a dedicated side port. The (DMI6000 B) came equipped with an epi-fluorescence condenser and a transmitted light path in a fully automated system, designed for the life sciences. The trans-illumination condenser arm was removed to give way to the uncaging setup described earlier (cp. Sec.2.2.2). Oblique, diffuse illumination was installed instead using an off-the-shelf light bulb or infrared (IR) light-emitting diode (LED), respectively, which yielded sufficient through-light contrast for my purposes. A high N.A. glycerol-immersion objective lens (HCX PL APO CS 63x/1.30 GLYC) was mounted on a piezo-stepper (PI-FOC P-721.LLQ) to be able to acquire z-stacks at high repetition rates. One camera port was equipped with a fast charged coupled device (CCD) camera (iXon DV885LC) to provide the option of wide field functional imaging with fluorescent reporters like calcium- or voltage-sensitive dyes [Lang et al., 2006; Albantakis and Lohmann, 2009]. The experimental chamber (cp. Sec.2.1.6) fit onto a motorized x/y-stage, custom-built by the mechanical workshop at the Max Planck campus in Martinsried.
Besides, the setup was prepared for future electrophysiological investigations. On that account it was supplied with micromanipulators (Junior RE/LE System), stimulus isolators for the injection of current and voltage pulses (A 360 and V-Stim), a microelectrode amplifier (AxoClamp 2B) in combination with a laboratory amplifier (Model 410) for signal filtering and a noise eliminator (Hum Bug) to reduce 50/60 Hz hum, an oscilloscope (HM507), and an IR sensitive CCD camera (KP-M2RP) at the DMI6000 B's second camera port, whose output was split between a liquid-crystal display (LCD) screen (UltraSharp 2001FP) and a video-to-universal serial bus (USB)-converter (DFG/USB2pro) connected to the personal computer (PC) (cp. Sec.2.3.6). Data acquisition (DAQ) was conducted with a custom software suite written in the LabVIEW programming language (courtesy of Volker Staiger).

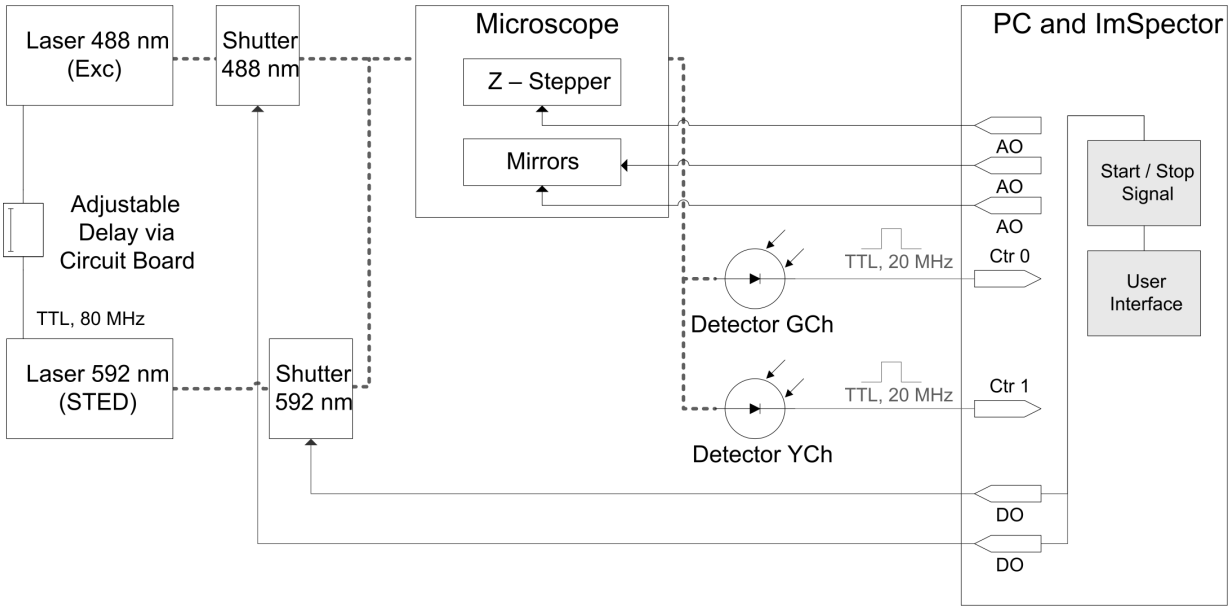

Figure 2.4: DAQ Block Diagram. Solid lines represent electrical signals, dashed lines the optical beam path. AO: analog output, Ctr: counter input, DO: digital output.

2.3.6 Operation of the Imaging Setup and Data Acquisition

As an interface to control the LSM and acquire images a PC (Precision T7500) was used. Images were taken with the ImSpector software suite [Schönle, 2006]. External hardware control was achieved via a peripheral component interconnect express (PCIe) plug-in card (PCIe-6363) connected to equivalent breakout boards (BNC-2090A). The scan-head and z-stepper were operated by analog voltage signals, beam-shutters by digital (TTL) signals. Detectors were connected to digital inputs, set-up as on-board counters, in the case of the SPCM-AQRH-13-FCs, and to an analog input in the case of the MD-963. Fig.2.4 shows an overview of the routing for DAQ. Raw data were stored in .msr-files, a binary format inherent to ImSpector. For post-processing images were manually exported to 8 −bit gray-scale tagged image file format (TIFF) files.

2.4 Electron Microscopy of Fixed Tissue Slices

To reconstruct post-synaptic densities from EM images membrane cultures were fixed after 15 to 20 DIV at 4 °C for 12 − 60 h in Fixative. Processing for EM followed standard procedures according to Knott et al. [2009]. In short, osmication was conducted in OSO_4 (1 % in 100 mM sodium cacodylate) for a period of 40 min. Slices were then washed 3

times in distilled water and dehydrated consecutively in 50 %, 70 % and 2 times 100 % ethanol, each for 10 min. They were washed for another 10 min in propylene (100 %) and equilibrated in propylene oxide (epoxy resin (ER), 100 %) for 24 + 2 h, before they were embedded in Resin for 48 h at 60 °C. Embedded tissue was cut into ultra-thin serial sections (dimensions: 150 x 250 x 0.07 μm^3) using an ultramicrotome (EM UC6). Samples were counterstained in a slide stainer (Ultrastainer) with uranyl acetate (0.5 %) and lead citrate (3 %). Images were obtained at a commercial transmission electron microscope (TEM) (JEM-1230), equipped with a SC1000 ORIUS CCD camera, using the DigitalMicrograph image acquisition and processing software. I employed the free software Reconstruct [Fiala, 2005] to first linearly align serial EM images (magnification: 50'000x), identify and count synaptic connections from 6 randomly chosen regions of interest (ROIs) and finally render 3D surface reconstructions of potentially non-macular PSDs.

2.5 Processing of Raw STED Images

8 −bit TIFF files were edited with two bundled distributions of the public domain program ImageJ [Abràmoff et al., 2004], MBF-ImageJ [Collins, 2007] and Fiji [Schindelin et al., 2012], either manually or using batch processing using custom-written code in the ImageJ Macro Language. The following analysis tools and plugins have been applied:

- Addition of related color channels of monochrome specimens
- Rendering of maximum intensity projections (MIPs)
- Background subtraction (rolling ball)
- Clipping of the dendrite signal
- Contrast stretching and histogram normalization
- Median filtering (radius: 1 px)
- Creation of sorted time series
- Registration with the *Linear Stack Alignment with SIFT* plugin
- Annotation

Distance measurements were taken from unprocessed MIPs.

2.6 Analysis of Spine-Neck Dimensions after Chemical LTP

After image processing (cp. Sec.2.5), spines were identified in MIPs of the image stacks, whose neck was clearly visible at each time point of the imaging session. Using MBF-ImageJ [Collins, 2007] cross-sectional profile plots of necks were compiled for each time point, averaging 3 px perpendicular to the necks' long axis, and saved to formatted text files (tab-separated values). With custom written routines in the Python programming language, Gaussian functions were fitted to the profile plots and their full width at half maximums (FWHMs) taken as measures for the corresponding spine-neck widths. The average of consecutive measurements, two before and four after pharmacological stimulation (cp. Sec.2.1.6), were computed for each spine-neck to form pre- and post-stimulus populations of neck widths, which were then compared by means of their median values.

2.7 Analysis of Spine Morphology after Light-Induced Plasticity

Annotation of Spines. In the first step, individual spines were tagged in average intensity projections of registered time series. Identified spines were then visually inspected at each time point with MBF-ImageJ [Collins, 2007] and annotated in appendant MS Excel files. Measurements of spine dimensions, if any, were performed on MIPs and exported to formatted text files (tab-separated values). Preferably impartial categorization criteria, considering absolute and relative proportions of spine dimensions, are summarized in Fig.2.5. They were based on former EM and light microscopy studies [Peters and Kaiserman-Abramof, 1970; Harris et al., 1992; Nägerl et al., 2008] and comprised spine morphology, head shape, as well as total spine length (stubby spines were considered long if $L > 0.5\,\mu$m and short if $L \leq 0.5\,\mu$m; thin / mushroom /filopodial spines were considered long if $L > 1\,\mu$m and short if $L \leq 1\,\mu$m). Branched spines were highlighted and counted as two separate heads. If in doubt or non of the classification criteria fit, a spine was registered ambiguous. For quantification, spines that belonged to the ambiguous class in all frames were not incorporated in the analysis, as well as spines, that were not visible in all frames. The latter occurred, when a spine had moved out of the imaging plane.

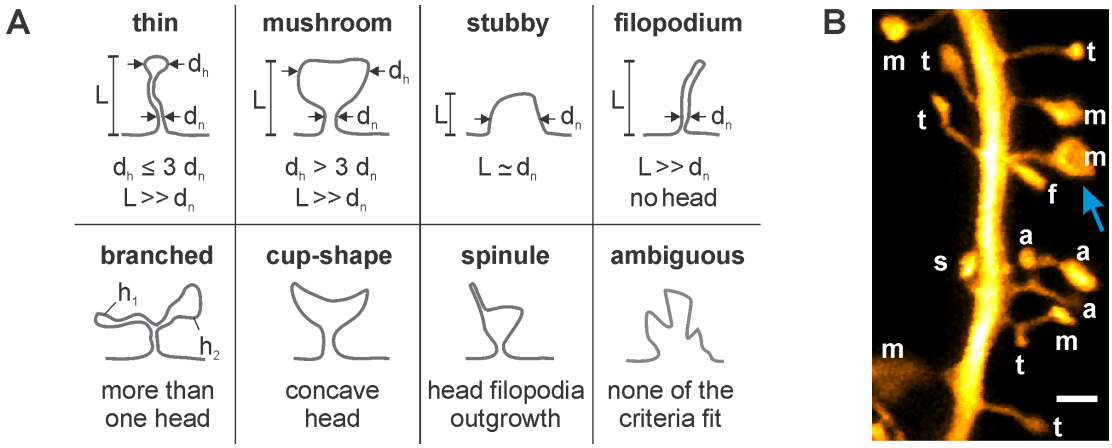

Figure 2.5: Spine Classification. *A* Annotation of spines was based on morphological criteria. A spine fell into one of the main categories in the first row (thin / mushroom / stubby / filopodia) and was then further classified according to its head shape and total length, so for example a stubby spine could still be considered cup-shaped. If in doubt, the ambiguous class applied. L: total spine length, d_h: spine head diameter. d_n: spine neck diameter. *B* Examples of spine classification; a: ambiguous, f: filopodium, m: mushroom spine, s: stubby spine, t: thin spine; the blue arrow indicates a cup-shaped head. Scale bar: 1 μm.

Statistical Analyses. Annotations were imported to MATLAB and analyzed with custom routines. Spines were sorted according to their main category, their head shape and their total length. First, the time course of spine morphing was analysed. To compute the relative amounts of spines in each category, they were pooled according to frame number, and the respective averages, as well as standard error of the means (S.E.M.s) of these collections determined. In a second step, morphological changes were evaluated statistically on a population level. To compute pre- and post-stimulus populations of spines in each categorical class, the respective fractions were rendered for individual experiments at each frame, and 3 baseline points, as well as 5 time points after stimulus application were averaged (cp. Fig.2.1). The resulting values were pooled according to spine class. Their distributions were compared with respect to statistical equivalence of the means between pre- and post-stimulus populations. For that, unpaired two-sample t-tests were conducted, where differences were considered significant, if the p-value was below 0.05. Different experimental conditions were analysed separately. To analyse stable spine fractions and the amount of spines changing morphology between time point 20 min and 30 min, respective values were determined from the sorted annotations for each individual trial and averages, as well as S.E.M.s computed for treated and untreated slices, respectively. Resulting distributions were compared with two-sample Kolmogorov-Smirnov tests, where differences were

again considered significant, if the p-value was below 0.05. Significance levels throughout the current thesis: $^{*}p < 0.05$, $^{**}p < 0.01$, $^{***}p < 0.001$.

Chapter 3

Results

3.1 Characterization of the LSM

Before biological experiments could be realized, the custom imaging system's characteristics had to be defined. For that, I decided to follow three steps: first, the physical, optical features had to be identified, next, a simple study in live tissue helped to familiarize with the system, and finally, I probed its performance in comparison to EM.

3.1.1 Resolving Power

After careful alignment of the imaging optics, the two laser beams of the excitation and depletion sources had to overlap in 3D. This was routinely checked at the beginning of an experimental session by scanning spherical gold nano-particles (cp. 2.3.4). Resolution improvement due to a STED effect was tested in a sample of fixated yellow-green fluorescent beads (FluoSpheres, Carboxylate-Modified Microspheres, 0.04 um), adherent to a glass coverslip [Wurm et al., 2010]. The actual resolving power of the LSM was dependent on depletion intensity, penetration of the specimen and the fluorescent reporter used to mark features of interest. Best results in live tissue were obtained with a fluorescent Lifeact fusion [Riedl et al., 2008] examining cellular structures close to the coverslip (distance $< 10\,\mu$m) using a STED power of 35 mW in the BFP[1].
Fig.3.1.A shows examples of cross-sectional views along three orthogonal spatial planes of

[1]Higher de-excitation intensities resulted in improved resolution, but also increased photodamage to untolerable extent.

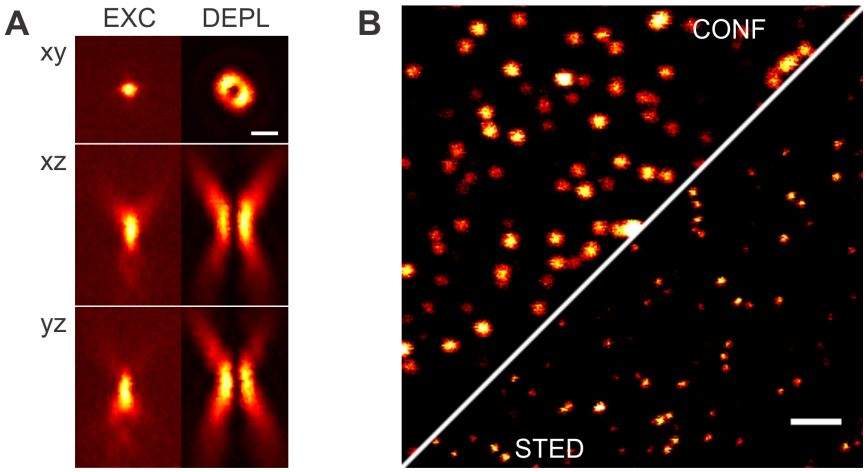

Figure 3.1: PSFs of the Imaging System. *A* Excitation and depletion PSFs in cross-sectional view along orthogonal planes. Scale bar: 0.5 μm. *B* Comparison of confocal and STED imaging of fluorescent microspheres. Scale bar: 1 μm.

the excitation and depletion PSFs, respectively: The excitation PSF appeared circular and more or less symmetric in the focal plane and exhibited a typical elongated shape along the optical axis [Diaspro et al., 2006]; extended side lobes were present above and below the axial focus in the x/z- and y/z-planes, pointing to spherical aberrations of the imaging system [Deng et al., 2010]. I tried to reduce them to a minimum adapting the correction collar of the imaging lens [Urban et al., 2011]. The excitation volume was determined to extend 205 ± 7 nm in the focal plane and 509 ± 11 nm along the optical axis.

Slight spherical aberrations were also present in the depletion PSF (cp. x/z- and y/z-planes). Besides, it displayed an asymmetry in the lateral dimension. Deng et al. [2010] ascribed similarly asymmetric toroidal intensity distributions to astigmatism of the optical system. Sources of astigmatic aberrations can, in general, relate to grinding and polishing of optical parts with respect to frictional side pressure, to poor lens centration, misalignment of optical components along the beam path, or to tension on reflective surfaces [Mahajan, 2011]. So far, I was not able to reliably identify the sources of astigmatic aberrations in the implemented imaging system. Since they did not severely affect the resolution obtained (see below), they were not investigated thoroughly.

The quality of the intensity zero, a prominent feature of the depletion torus, had to be determined differently, due to its dependence on the circularity of the light's polarization [Keller, 2006]. The pellicle beam splitter, introduced to image back scattered light (cp. 2.3.4), altered particularly this characteristic and had to be taken out of the beam path not to disturb the measurement. I took the relation of fluorescence intensities in confocal and

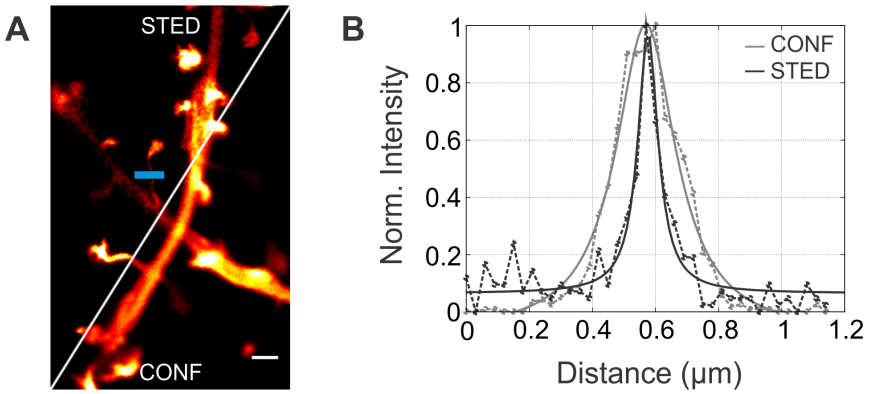

Figure 3.2: Determination of the Resolution of the STED-LSM. *A* Comparison of confocal and STED imaging of living neurons, labeled with Lifeact::EYFP via viral injection. Scale bar: 1 μm. *B* Lorentzian fits (solid lines) to 3 px wide profile plots (dashed lines) through the spine neck highlighted in A with the blue line. STED improves the resolution roughly by a factor of 3 when comparing the FWHMs of the fitted curves.

STED images as a qualitative gauge for wavefront pattering: if a structure imaged with STED appeared significantly darker than imaged confocally, the central minimum of the depletion PSF was not low enough to allow for sufficient spontaneous light emission and the fluorophores were quenched over the whole excitation volume. In experiments imaging yellow-green fluorescent beads at an excitation power of 3 μW and a depletion power of 15 mW (both measured in the BFP of the imaging lens), I determined an empirical value of below 20 % signal loss to be reasonable; Fig.3.1.B shows an example of the resolution improvement due to STED in a fluorescent bead sample.

The effective resolution obtained in live tissue with the current STED-LSM is illustrated in Fig.3.2. A three pixel wide line profile of a spine neck was plotted from confocal and STED images, and Lorentzian functions fit to the data points. Their FWHMs served as a measure for the resolution. I gained a resolving power of at least 77 nm with STED imaging (excitation power: 6 μW, depletion power: 35 mW, both in the BFP), a roughly three-fold increase compared to the best confocal resolution measured (232 nm)[2]. Even though better STED-resolutions had been reported down to $60 - 66$ nm in various biological specimens [Willig et al., 2006; Hein et al., 2008], the estimated value for the present system compared very well to published data from living cells labelled with fluorescent proteins ($77 - 80$ nm, [Nägerl et al., 2008; Tønnesen et al., 2011]). In general, resolution can be tuned with depletion power and will have to be weighed against phototoxicity and photobleaching,

[2]This is about 10 % above Abbe's theoretical resolution limit for green light of 532 nm wavelength, which corresponds to 205 nm.

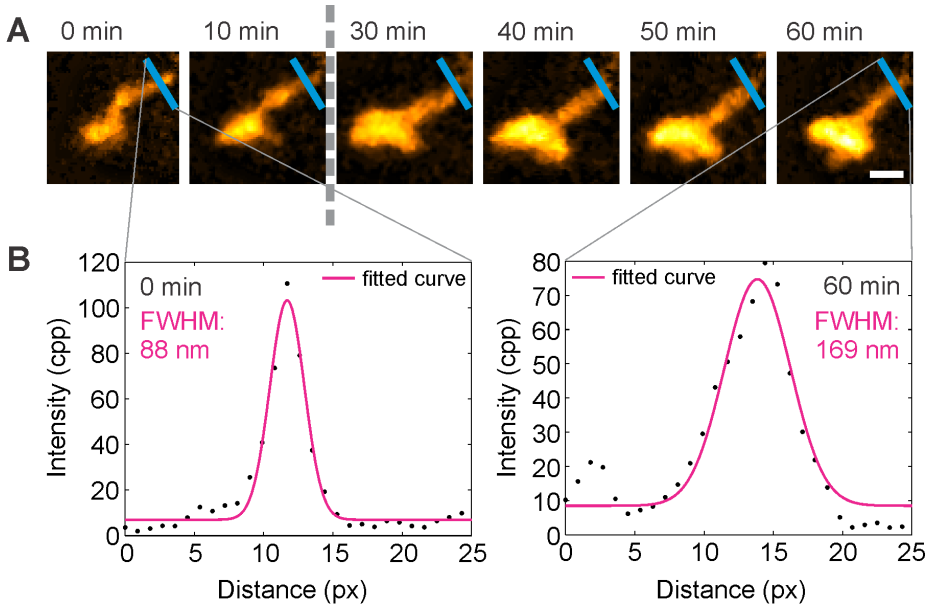

Figure 3.3: Change of Spine Neck Dimensions in Response to Chemical LTP – Examples. *A* Time-lapse series exemplifying the dynamics of spine stalks during cLTP; the dashed line marks the pharmacological induction of LTP. Scale bar: 500 nm. *B* Intensity profiles (3 px average) indicated by the blue lines in *A* at time points 0 and 60 min with Gaussian fits to determine respective diameters of the spine neck.

which is much less of an issue in fixed specimens labelled with synthetic dyes.
Imaging speed depended on photon counting efficiency. In specimens bright enough for experimental usage, photon counts above about 50 cpp resulted in a sufficient signal to noise ratio to give acceptable contrast. Therefore, pixel dwell times of $10 - 30\,\mu$s had to be applied. Given a typical FOV of 30 x 30 μm^2, a Nyquist-Shannon compliant pixel size of 30 x 30 nm^2 and four z-planes to cover dendritic stretches in 3D, I obtained frame rates of $40 - 120$ s. Subsequent z-planes were usually separated 750 nm to gather fluorescence from non-overlapping sections. Faster frame rates were attained by reduction of the FOV, keeping pixel size and dwell time constant.

3.1.2 Applicability to Neurobiology

Spine Neck Width in Response to cLTP. As a first proof of principle study, I decided to investigate spine neck dimensions with respect to the induction of cLTP. In total, four organotypic slice cultures of transgenic mice pups were used for the study after 14 to 96 DIV. Of these, three slices were treated as described in Sec.2.1.6 and one served as a control, i.e. no TEA (Tetraethylammonium, Et_4N^+) was added to the bath. This cation

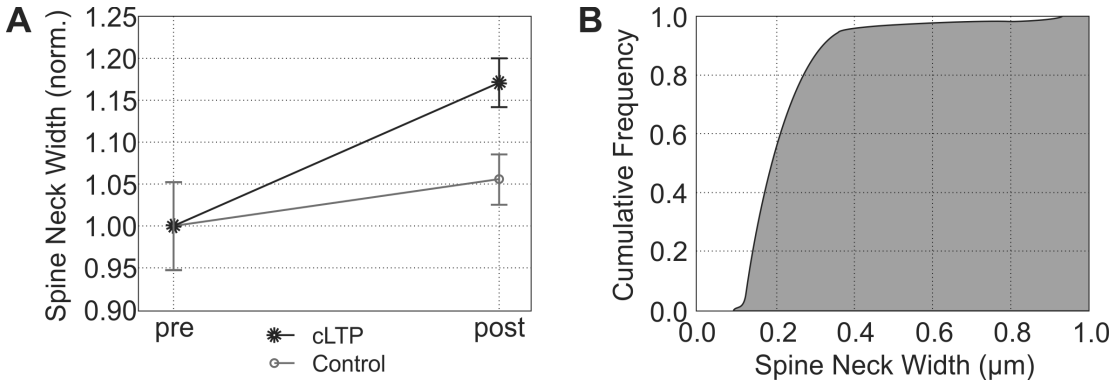

Figure 3.4: Change of Spine Neck Dimensions in Response to Chemical LTP – Summary. *A* Comparison of pre- and post-stimulus populations (median ± standard error). cLTP: n = 12 spines; control: n = 9 spines. *B* Cumulative histogram of neck widths, pooling all measurements together (cLTP + controls); n = 126 measurements.

blocks potassium channels in post-synaptic terminals [Hille, 1967] and has been shown to pharmacologically induce LTP at hippocampal CA1 synapses in a calcium-dependent way [Aniksztejn and Ben-Ari, 1991; Huber et al., 1995]. Twenty-one spine necks were analysed (12 stimulated and 9 controls) following Sec.2.6. Fig.3.3 shows an example of a time-lapse recording (A) and the estimation of spine neck diameters via Gaussian fit curves (B). To determine pre- and post-stimulus populations, two baseline values and four measurements after LTP induction were averaged from individual experiments.

Fig.3.4 summarizes the results: First, he cumulative histogram (Fig.3.4.B) subsumes all neck widths measured, indicating 55 % of them to fall within the scope of super-resolution imaging below 200 nm, and second, when normalized to the initial neck width, i.e. before stimulation with TEA, a 17 ± 3 % increase in the median neck diameters became prominent, whereas in the control cases no such change was noticed within the 5 % error range (Fig.3.4.A). The modification of their neck widths is a proposed dynamic feature of post-synaptic spines, potentially regulating molecular diffusion and therefore morphological and functional plasticity [Van Harreveld and Fifkova, 1975; Fifková and Van Harreveld, 1977; Fifková and Anderson, 1981].

At the same time I performed these experiments, Urban et al. [2011] published a similar study on cultured slices labelled with a fluorescent Lifeact probe. The necks reported in their publication were thinner than those quantified here by a factor of approximately 1.4 (170 nm vs. 119 nm), and they observed an increase in neck widths of 22 % on average after chemical induction of LTP. Considering, that Lifeact is selectively assigned to the cytoskeleton, smaller neck diameters are to be expected when compared to measurements

on volume markers used in my experiments. The different label could also account for the larger changes in neck width measured by Urban et al. [2011] in the wake of LTP: massive recruitment of actin to widen the necks might not reflect the effective volumetric increase happening, such that Urban et al. [2011] might have overestimated the actual changes. On the other hand, they reported their imaging system to outperform my LSM with respect to the achievable resolution by a factor of 1.2 (down to 60 nm). Therefore, it could as well be me to underestimate the actual size adjustments, due to an overestimation of the spine necks' baseline extent.

All in all, these initial experiments confirmed the applicability of the custom LSM to neurobiological research. I was able to adapt state-of-the-art STED nanoscopy to the needs of standard *in-vitro* assays and quantified spine neck changes with sub-100 nm resolution in time-lapse recordings. As pointed out by Urban et al. [2011] an essential benefit of our systems was gained by the use of a special objective lens (HCX PL APO CS 63x/1.30 GLYC), since the combination of glycerol immersion[3] and correction collar allowed for modest tissue penetration. Besides, telecentric mirror scanning turned out to be essential for fast time-lapse imaging without noteworthy disturbances of the specimens, especially regarding future electrophysiological studies.

A drawback of the actual implementation was the lack of temperature control of the bath chamber. All experiments were carried out at room temperature, though physiological conditions required 35 °C. Addition of temperature control is possible, but would mean a further upgrade of the system. Simple filaments, heating up the experimental chamber, as generally used in many labs, would not be sufficient here, since they introduce temperature gradients in the bath, especially in the imaging area, where the lens poses a heat sink. As a consequence, additional aberrations would arise, making corrections in a simple manner, as by a collar, hardly manageable. Alternatively, incubation or environmental chambers combined with a heated, temperature adapted imaging lens could solve this problem, but are usually costly and inconvenient in the running.

Incubation of Roller Tube Cultures in Glass Bottom Dishes. Handling of standard roller tube cultures turned out an elaborate and error prone procedure performing the trials described above (cp. Sec.2.1.6). Duplication silicone (Picodent Twinsil) needed $10-15$ min for setting. During that time cultured slices could not be perfused with ACSF and had to reside in small droplets of Roller Tube Culture Medium. Though I kept them

[3] This means better refractive index matching of the immersion liquid and the tissue at reasonably high N.A.

Table 3.1: Quantification of Non-Macular PSDs in Organotypic Slice Cultures.

ROI	Exc. Synapses	Macular PSDs	Non-Macular PSDs	Non-Macular Proportion
1	16	12	4	0.25
2	11	7	4	0.36
3	9	7	2	0.22
4	10	8	2	0.20
5	14	9	5	0.36
6	6	5	1	0.17
Total	*66*	*48*	*18*	*0.27*

warm at 35 °C, the pH of the medium could hardly be controlled. In addition, great care had to be taken, to prevent desiccation of the slices. I therefore developed an alternative preparation protocol to culture hippocampal slices in glass bottom dishes together with the technical staff in the Bonhoeffer lab (see Sec.2.1.2). With that I was able to drop the intermediate step of pasting slices on coverslips into an experimental chamber, which saved me about half an hour between subsequent imaging sessions and induced less stress on neurons. Therefore experimental throughput, measured by the number of slices that survived a whole imaging session, could be boosted by 66 % (from three to five slices per day). I observed no differences in the quality of organotypic slice cultures prepared one or the other way, cells displayed comparable morphological characteristics (size of cell body, amount of dendritic branching, spine density). Roller tube cultures in glass bottom dishes were incubated for extended periods of time of up to 6 weeks.

3.1.3 Post-Synaptic Density: A Comparison of EM and STED Imaging

To assess, whether STED nanoscopy represents an appropriate methodology to investigate the structure of PSDs, I first quantified the proportion of non-macular shapes in my model system. For that, an organotypic tissue explant was processed for EM as described in Sec.2.4. At six randomly chosen regions of interest (ROIs) I identified excitatory synapses and quantified the fraction of non-macular PSDs, i.e. those electron dense structures

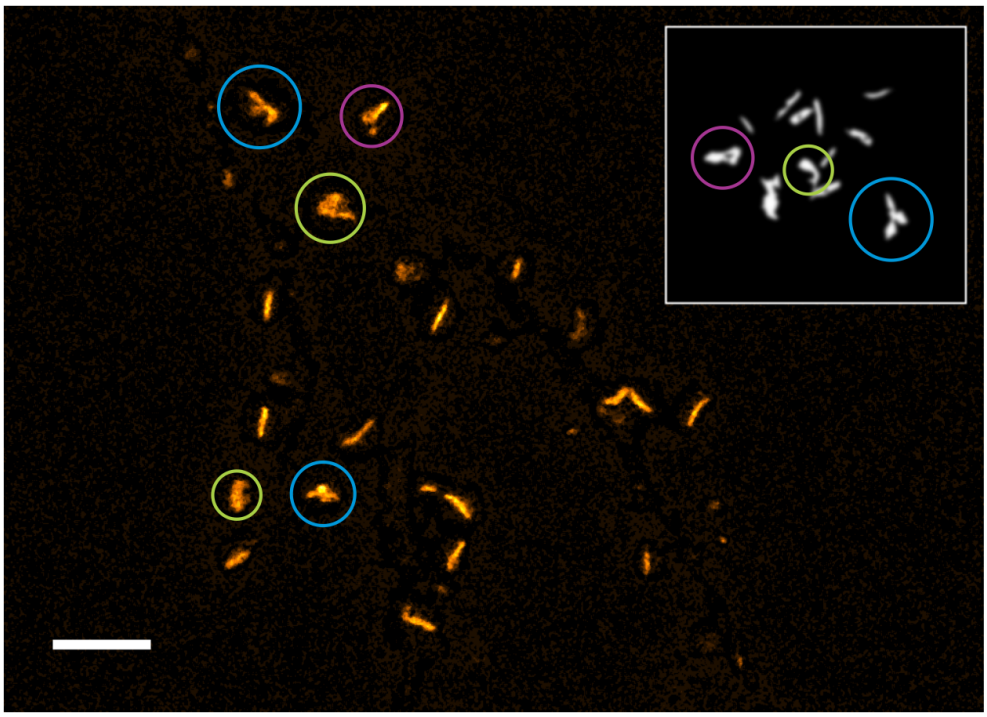

Figure 3.5: Comparison of STED-LSM with EM. STED image of fluorescently labelled PSD (PSD-95::EGFP). The dendrite signal was removed in the background subtraction step of the post-processing of the image for better visualization of the relevant features. *Inset* Simulated image from EM reconstructions scaled to size (details in the text). Colored circles highlight structures of similar shape in both pictures. Elongated PSDs presumably represent those oriented perpendicular to the focal plane. Scale bar: 3 μm.

that displayed perforations; the results are summarized in Tab.3.1. Accordingly, about one third (27 %) of excitatory synapses in CA1 *stratum radiatum* appeared perforated or non-macular in organotypic slice cultures after 17 DIV. Former EM studies reported non-macular fractions between 12 % in dissociated neuronal cultures after 12 DIV [Neuhoff et al., 1999] and 70 % in acute hippocampal slices from adult rodent brains [Stewart et al., 2005]. In hippocampal slice cultures of neonate rats Toni et al. [2001] found 22.4 ± 2.3 % of Schaffer collateral synapses to be perforated after 12 DIV, which fits very well to my rough assessment.

I then reconstructed the identified perforated assemblies from each region of interest (ROI) in 3D to get an idea of their dimensions and shapes, determining the average extent of a perforation to be 65 ± 5 nm, and therefore slightly below the resolving power of the LSM (cp. Sec.3.1.1)[4]. Nevertheless, I convolved a two dimensional / two dimensions (2D)

[4]Value corresponds to mean ± S.E.M..

projection of those reconstructions in their original orientation with a Gaussian kernel (FWHM: 75 nm), to get a blurred image of the structures, "simulating" fluorescence laser imaging; the inset in Fig.3.5 shows the outcome of this procedure. Taking into account the random orientations of synapses in a piece of tissue, I estimated one third of complex PSDs, i.e. about 10 % of all PSDs, in a piece of tissue to be detected with the custom STED microscope.

In Fig.3.5 I show an example of a STED image of fluorescently labelled PSD-95 taken in a tissue slice after 19 DIV. Most of the PSDs seemed to be elongated structures, but a few (encircled) resembled similar morphologies to those non-macular assemblies found with EM (cp. inset). As to be expected, circular perforations were not clearly visible. However, according to the predictions above, I was able to verify complex structured PSDs with STED imaging.

This shows, that STED nanoscopy can be beneficially employed to study PSDs in live tissue, though there is still room for optimizations to reliably resolve perforations. For time-lapse imaging, photobleaching poses a major problem to study PSD-dynamics. Unlike volume markers, where bright dye molecules continuously replace faded fluorophores via diffusion, PSD-95 proteins have a relatively slow molecular turnover in the range of a few hours [Okabe et al., 1999; Gray et al., 2006]. In my hands, the brightness of the PSD-95-GFP fusion went down by about 50 % in the wake of STED illumination, such that after a maximum of three to five frames hardly any information could be extracted from STED-images.

3.2 Local Induction of Spine-Plasticity

Following the experimental paradigm described in Sec.2.1.6 and Sec.2.2.2 I induced morphological spine plasticity in 37 pyramidal cells of hippocampal CA1. Cultured tissue slices from transgenic animals (Thy1-GFP-M mice [Feng et al., 2000]) were used after 7 to 20 DIV. Fourteen additional slice cultures served for control conditions, where in eight cases a photo-stimulus was applied without caged glutamate being present in the ACSF, and in six cases no photo-stimulus was applied when caged glutamate had been added to the bath. Typically a set of control slices preceded a set of stimulated ones in a test run, to reduce batch related variabilities. Not taking into account spines, that had not been visible, or those, that had fallen into the ambiguous class throughout the whole experimental session, I incorporated in total 1505 stimulated and 517 control spines to my analyses (see

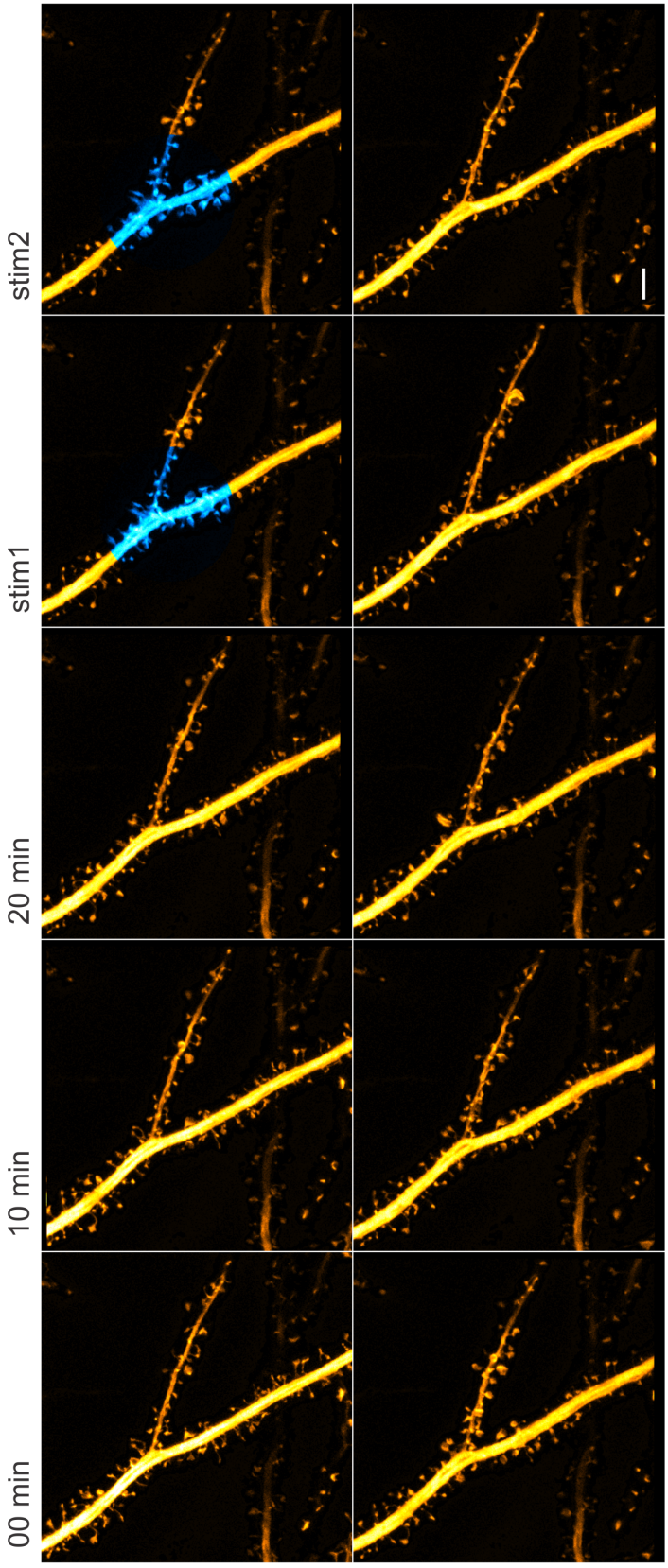

Figure 3.6: Time-Lapse Imaging of Glutamate Uncaging In-Vitro. STED time series of a CA1 pyramidal cell in an organotypic slice culture from a Thy1-GFP-M transgenic mouse pup. The blue spot marks the stimulus area. The bath contained 2 mM of caged glutamate. Scale bar: 3 μm.

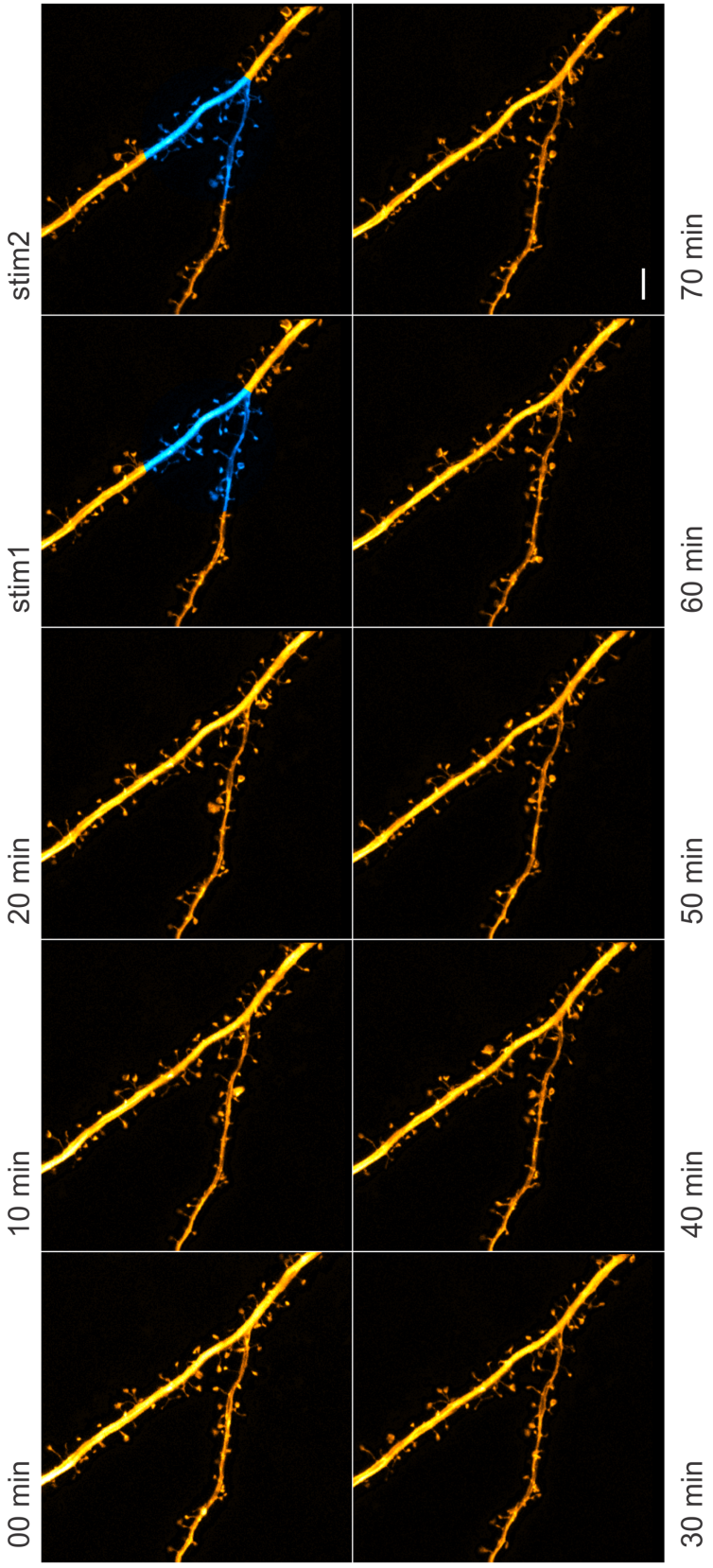

Figure 3.7: Time-Lapse Imaging of Control Slices In-Vitro. STED time series of a CA1 pyramidal cell in an organotypic slice culture from a Thy1-GFP-M transgenic mouse pup. The blue spot marks the stimulus area. The bath contained no caged glutamate. Scale bar: 3 μm.

Sec.2.7). Spine density was measured to be 1.18 ± 0.05 spines/μm (see Appx.A), which corresponded well to published values from primary cultures (13.1 spines/10 μm [Izeddin et al., 2011]) and moreover from hippocampal organotypic slice cultures (1.3 spines/μm, [Oe et al., 2013]), as well as from *in-vivo* quantifications in the transgenic mouse line used (1.4 spines/μm [Oe et al., 2013]).

Fig.3.6 shows a classic example of a stimulated neuron as imaged with the STED system in time-lapse recordings. After 3 baseline images a light stimulus released glutamate in a localized spot around the center FOV. Consistently, I focused on main apical dendrites at a distance of their first or second branch point from the soma. After stimulation imaging went on at a 10 min interval for another 50 min. Alongside spontaneous movements of spines, clearly stimulus related dynamics, mainly volumetric enlargements, could be observed in response to the photolysis reaction. In contrast, when no caged glutamate was present, the light stimulus did not induce additional dynamics (cp. Fig.3.7). The same held true for control slices with caged glutamate in the bath, but no photo-stimulus applied. Further analyses focused on the morphological changes of individual spines, as well as overall modifications of the fractions of different morphological criteria, particularly of total spine size, spine classification and head shape. For that, frames to confirm successful photolysis of MNI-glutamate taken directly after the stimulus had been applied (stim1 and stim2 in Figs.3.6 and 3.7), were not considered, as they were out of line with the regular time-lapse interval.

3.2.1 Tracking of Morphological Changes over Time

Following Sec.2.7 spine morphology was captured and documented in living tissue under treatment and control conditions. The results are compiled in Fig.3.8, where all spines investigated are displayed color coded according to their morphological category (A) and their head shape (B), respectively, for each time point imaged. Traces were sorted to make interpretation of the results easier. Several aspects of the data could be discerned from these graphs at a glance. A quantitative analysis of changing fractions on a population level follows in the subsequent sections.

The first prominent features were stable fractions, i.e. spines which did not change throughout the whole experimental session. They are subsumed in Fig.3.9. Starting from comparable distributions of morphological categories, in both, treated and untreated slices (cp. time 0 min in Fig.3.8), the largest proportion of stable spines belonged to the mushroom class (dark blue), making up a quarter in approximation of the spines examined (cp. Fig.3.9

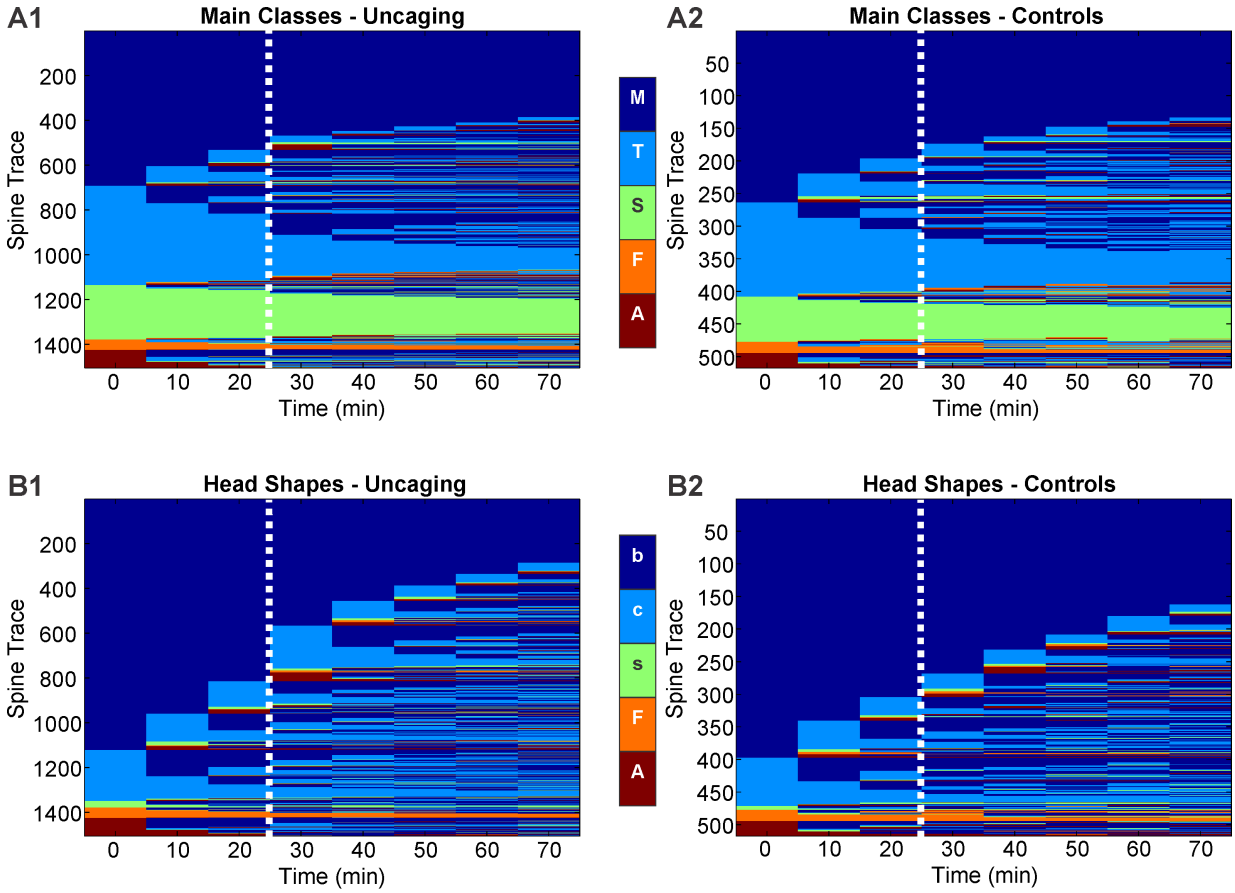

Figure 3.8: Tracking of Spine Morphology over Time. Sorted traces of individual spines as classified by visual inspection at each imaging time point for uncaging and control experiments (both control conditions pooled together), respectively. The dashed lines mark the stimulus. *A* Morphological main classes; M: mushroom, T: thin, S: stubby, F: filopodia, A: ambiguous. *B* Spine head shapes; b: bulbous, c: curved, s: spinules, F: filopodia, A: ambiguous (the latter two lacked a classifiable head).

panel A1). The next largest quota (roughly 10 %) was made up by stubby spines (green) irrespective of the treatment. A similar amount of thin spines (light blue) was stable in controls, whereas in uncaging trials less thin spines (about two thirds compared to controls) stayed within their category[5]. If related to their own subgroup (cp. Fig.3.9 panel A2), it appeared that ≈ 79 % of thin spines, ≈ 44 % of mushroom spines and ≈ 38 % of stubby spines *changed* shape during an uncaging session. In controls these fractions came out as 58 % of thin spines, 47 % of mushroom spines and 41 % of stubby spines. Thus, under control conditions, most of the thin spines were plastic and the least stable spines

[5]Filopodia and ambiguous proportions were neglected in this respect, since they were small.

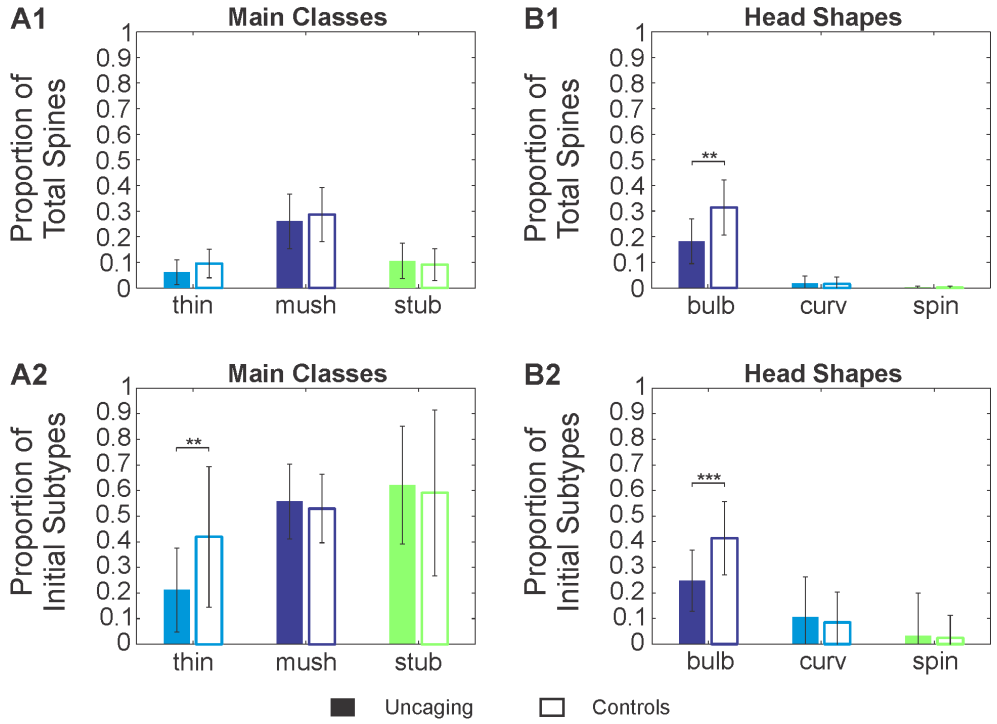

Figure 3.9: Stable Spine Fractions. Percentage of spines that did not change categories throughout experimental sessions. *A* Morphological main classes. *B* Spine head shapes. The upper panels (1) show ratios of the number of stable spines of a category over the total number of spines analysed, the lower panels (2) display ratios of the number of stable spines of a category over the number of spines that fell initially into the same category. Uncaging: n = 1505 spines, N = 37 slices; Controls: n = 517 spines, N = 14 slices.

were thin spines. On the other hand, most stable spines were mushroom spines, though about half of them appeared plastic. With glutamate uncaging, even less stable spines belonged to the thin category and the amount of initially thin spines changing shape grew by 21 %.

Glutamate uncaging facilitated in addition dramatic spine head morphing in comparison to the control conditions. This was reflected in a reduced proportion of stable heads (cp. Fig.3.9 panels B1 and B2): 25 % of initially bulbous heads (dark blue) kept their shape after glutamate uncaging, but 41 % in controls. On the other hand, the appearance of spine head filopodia (= spinules, green) was rather infrequently detected (cp. Fig.3.8 panels B1 and B2) and hardly stable at all (cp. Fig.3.9 panel B1). Curved spines (light blue), were as well highly dynamic throughout the testing period, their stable proportion was less than 2 % under all experimental conditions (cp. Fig.3.9 panel B1). Most stable heads had a bulbous shape, irrespective of the treatment ($\approx$ 18 % and $\approx$ 31 %, respectively).

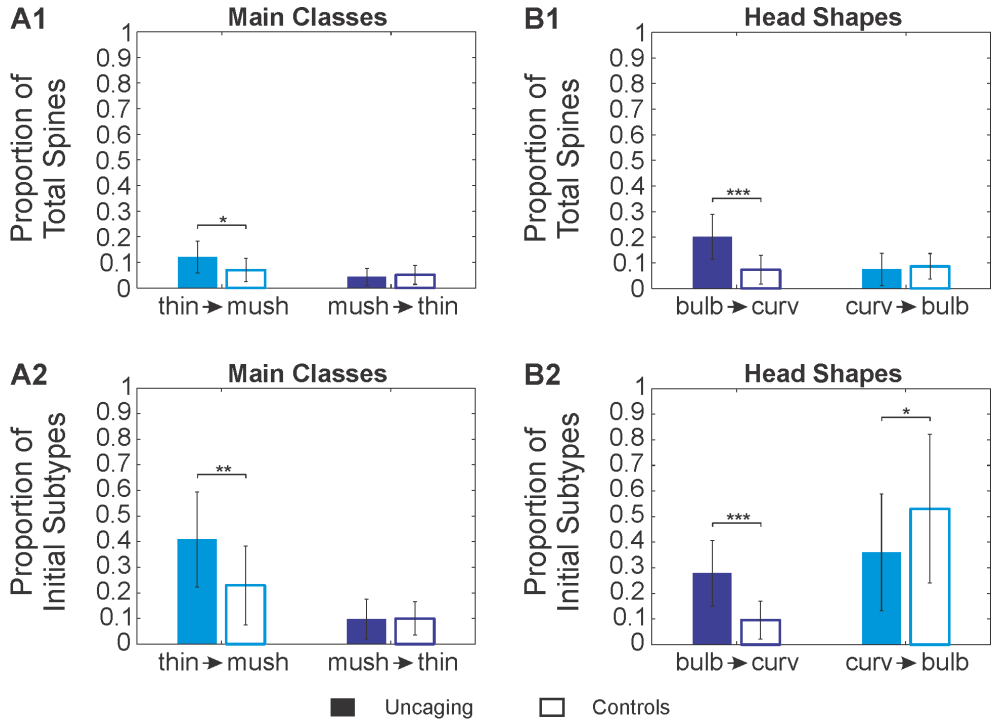

Figure 3.10: Stimulus Locked Changes in Spine Fractions. Percentage of spines that did change categories after LTP induction. *A* Morphological main classes. *B* Spine head shapes. The upper panels (1) show ratios of the number of changing spines of a category over the total number of spines analysed, the lower panels (2) display ratios of the number of changing spines of a category over the number of spines that fell into the same category before stimulation. Uncaging: n = 1505 spines, N = 37 slices; Controls: n = 517 spines, N = 14 slices.

Another striking observation concerned stimulus related changes, meaning those from time 20 min to 30 min (cp. Fig.3.10). Though subtle, a larger amount of thin spines changed to the mushroom category after the stimulus in treated slices than in controls (41 % vs. 23 %, cp. Fig.3.10 panel A2). In addition, the total amount of mushroom spines changing to the thin category was markedly smaller than the total amount of thin spines changing to the mushroom category in treated slices (4 % vs. 12 %), whereas in controls they were more or less equal (5 % vs. 7 %, cp. Fig.3.10 panel A1). After glutamate uncaging also a higher fraction of the "new" mushroom spines kept their class, but in controls most of them remained flexible (cp. Fig.3.8 panel A1). In essence, this indicated an evolution of a subset of thin spines to mushroom spines due to glutamate uncaging, that is, the induction of LTP.

Analogous observations were made for head shape changes directly after the light stimulus. Whereas roughly 220 of 800 spines (28 %) altered their head shape from bulbous

to curved in treated slices (≈ 20 % of all spines), that fraction in controls was less than half as large (≈ 7 % of all spine heads and 10 % of initially bulbous heads, cp. Fig.3.10 panels B1 and B2). Though most of them in treated slices had turned back to bulbous heads already 10 min later, this change made up the complete surplus of unstable spines in treated slices when compared to controls (cp. Fig.3.8 panels B1 and B2). In controls the amount of spines changing head shape from bulbous to curved was basically compensated by the amount of spine heads changing from cup-shaped to bulbous (9 %), whereas in treated slices the amount of bulbous to curved changes was nearly three-fold as large as the amount of curved to bulbous changes (≈ 7 %, cp. Fig.3.10 panel B1). Remarkably, to compensate the absolute changes in control slices, more than 50 % of the curved spines had to alter their head shape (cp. Fig.3.10 panel B2). Posing a minor fraction also in treated slices, ≈ 36 % of the curved spine heads changing to bulbous shapes did not outbalance the opposed shifting.

Overall, most spines varied their head shape and morphological class quite recurrently and sometimes in between all categories. This held true, again, for treated and untreated slice cultures. Along the lines of Parnass et al. [2000] and Nägerl et al. [2008] my observations support the idea of morphology being a highly dynamic characteristic of dendritic spines. Therefore, structural classification might be much less predetermined than to be speculated from former studies on fixed tissue [Peters and Kaiserman-Abramof, 1970; Harris et al., 1992]. Also movements of spines were most common (see Figs.3.6 and 3.7): heads were shaking or swirling around, necks bending and stretching. Here the strength of STED nanoscopy became most obvious, as subtle morphological details like head curvatures or head-to-neck-diameter ratios of a high number of individual post-synaptic compartments could be traced in live cells over time.

An astonishing by-product of my study is depicted in Fig.3.11. Here I give examples of developing branched spines, being observed at super-resolution in live dendrites. In both cases, what was to become the second head started evolving from a protrusion in the existing neck. Within $20 - 30$ min that protrusion appeared to grow to its final size and even advanced a cup-shape in the case of Fig.3.11.A. Within another $20 - 30$ min the new born head detached from the original neck to form an additional compartment. The primary head seemed to be rather unaffected from these processes and showed the typical dynamics, i.e. subtle movements or head shape changes. In both cases the outgrowth of the additional branch seemed to be completed at the last imaging point after 70 min. I detected the outgrowth of additional heads in four cases.

Other rare events included the vanishing of one branch of a multi-headed spine observed in two slices, moving protrusions in spine necks, that could indicate molecular transport (not quantified), and two spines stably "facing" each other, potentially contacting the same pre-synaptic bouton (four slices). Additionally, several three-headed spines were found and events observed, where spines / necks seemed to wander along the dendrite, where spines seemed to split up, or where two spines seemed to merge. All latter perceptions were not a major consideration within the scope of the work at hand, and therefore not systematically investigated. Thus, their mentioning here is solely meant as a side note for the sake of completeness. However, they yet again prove the power of super-resolution light microscopy, as one can get a glimpse of what kind of phenomena come at reach by the method.

The greatest handicap of my investigation was probably the limited resolution along the optical axis, being no better than in a normal confocal system. I therefore may unwillingly overestimate inter-class changes of spines, as I restricted my analyses to 2D projections of 3D structures. A mushroom spine, for instance, with a head being elongated in only one spatial domain, could be classified as thin spine, when inspected from the "wrong" perspective. Else, very small mushroom spines, with necks shorter than their heads, could be seen as stubby spines due to diffraction of light. This issue is intrinsic to my methodical approach and can only be circumvented by 3D STED implementations (see for example Hein et al. [2008]; Wildanger et al. [2009]) and Nyquist-Shannon compliant z-scanning. Consequently, potential inter-class changes based on my data have to be interpreted with great caution.

3.2.2 Effects on Classification of Spines

Further insight in the ongoing structural dynamics is gained, examining fractions of spines belonging to the main morphological categories (thin, mushroom, stubby spines and filopodia) as depicted in Fig.3.12. Panels A1 to A3 reveal the corresponding mean fractions over time for the three different experimental conditions, panels B1 to B3 a comparison of the matching pre- and post-stimulus population distributions, derived from averaging the baseline and post-stimulus fractions of single experiments (cp. Sec.2.7). Hence, neither the stubby spine section, nor filopodia went through significant changes during the trials, regardless of the induction of plasticity. Stubby spines settled at a stable quota of almost 15 %, filopodia at about 5 % in all preparations.

However, proportions of thin and mushroom spines were altered after the photolysis of

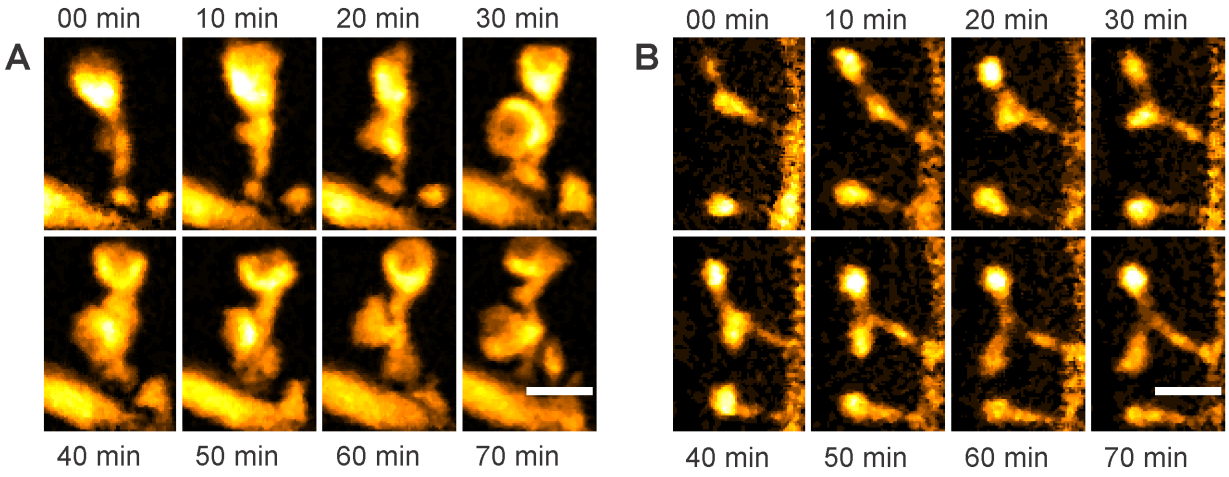

Figure 3.11: Development of Branched Spines. Two examples of spines branching to grow an additional head as imaged with the STED-LSM. Scale bars: 1 μm.

caged glutamate in opposite directions: the thin fraction dropped from 30 % to 23 % on average, whereas the mean mushroom fraction increased by the very same amount from 48 % to 55 %, both changes appearing to be highly significant on the population level and becoming obvious right after the photo-stimulus had been applied. Potentially due to biological variability standard errors are large (±10 %), such that the changing fractions still fall within their limits.

Starting at comparable baselines on average, no such modifications became obvious in controls without caged glutamate addition (panels A2 and B2) and in controls with the caged construct being present, but no photo-stimulus applied (panels A3 and B3). In the latter case, the corresponding baselines on average exhibited a 5 % shift compared to the other two experimental conditions. However, within the standard error range, this can most probably as well be considered biological variance.

Baseline levels of categorical fractions in comparable tissue preparations were reported to correspond well with my data: Roelandse et al. [2003] found 51 ± 11 % mushroom spines, 25 ± 4 % thin spines and 24 ± 11 % stubby spines in 4 organotypic hippocampal slice cultures after 30 DIV; McKinney et al. [1999] on the other hand, found 24 ± 6 % mushroom, 34 ± 4 % thin and 42 ± 5 % stubby spines in 60 organotypic hippocampal slice cultures after 14 DIV. Though both studies were performed on roller tube cultures, they support the great biologic variability I have observed.

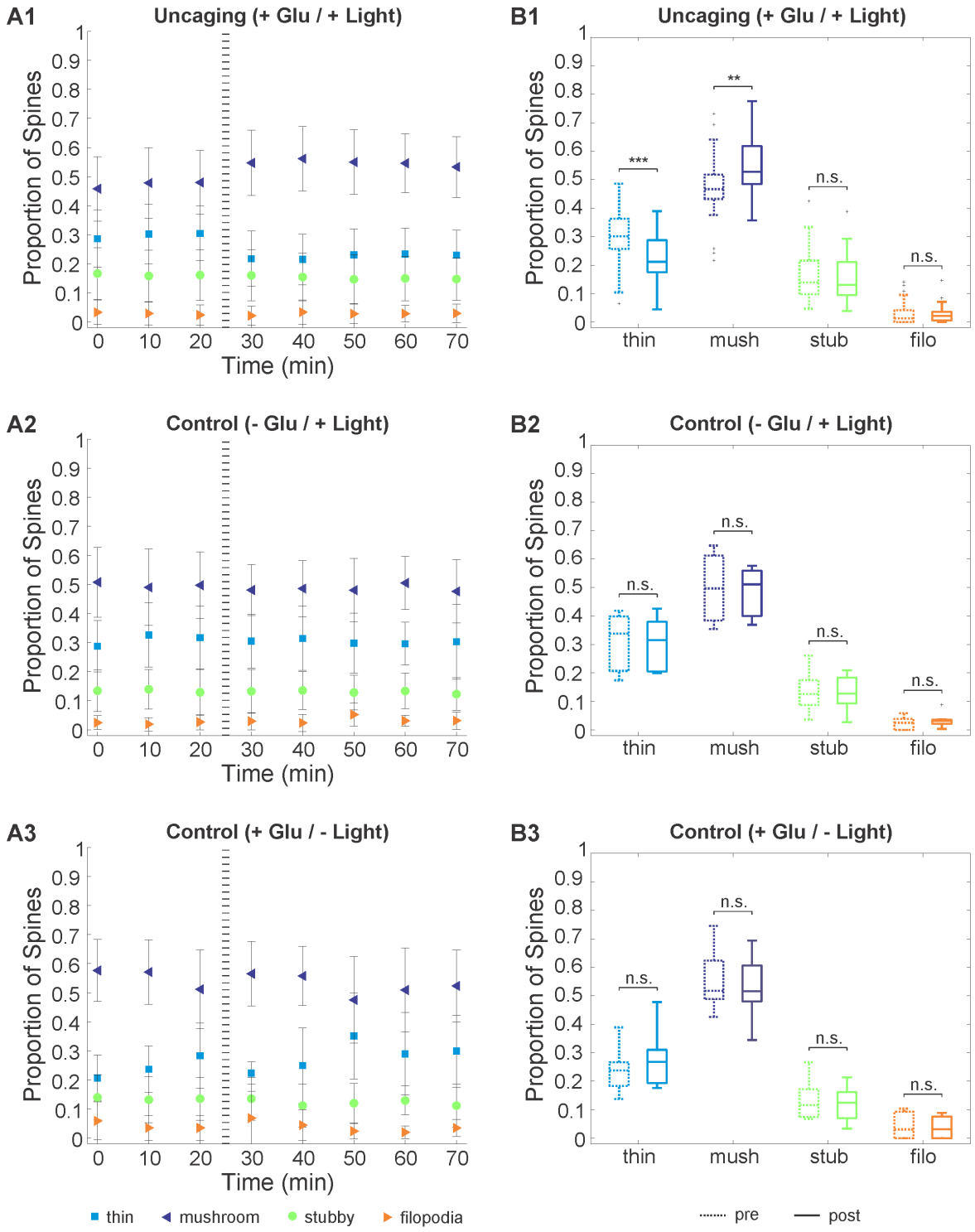

Figure 3.12: Effects of Glutamate Uncaging on Main Spine Classes. *A* Fraction of spines belonging to a morphological class in the lapse of time (mean ± S.E.M.). The dashed lines mark the stimulus. *B* Comparison of pre- and post-stimulus populations. (1) Uncaging: n = 1505 spines, N = 37 slices, (2) Controls: n = 387 spines, N = 8 slices, (3) Controls: n = 130 spines, N = 6 slices.

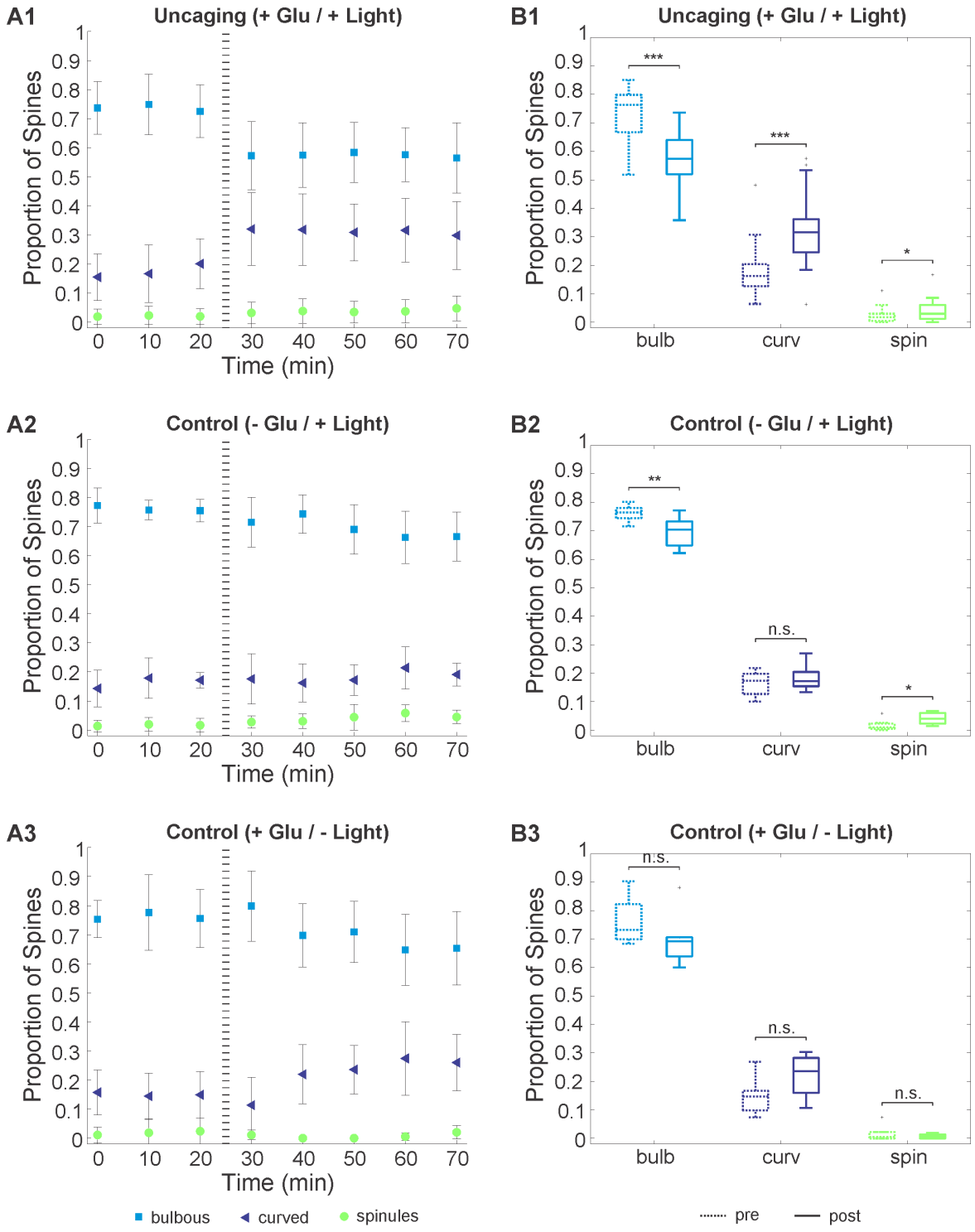

Figure 3.13: Effects of Glutamate Uncaging on Spine Head Shapes. *A* Fraction of spines belonging to a head shape class in the lapse of time (mean ± S.E.M.). The dashed lines mark the stimulus. *B* Comparison of pre- and post-stimulus populations. (1) Uncaging: n = 1505 spines, N = 37 slices, (2) Controls: n = 387 spines, N = 8 slices, (3) Controls: n = 130 spines, N = 6 slices.

3.2.3 Effects on Head-Shapes

Next, I investigated proportional modifications of spine head shapes. The results are subsumed in Fig.3.13, again illustrating the corresponding mean fractions over time in panels A1 to A3 and a juxtaposition of their distributions before and after stimulation in panels B1 to B3. In accordance with the analysis of single spine tracking (cp. Sec.3.2.1), the advent of spinules was a rather rare event, as the proportion of spine heads growing filopodia remained steadily below 5 % in all experiments conducted. A slight increase in the spinule fraction was observed at a significance level of 5 % in treated slices and in controls lacking the caged compound. This change was relatively small ($1-2\,\%$) and did not reach beyond the standard error range ($\pm 3\,\%$).
Panels A1 and B1 show highly significant transitions in the proportions of bulbous and curved spine heads, clearly related to the photo-stimulus. Already at the first post-stimulus imaging point the number of cup-shaped heads doubled on average from an initial fraction of 15 % to about 30 % and stayed at that level until the end of the trial period. Accordingly, the quota of bulbous heads declined from 75 % to nearly 60 %. Again, the standard errors are large ($10-15\,\%$), but are a minor concern against the backdrop of the population data in panel B1. The upper and lower quantiles of respective pre- and post-stimulus distributions do not have any overlap and their means differ at a significance level of 0.1 %.
In the controls without glutamate being present, no prominent drop at time 30 min was observed. However, their time course displays an approximately $5-10\,\%$ decrease in the number of bulbous heads at time point 60 min, hardly compensated by a corresponding increase in the curved fraction. When comparing population distributions, this is reflected in a significant drop of bulbous heads in panel B2. Nevertheless, that is probably due to the error range of the corresponding baseline (cp. panel A2) being unusually small when compared to the other experimental conditions. In addition, I conducted analyses where only the time points 30 min to 50 min served to make up the post-stimulus populations; under those circumstances, no significant change could be verified in the controls, leaving the results for the stimulated slices unaffected.
Under control conditions lacking the photo-stimulus (panel A3) I observed a gradual increase of curved and a decrease of bulbous heads (10 % on average), both of which did not prove statistically significant, and were therefore regarded biases of the experimental paradigm. Since they were more pronounced in controls with caged glutamate being present in the bath, it might very well be, that, though spectrally far from the ideal uncaging wavelength, photolysis was partially induced by the imaging lasers. Persistent

head changes are therefore hard to infer from the data at hand.
In the past, changing spine head shapes were investigated by Desmond and Levy [1986a], who reported a proportion of 27.2 % of curved heads after LTP induction in detate gyrus granule cells. Their controls exhibited about 20.7 % cup-shaped spine profiles in adult rats. Roelandse et al. [2003] found a 50:50 baseline ratio of curved:round heads in cultured hippocampal slices (roller tube cultures, after 35 DIV) and a 60:40 ratio in adult mice (6 weeks), focusing on CA1 pyramidal neurons. Both studies employed EM on fixed tissue.

3.2.4 Effects on Total Spine Size

In the course of annotating, spines were categorized into two distinct size classes: long and short (stubby spines were considered long if their total length $L > 0.5\,\mu$m and short if $L \leq 0.5\,\mu$m; thin / mushroom / filopodial spines were considered long if $L > 1\,\mu$m and short if $L \leq 1\,\mu$m). Panels A1 to A3 in Fig.3.14 display the mean fraction of spines belonging to each size class (± S.E.M.) over time for the three different experimental conditions probed.

Compared to the control cases, in stimulated slices the baseline fractions were "inverted", since more short spines than long spines were found. After stimulation, in all cases the number of long spines exceeded the number of short spines. The time course of the mean values showed a slight tendency toward an increase in the number of long spines of about 5 % (panels A1 and A2), whereas in panel A3 the fractions inspected were rather stable. However, standard errors are large ($10 - 20\,\%$) and the overall impression left to the observer is more a 50:50 balance of long and short spines irrespective of the experimental condition. That is reinforced by panels B1 to B3, comparing pre- and post-stimulus populations of the average length fractions from constituent experiments with boxplots (cp. Sec.2.7). The main part of the spines imaged was quite evenly split between the long and short class, again no matter what condition was taken into consideration. In controls, no significant change was observed due to a potential stimulus. In "real" experiments the mean of the distributions changed at a significance level of 5 % in favour of larger spines, which seems surprising, since stimulated spines followed a similar time trend as spines under control conditions with no caged glutamate present. However, the latter do not change significantly.
Taking into account the low significance level of the changes described for stimulated spines and the large errors on the back of this, uncaging related modifications in spine size based on my analysis are only weakly supported. Though former light-microscopic studies have reported increasing spine lengths in response to cLTP [Hosokawa et al., 1995], I am not

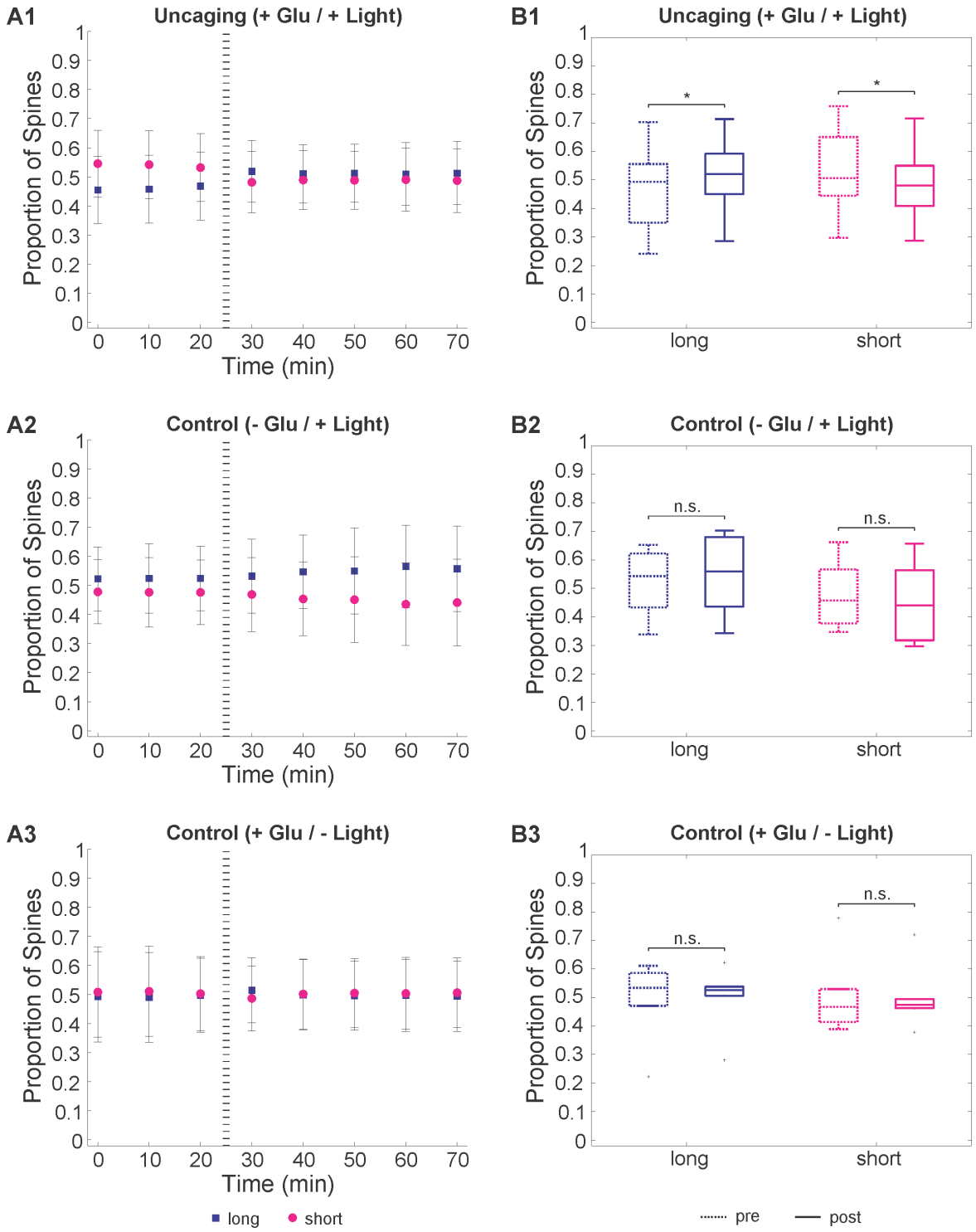

Figure 3.14: Effects of Glutamate Uncaging on Total Spine Size. *A* Fraction of spines belonging to a size class in the lapse of time (mean ± S.E.M.). The dashed lines mark the stimulus. *B* Comparison of pre- and post-stimulus populations. (1) Uncaging: n = 1505 spines, N = 37 slices, (2) Controls: n = 387 spines, N = 8 slices, (3) Controls: n = 130 spines, N = 6 slices.

convinced at this point, to have observed any effect. Further investigations are necessary, including a continuous length measure. In addition, a distinction between transitions in spine neck and head dimensions could give more conclusive insights into the ongoing processes. Still, manual quantification of these characteristics are tedious and have therefore not been considered an option for the time being. Automated analyses unfortunately failed, because suitable, rigorous algorithms for feature detection in low contrast images were missing. One has to pay great attention, when processing imaging data, as most operations improving the signal-to-noise affect distance measures and result in non-linear representations of the data. In contrast, the most efficient feature detectors work best on deconvolved, noise filtered, contrast enhanced images [Rodriguez et al., 2008]. From what I have learned, even specialized, expensive proprietary image analysis tools like Bitplane's Imaris have trouble to reliably track spines over several images, at least when processing my data.

Chapter 4

Discussion

4.1 Evaluation of the Methodical Approach

In the previous chapter I gave experimental proof of my efforts to set-up a STED nanoscope, adapted to the needs of neurobiological *in-vitro* research. I gathered super-resolved images of living neuronal structures in longitudinal experimental sessions, keeping cultured hippocampal slices intact for an elapsed time of 1.5 h. The resolving power of the custom optical design stood within the limits of the latest state of the art for live tissue imaging published by other labs [Nägerl et al., 2008; Tønnesen et al., 2011]. With this, I was able to follow rapid morphing of dendritic spines, and detected drastic changes of their structural features in response to locally induced NMDAR dependent plasticity or widespread cLTP. Also, sub-wavelength structural details of PSDs could be resolved in live tissue and were correlated to EM recordings.

One advancement for the investigation of cultured brain slices at super-resolution, made within the course of the current thesis, was the development of a modified protocol to incubate roller tube cultures in glass bottom dishes (cp. Sec.2.1.2). I anticipate this procedure to become the standard method for slice cultures to be used in conjunction with nanoscopic imaging at inverted microscopes, as it keeps growing slices directly on a glass substrate, a major benefit of Gähwiler's original idea [Gähwiler, 1981] with respect to penetration depth, scattering or aberrations of the imaging light[1], but it obviates the need

[1] Using membrane cultures for the most part of my work, I had to compensate for these issues by turning the slices upside down.

for elaborately pasting coverslips into an experimental chamber before an imaging session. Therefore higher throughput of trials can be yielded and the easier handling makes slice treatment less stressful for cells, i.e. less discard is created. Moreover, slices are accessible to micro-electrodes enabling electrophysiological experiments. In addition, they can nearly as easily be stained or genetically targeted as primary cell cultures by standard laboratory techniques using antibodies, biolistics [McAllister, 2000], SCE or viral injection. Also *in-situ* fixation, subsequent to an imaging session, should be feasible without serious problems and poses an interesting option for combined LSM-EM experiments, especially in view of near infrared branding (NIRB) [Bishop et al., 2011].

Local stimulation of dendrites using (near) UV photolysis of caged compounds appeared yet again a powerful supplement to light-microscopic techniques. I implemented a simple and cheap version of this prominent method, which is much less invasive than electrical and as easy to apply as chemical stimulation. Though its 2PE derivative holds the option to interfere with neurons at single synapse resolution, I see its strength in taking effect on intermediate spatial scales. In that sense, a local stimulus covers short stretches of dendrites within the FOV. If applied to opto-genetics[2], with the current system channelrhodopsin assisted synapse identity mapping (CASIM) (see Gökçe [2013]) could be pushed to nanoscale resolution or spine plasticity studied at those particular synapses, that receive an actual input from the real network. Calcium imaging or electrophysiological recordings could provide a functional readout and have both been incorporated to the system already. However, the present setup still contains several issues for improvement, the most straight forward probably comprising the implementation of nanoscale 3D sectioning with a second de-excitation PSF, patterned like a donut in the x/z and y/z focal planes [Klar et al., 2001]. As well, due to its one-photon character, the STED-LSM is fundamentally limited to a penetration depth of approximately 50 μm, which puts a constraint on the specimens to be used. Stimulated emission by two-photon absorption should admittedly be possible in theory, but I am not aware of any practical implementation, presumably due to a very low cross-section of such a transition bringing about immense energies to saturate the process. Still, the combination of 2PE with one-photon STED in the red spectral region have at least tapped into acute slice preparations [Ding et al., 2009; Bethge et al., 2013; Takasaki et al., 2013]. Next, as pointed out in Sec.3.1.2, the current setup was designed for investigations at room temperature; ways to adapt it to physiological conditions have been suggested there. A further intrinsic drawback of STED imaging is its reliance on high light

[2]One could for example selectively target CA3 axons with Channelrhodopsin-2 [Nagel et al., 2003].

intensities of several hundred MW/cm^2, giving rise to phototoxicity and photobleaching. The advent of new probes, especially designed for efficient and reversible on- / off switching, will hopefully provide a remedy in this respect (see for example Testa et al. [2012]). As for its aptitude to image specimens labelled with multiple colors, the present LSM is limited to green / yellow fluorescent reporters, i.e. GFP, YFP, or Fluorescein derivatives like Alexa Fluor 488 (Life Technologies), Atto 488 (ATTO-TEC), Oregon Green 488 (Life Technologies), and so on. The major constraint is posed by the laser pair employed for de- / excitation. If one wanted to stick with this combination of light sources (cp. Fig.1.6), it could be feasible to use fluorescent dyes with an emission maximum closer to the 592 nm line of the depletion laser, if the contribution of anti-Stokes excitation (AStEx) by the STED beam to the (background) fluorescence signal can be effectively subtracted or filtered from respective images. Besides a method introduced by Vicidomini et al. [2012] based on time-correlated single photon counting (TCSPC)[3], frequency dependent lock-in detection (ModSTED) [Ronzitti et al., 2013] could be a quick way to achieve this: intensity modulations imposed onto the excitation light leave a traceable signature on fluorescence emission; hence, excitation induced fluorescence can be distinguished from the AStEx induced fluorescence. Modifications necessary to implement ModSTED at the actual imaging system are potentially reduced to a lock-in amplifier in the detection unit, since the excitation pathway has already been equipped with a modulator (cp. EOM in Fig.2.2).

4.2 Local Induction of Morphological Spine Plasticity

Spine motility and morphological changes associated with synaptic long-term plasticity are exceptional attributes of living brains, and might very well represent the cellular correlates of learning and memory consolidation [Maletic-Savatic et al., 1999; Engert and Bonhoeffer, 1999]. Classically, plasticity can be induced in CA1 pyramidal dendrites of the hippocampus by LTP protocols applied to Schaffer collateral synapses (see Bliss and Collingridge [1993] for review). It is mediated by NMDA receptors, when strong influx of calcium ions activate signalling cascades via phosphorylation processes [Collingridge et al., 1988]. Besides extensive investigations utilizing EM, a considerable number of light-microscopic studies have exposed drastic alterations of dendritic spine structure related to LTP (see for instance Bosch and Hayashi [2011] for review). Morphological changes comprise spine enlargement [Van Harreveld and Fifkova, 1975; Hosokawa et al., 1995; Matsuzaki et al., 2004;

[3]This advanced detection scheme usually involves the need for expensive hardware.

Okamoto et al., 2004; Kopec et al., 2006; Zhang et al., 2008], widening of the stalk [Fifková and Anderson, 1981; Urban et al., 2011], larger and more perforated PSDs [Desmond and Levy, 1986b; Calverley and Jones, 1990; Harris et al., 1992; Toni et al., 2001; Stewart et al., 2005; Meyer, 2013], more bifurcated spine-heads and multi-synapse boutons [Trommald et al., 1996; Toni et al., 1999; Fiala, 2005], a gain in spine density, i.e. an outgrowth of new spines, [Andersen and Soleng, 1998; Maletic-Savatic et al., 1999; Engert and Bonhoeffer, 1999; Kwon and Sabatini, 2011], as well as the formation of spine-head filopodia [Richards et al., 2005; Tao-Cheng et al., 2009] and an increase in the number of concave spine heads [Desmond and Levy, 1986a] (also see Sec.1.2.3).

In the work at hand, I have provided evidence of structural transformations of spines in live tissue, time-locked to the local photolysis of caged glutamate, resembling a prototypical plasticity induction protocol. Shape changes have been classified according to approved criteria [Peters and Kaiserman-Abramof, 1970] and quantified over time. Conveniently, the application of STED nanoscopy has enabled me to reveal changes at sub-100 nm resolution. Though the real advantage of light microscopy – to be able to conduct individual measurements on a specimen over time to track single transitions instead of quantifying random samples of whole populations – does not come into effect with the statistical analyses applied to my data, it entails important information about the reliability of the method. Because it tailors the results of individual traces to overall proportions, they can now be compared with studies based intrinsically on population data, like previous EM experiments.

Thin spines have proven fewest of all to be stable, at the same time holding the largest dynamic percentile. After LTP induction a 7 % growth in the amount of mushroom spines has been observed at an equal expense of thin spines. The shift has been locked to the stimulus and stable over time. No such transitions have been found under control conditions. That, plus the high statistical significance of the changes, outbalances the large error range of my data and indicates uncaging related modifications in spine classification. Furthermore, I have determined a 10 % increase in the proportion of cup-shaped spine heads balanced by an equivalent decline in bulbous ones. Controls have shown a substantially different time course, and dissimilar relations of the pre- and post-stimulus distributions, however, curved heads have hardly turned out to be stable in the lapse of time. Though subtle, population differences have statistically proven highly significant. Hence, I am confident to consider the induction of cup-shaped spine heads due to glutamate uncaging a genuine effect. In addition, I have been successful to observe a few occurrences of spine branch-

ing and have infrequently detected the outgrowth of spinules, neither of them particularly locked to potentiation, though. Corresponding time courses have been hardly different in slices under treatment and controls, respective statistics are weak and inconclusive. The findings of Richards et al. [2005] support my observations of spinules being a rather rare phenomenon; they reported the occurrence of less than 1 spine head filopodium per 10 μm dendrite per hour in organotypic slice cultures after over six weeks *in-vitro* in response to glutamate iontophoresis. Although Schätzle et al. [2011] examined spinules in much higher quantities (up to about 50 %), their pharmacological induction protocol affected muscarinic acetylcholine receptors, i.e. molecular pathways potentially different from the glutamatergic system addressed by my experiments. Their baseline levels, on the other hand, compare quite well to my data ($< 5\,\%$, see Sec.3.2.3): they reported $2.87 \pm 2.09\,\%$ spinules in hippocampal slice cultures of transgenic mice after at least three weeks *in-vitro*.

4.2.1 Rapid Spine Motility

With super-resolution time-lapse imaging I have examined great frame-to-frame variability in spine head shapes and overall structure, as well as massive movements like bending necks and swirling heads. Though its function is still a mystery, rapid spine motility has been discovered to occur throughout the whole CNS by *in-vitro* [Dunaevsky et al., 1999; Parnass et al., 2000; Nägerl et al., 2008] and *in-vivo* [Lendvai et al., 2000] studies. It has been found to be developmentally regulated and the underlying molecular mechanism to be actin-dependent, as reviewed for example by Matus [2000].

My observations heavily support the idea of morphology being a continuous characteristic of dendritic spines suggested by Parnass et al. [2000] and Arellano et al. [2007]. A strict distinction of segregated subtypes leaves the misleading impression of static synaptic compartments and therefore completely ignores their consecutive morphing within a continuum of intermediate shapes. Nevertheless, classic categorization of spines according to morphological criteria has its pragmatic virtue: in my analysis, it has promoted tracing the overall dynamics of a large number of post-synaptic compartments (> 2000 spines) in relatively short time ($\approx 100\,\mathrm{h}$). In contrast to exact dimensions, different shapes have been relatively easy to grasp by human annotators, potentially because our visual system is extraordinarily well trained in such a task. Beside my own experience with automated feature detection in low contrast fluorescence images (see Sec.3.2.4), this is known from EM reconstructions, where human annotation has been shown to perform superior to automated algorithms [Helmstaedter, 2013].

How do correlations of spine structure and function, that have been reported in the past, such as an equivalence of the PSD area with spine (head) volume [Harris and Stevens, 1989; Arellano et al., 2007] or the regulation of diffusional and electrical coupling between spines and dendrites at the stalk [Majewska et al., 2000a; Grunditz et al., 2008], fit into a picture of constant dynamics? I think, spontaneous spine motility does by no means have to be in opposition to such correlations, as they simply describe complementary aspects of spines. Meyer et al. [2014] have shown just recently, for instance, how differently morphological and functional changes evolve over time: in their trials long-term synaptic plasticity strongly correlated with *rapid* volumetric spine enlargements followed by a *slow* increase of the amount of PSD scaffolding proteins. A previous study by Ehrlich et al. [2007] provided evidence along similar lines, suggesting PSD-95 to be required for activity-dependent synapse stabilization after initial phases of synaptic potentiation. Other proteins shown to be involved in spines stabilization include cell adhesion molecules (CAMs) like N-cadherine [Bozdagi et al., 2000, 2010; Mendez et al., 2010] and glutamate receptors [Kopec et al., 2007]. Besides, Lohmann et al. [2005]; Lohmann and Bonhoeffer [2008] observed structural and functional interactions between pre- and post-synaptic partners well before a functional synapse had been formed, indicating a rapid synaptic partner selection process by dendritc filopodia. Assuming that spine motility in adult brains serves a similar purpose as during synaptogenesis in early development, it was highly likely, that spines are indeed constantly probing their surroundings. Synaptic efficacy would eventually only be enhanced, however, if a contact was stabilized in the long run. Involving protein synthesis and trafficking, this was on the lines of the so called "synaptic tagging and capture hypothesis of protein synthesis-dependent LTP" (see Redondo and Morris [2011] for review).

4.2.2 Spine Enlargement and Morphological Class Changes

In the analysis of spine size, my attempts to decipher plasticity related modifications have initially been rather coarse, drawing a hard line at their total length to let dendritic spines be considered either long or short (see Sec.3.2.4). Still, I have observed a significant trend towards larger spines on a population level after LTP induction, that goes along the lines of earlier glutamate uncaging studies [Matsuzaki et al., 2004; Zhang et al., 2008]. Absolute enlargements could potentially be examined more thoroughly by restricting actual volume measurements[4] on individual potentiated spines, as performed by Matsuzaki et al. [2004].

[4]This could be done via the determination of the maximum brightness within a compartment, for example.

I have omitted those quantifications for the time being, since, to my understanding, it would most probably have not contributed additional insight to my assessment of plasticity. Transient spine enlargements due to the photolysis of caged glutamate have been determined to up to 400 % [Matsuzaki et al., 2004] and persistent growth to between 75 % [Meyer, 2013] and 200 % [Matsuzaki et al., 2004].
In my analysis, the emphasis has been on the structural morphing of dendritic compartments. In this regard, the overall proportions of spines belonging to the thin and mushroom morphological categories has changed significantly during uncaging sessions, time locked to the induction of plasticity and in opposite directions. Hence, I am confident to have observed a subset of thin spines evolving to mushroom spines. This conclusion is supported by the analysis of individual spine traces (cp. Fig.3.8), showing that about two thirds of the spines changing from the thin to the mushroom class after stimulation have stayed in that category for at least 20 min and quite half of them even until the end of an experiment. A tendency towards more mushroom shapes holds two aspects: on the one hand, it approves the trend to larger spine structures associated with LTP, since it necessitates at least head growth, on the other hand it advocates an evolutionary viewpoint of potentiation, in its sense of a rudimentary learning paradigm.
Quite a few investigations promote a similar shift from plastic / less evolved thin spines towards more stable / evolved mushroom spines during development (see for example Holtmaat et al. [2005]; Zuo et al. [2005]) and associated with the induction of LTP (e.g. Matsuzaki et al. [2004]; Kopec et al. [2006]). As subsumed in Sec.1.2.2, mushroom spines carry larger PSDs, more receptors and intracellular components, as well as more astroglial contacts than thin spines. I have related the particular transition from thin to mushroom spines to NMDAR mediated LTP on a (sub-) population level. Therefore my findings supplement previous work and support the present understanding of dendritic spines to "learn to be mushroom spines that remember" [Bourne and Harris, 2007].

4.2.3 Shape Changes of Spine Heads

Already in the last century Desmond and Levy [1983, 1986a] have found an increase in the number of concave spine heads in correlation with the induction of LTP in granule cells of the dentate gyrus. Roelandse et al. [2003] have been the first to detect cup-shaped heads with light microscopy in developing hippocampal pyramidal cells, though their images have been rather blurry and curvatures only vaguely perceptible. With the advent of super-resolution imaging techniques, Nägerl et al. [2008] and Izeddin et al. [2011] have

shown the aptitude of STED and PALM, respectively, to reveal spine head curvature reliably. In the present work, the occurrence of cup-shaped heads is quantitatively investigated in association with NMDA dependent LTP.

Beside their profound contribution to overall spine motility, convex spine head curvatures have significantly more often been observed after the induction of plasticity than during baseline recording. Though most of the cup-shapes did not persistently stay over time, a proportional stimulus-locked doubling of their appearance has been detected on the population level. Visually inspecting corresponding images, I observed post-synaptic compartments reaching out for their potential pre-synaptic partners (cp. e.g. Figs.3.6 and 3.7). That way they could increase the interface area to a bouton and shield it from its environment to prevent adjacent post-synaptic compartments from "docking".

On that account, I propose a scenario, where the sudden increase in local glutamate concentration due to photolysis of the caged compound, triggers some kind of collective "probing mode" in spines within the reach of action of the uncaging spot, akin to spontaneous motility of dendritic filopodia during development [Lohmann et al., 2005; Lohmann and Bonhoeffer, 2008]. Hence, a great deal of dendritic spines are "encouraged" to increase the contact areas to their respective boutons, in the "expectation" of further input. Since a stabilizing signal has been missing in my experimental paradigm, head curvatures have not been persistent, too. Additionally, cup-shaped spines have been abundant in slices under control treatment. Hence, the presumed "probing mode" could potentially be considered an inherent characteristic of dendritic spines. In that case, the amount of cup-shaped heads could probably serve as a measure for spine motility. Glutamate uncaging would then predominantly affect exactly this motility and spine morphing would display its mere consequence.

Due to a lack of analogous investigations, it is hard to assess my findings on grounds of plausibility. Nägerl et al. [2008] have examined spine morphological transitions in regard to cLTP in hippocampal slice cultures, but they report $40 - 60\,\%$ of the spines to have changed shape *at all* after stimulation, without deeper quantification of distinct structural aspects, like the occurrence of curved spine heads. Furthermore, their pharmacological stimulation protocol mediated spine plasticity via the potassium channel blocker TEA in an NMDA independent way [Aniksztejn and Ben-Ari, 1991]. In their super-resolution based study, Izeddin et al. [2011] have measured the distribution of actin molecules in rat primary hippocampal neurons, and found actin-free regions in spine heads, that they related to pre-synaptic boutons and PSDs, respectively. Apparently, what they are referring

to corresponds to cup-shaped spine heads. With a focus on the method, they have not addressed spine plasticity at all. Similarly, it is hard to compare my data to the work of Roelandse et al. [2003]. They focused on developmental aspects of spine morphology, and did not show quantifications of the number of cup-shaped spine heads from light-microscopic data. Instead they performed EM on microwave-fixed tissue. The only studies associating the appearance of curved spines with the induction of (electrical) LTP are the ones from Desmond and Levy [1983, 1986a]. They have observed a 31.4 % increase in the proportion of the total synapses that are concave. However, there images have been taken on perfusion fixed brain tissue (EM) and comprised a different region of the hippocampus (dentate gyrus).

4.2.4 Spine Branching

One particular sequence of structural changes during LTP that has been speculated about for quite some time in the literature, is spine splitting (see for instance Hering and Sheng [2001]; Yuste and Bonhoeffer [2001]). Based on correlations of the number of perforated PSDs and the number of multiple spine boutons with LTP, the idea has been that large mushroom spines break / split into two separate compartments, when potentiated. A couple of branched spine heads formed like this, would then contact the same bouton.
Fiala et al. [2002] have shown that branched spines do, in general, not share a pre-synaptic partner. Hence, spine splitting is very unlikely to underlie the formation of multiple synapse boutons or the formation of branched spines. Nevertheless, it has just recently still been considered a viable mechanism [Verzi and Noris, 2009]. Alternatively, Rusakov et al. [1996] have suggested spine fusion to guide the creation of branched spines. On grounds of super-resolved time-lapse images (cp. Fig.3.11), I can neither support the idea of spine splitting, nor of spine fusion. Instead, I have observed an outgrowth of new heads from the stalks of spines.
Along the lines of Fiala et al. [2002], additional spine heads seem not to synapse with the same bouton as their companions, since they usually grow out in different, and even in opposite directions. The formation of the new head has been initiated at a thickening in the spine neck, about 1 μm away from the dendritic shaft, corresponding to half of the total length of the initial spine, and has supposedly been completed within one hour. However, due to a small sample size (n=4) and the lack of a systematic assay, at this stage my findings have to be treated with great caution.

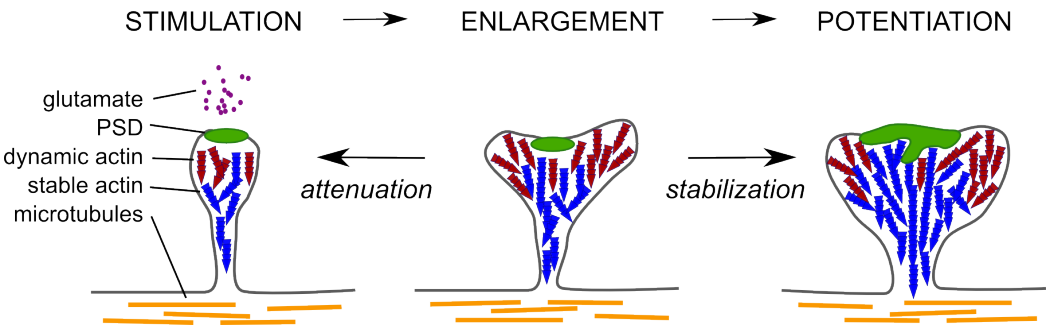

Figure 4.1: Simplified Model of Actin Driven Spine Plasticity. Glutamate acts as a stimulus to induce enlargement of spines via the regulation of the actin cytoskeleton. If stabilized, changes lead to the establishment of a mushroom spine. Adapted from Kasai et al. [2010].

4.2.5 Mechanism Driving Spine Plasticity

A lot of research has been conducted to reveal the molecular mechanisms driving morphological spine plasticity, which can hardly be covered in its entirety within the scope of this thesis. Therefore, I would like to focus on one of the key players of spine morphing, that is, actin. The review of Matus [2000] is a classic, dealing with the involvement of actin filaments in the formation of dendritic spines during development and their structural plasticity at mature synapses. More recent reviews on that topic have been published for example by Bosch and Hayashi [2011] and Kasai et al. [2010], the latter notably organizing the fundamental findings on spine structure and function into 15 "spine learning rules (SLRs)", as they call them.

Post-synaptic compartments are essentially free of microtubules, such that actin constitutes their main cytoskeletal component. Filaments are anchored in the plasma membrane and the PSD. On the one hand, they build a fine mesh inside spine heads, on the other hand, they form long parallel strands within the spine neck [Fifková, 1985; Korobova and Svitkina, 2010]. In resting spines, actin fibers organize in two groups: a dynamic and a stable pool [Star et al., 2002; Honkura et al., 2008]. The dynamic pool is located at the apex of a spine and appears to generate an expansive force, that maintains spine volume. The stable pool, by contrast, is located at the base of a spine and is supposed to act as a foundation for the dynamic pool to generate force on [Kasai et al., 2010]. Analysis of actin dynamics have revealed, that monomers polymerize at the apex and depolymerize at the base of spines [Honkura et al., 2008; Frost et al., 2010] (although see Tatavarty et al. [2009]). The involvement of (F-) actin polymerization in synaptic plasticity has been

shown by Matsuzaki et al. [2004]; Okamoto et al. [2004]; Honkura et al. [2008] as well as Kim and Lisman [1999]; Krucker et al. [2000].

A potential model of spine dynamics by regulation of the actin cytoskeleton is illustrated in Fig.4.1. In accordance with my observations, it resembles the current opinion in the field (see Honkura et al. [2008]; Kasai et al. [2010]; Bosch and Hayashi [2011]). The release of glutamate from pre-synaptic vesicles into the synaptic cleft mediates calcium influx into the post-synaptic compartment. Calcium can enter a spine through NMDARs [Collingridge et al., 1988] or through voltage gated channels in an AMPAR dependent way [Fischer et al., 2000], and regulates confinement of actin at the spine neck. Additionally, the kinetics of actin de- / polymerization in the stable and dynamic pools are adjusted. Whereas the turnover in the stable pool is decreased, polymerization of the dynamic pool continues. Hence, the spine enlarges. The PSD poses an inherent obstacle to the expansion, which can therefore only take effect at the periphery of a spine. Eventually, a growth of the stable pool fixates morphological changes and provides a scaffold for the recruitment of synaptic constituents with slower turnover (e.g. adhesion molecules, PSD scaffold, receptors , etc.). If no stabilization is triggered, spine enlargement is reverted to baseline dynamics.

Continuous expansion by actin filaments is probably balanced by a contractile force exerted by surface tension of the plasma membrane and counteracted by the remaining neuropil, i.e. extracellular matrix (ECM)[5], glia, axons, etc. [Kasai et al., 2010]. This could give rise to spine motility and the spontaneous morphing I have observed in the current study. Rapid spine enlargements mainly mirrored by an increase in cup-shaped heads in response to glutamate uncaging, would be readily explained by the above model. Also, the transience of curved heads could be ascribed to the different character of the dynamic and stable actin pools. Moreover, if the model applied, enlargements would take effect mainly at the periphery of a spine, such that the stable pool would expand at an angle to the spines' longitudinal axis. Hence, a stable shift of a subset of thin spines due to potentiation, as I have detected, could be justified at once.

Considering the complex sub-structure of synaptic PSDs, an interesting corollary follows from the above model. Since mainly guided by the balance of expanding and contractile forces, as well as the composition of the surrounding densely packed neuropil, spines and therefore, PSDs can by no means grow freely. Hence, I propose that complex shapes are a result of that convoluted growth process, as opposed by a break-up of initially disk-like PSDs into non-macular pieces. Though posing an ambitious scheme, this issue could po-

[5] A recent study from Orlando et al. [2012] showed an involvement of the ECM in spine dynamics, for instance.

tentially be resolved with the experimental setup at hand. Given a suitable marker for PSDs in live tissue, time-lapse STED nanoscopy should be able to detect their structural changes. Though, the fluorescent label needs to be specific, bright, and photostable not to bleach too fast. In addition, it must not interfere with the endogenous expression of PSD constituents. One option could be to follow a replacement strategy, where the endogenous expression of proteins is silenced with short hairpin RNA (shRNA) via ribonucleic acid (RNA) interference [Fire et al., 1998] and replaced by the expression of a fluorescent fusion. Fluorescent intrabodies [Chen et al., 1994] could pose viable alternatives. Also the labelling of extracellular components of the PSDs might be an option and leaves the door open to use nanoparticles as reporters, that can be particularly designed for STED imaging and keep the advantage of quasi-indefinite photostability.

Chapter 5

Conclusion

In the course of the current thesis, I have investigated the sub-structure of post-synaptic compartments in living hippocampal CA1 pyramidal cells. Time-lapse super-resolution STED imaging, performed at a custom built LSM, has facilitated tracing dendritic spine dynamics in association with the local induction of NMDA receptor mediated LTP via UV photolysis of caged glutamate. My experiments have revealed the evolution of a subset of thin spines to mushroom spines in two steps: first, the application of a stimulus has triggered massive spine enlargement, mirrored by a strong increase in the proportion of spines with curved heads, and second, in a subgroup of enlarged spines changes have been stabilized to be condensed in a growing proportion of mushroom spines. My observations have proven plausible against the backdrop of the relevant literature and have been related to the current understanding of the molecular mechanism underlying morphological spine plasticity.

5.1 Résumé

The efforts to build-up of a confocal STED-LSM are by no means comparable to the design of for instance a 2PE-LSM. Where in the latter case one can consider oneself to be home and dry after "overfilling" the imaging lens' back aperture to generate a decent PSF, the actual challenge in the former case has just started there. The gathering of super-resolved images has been found to be highly sensitive to all kinds of parameters – superposition of

the PSFs, synchronization of laser sources, polarization of de-excitation light, immersion liquid, detection efficiency, and many more. The slightest deviations from the ideal configuration bring about devastating consequences in the resolution obtained. Still, fluorescence nanoscopy is not sorcery, and latest developments like EasySTED [Reuss et al., 2010] will contribute to super-resolution imaging becoming a standard laboratory technique in the future. Also, commercialization of diverse nanoscopic concepts has been considerably promoted in recent years.
As for the examination of structural spine plasticity, I have been able to follow morphological changes over time at sub-100 nm resolution in live cells. My findings can be considered a supplement to previous investigations and poke into questions of how long structural changes last and how the induction of synaptic plasticity affects the motility of spines. They are in good agreement with the current knowledge on actin driven spine morphing and give rise to new, testable hypothesis on the evolution of non-macular PSDs.

That said, it's probably fair to take a look back to the early times of modern neuroscience, when Santiago Ramón y Cajal first had spotted dendritic spines, a ground breaking discovery of great physiological relevance, according to his own judgement [Yuste, 2002]. He not only proposed spines to be the primary sites of neuronal communication, but also accorded them dynamic entities, that mediate learning and memory consolidation [Tashiro and Yuste, 2003]. For his reasoning, he did not need any live-cell, or in fact super-resolution imaging. He had to reflect about his finding on purely logical grounds and may not even have considered spines to be static. Constituent of a living organ in an alive organism, that has its part in a changing ecosystem, it might have felt natural to associate neurons and synapses to be constantly on the move. Nevertheless, imagining Cajal to have been equipped with means of modern imaging technology, he would most certainly have entered the history books as the "Leonardo da Vinci" of Neuroscience.

5.2 Outlook

Super-resolution imaging has become a fast-growing branch of optic research and clever developments are announced nearly every month. With respect to neurobiological applications, there is great potential in targeted switching concepts like STED or RESOLFT, especially, if they can be adapted to 2PE with improved probes, specifically tailored to low light intensities and high photostability. Due to their technical similarity to standard laser scanning modalities, this could finally facilitate long-term *in-vivo* imaging at super-

resolution.

A great advancement regarding the frame rates of image acquisition has been the invention of parallelized nanoscopy with patterned illumination using standing light waves to provide isotropic resolution in the focal plane [Chmyrov et al., 2013]. Here, the authors took advantage of both, RESOLFT and saturated structured illumination microscopy (SSIM), to dramatically speed up far-field super-resolution imaging. Hence, the fusion of complementary aspects of unlimited optical resolution might show the right way to new fundamental breakthrough.

Furthermore, quantitative fluorescence readout, like with the combination of STED and raster image correlation spectroscopy (RICS) [Hedde et al., 2013] or super-resolved fluorescence correlation spectroscopy (FCS) [Eggeling et al., 2009], will provide further insight into intracellular molecular pathways and protein trafficking.

A more than interesting by-product of these mainly TCSPC based methods, is STED lifetime imaging [Auksorius et al., 2008]. With an arrangement to measure fluorescence lifetime, the possibilities for multi-color nanoscopy are multiplied (see for example Bückers et al. [2011]). It basically adds another dimension to the detection, such that each pixel not only contains information on fluorescence brightness and spectral color, but also on the fluorescence lifetime of a fluorophore. Therefore, multiple markers in a specimen can be discerned on grounds of photon counts in a 2D space (color and lifetime). I foresee a major aptitude of STED lifetime imaging for neuronal connectomics, as it will be able to reveal synaptic connections in live tissue, e.g. from the Brainbow mouse line [Livet et al., 2007], and can additionally be applied to correlative EM, when complemented by serial block-face scanning [Denk and Horstmann, 2004] or array tomography [Micheva and Smith, 2007].

Appendix A

Determination of Spine Density

Table A.1: Statistics of Spine Density Measurements.

Population Size	51	Third Quartile	1.41
Mean	1.18	Variance	0.11
Median	1.15	Standard Deviation	0.34
Minimum	0.15	Quartile Deviation	0.23
Maximum	2.23	Mean Absolute Deviation (MAD)	0.27
First Quartile	0.95	Standard Error of the Mean (S.E.M.)	0.05

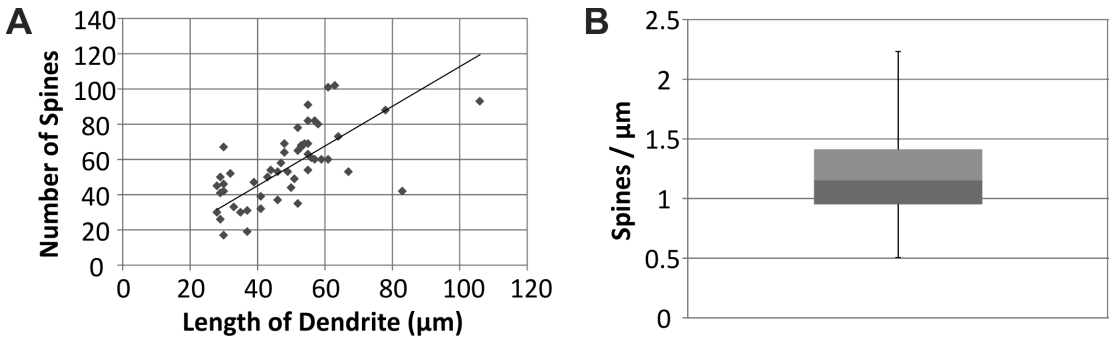

Figure A.1: Determination of Spine Density. *A* Scatter plot of all dendritic stretches analysed. *B* Boxplot of spine density distribution.

Average intensity projections of registered time series were rendered with MBF-ImageJ [Collins, 2007] and the total length of dendritic stretches measured on segmented line

reconstructions. Spines were tagged and their total count verified. Statistical analysis and graphs were compiled with MS Excel. Fig.A.1 and Tab.A.1 summarize the results. For this analysis all experiments were pooled together, i.e. I did not distinguish between uncaging trials and controls. The slope of the linear regression in Fig.A.1.A corresponds to the mean spine density. The border between light and dark gray in Fig.A.1.B resembles the median spine density.

Appendix B

Materials

B.1 Media and Solutions

ACSF for cLTP 2.5 mM calcium chloride, 1.25 mM monosodium hydrogen phosphate, 10 mM glucose, 1.3 mM magnesium chloride, 2.5 mM potassium chloride, 26 mM sodium bicarbonate, 126 mM sodium chloride, pH 7.2.

ACSF for Glutamate Uncaging 4 mM calcium chloride, 10 μM D-serine, 1.25 mM monosodium hydrogen phosphate, 25 mM glucose, 2.5 mM potassium chloride, 25 mM sodium bicarbonate, 127 mM sodium chloride, 1 μM TTX, 1 mM Trolox; pH 7.2.

Chicken Plasma Solution reconstituted in distilled water.

Dissolved Kynurenic Acid 946 mg of kynurenic acid were dissolved in 5 mL NaOH (1 M) and 45 mL distilled water.

Electroporation Solution 167 ng pCI-hSyn-PSD95::EGFP, 33 ng pCI-hSyn-tdimer2GFP and 50 μM Alexa Fluor 594 were dissolved in 50 μl HEPES-buffered ACSF.

Fixative 2.5 % (v/v) glutaraldehyde, 2 % (w/v) paraformaldehyde, 154 mM sodium chloride, 80 mM disodium hydrogen phosphate, 20 mM monosodium hydrogen phosphate.

GBSS 1.5 mM calcium chloride, 840 μM disodium hydrogen phosphate, 5.5 + 0.36 mM glucose, 1.03 mM magnesium chloride, 280 μM magnesium sulfate, 210 μM monopotassium phosphate, 4.98 mM potassium chloride, 2.7 mM sodium bicarbonate, 136 mM sodium chloride.

Glucose Solution 50 g of glucose were dissolved in 50 mL distilled water.

HEPES-buffered ACSF 2 mM calcium chloride, 10 mM glucose, 10 mM HEPES, 2 mM magnesium sulfate, 5 mM potassium chloride, 125 mM sodium chloride, pH 7.4.

Membrane Culture Medium 48 % (v/v) MEM medium, 25 % (v/v) HBSS, 25 % (v/v) horse serum, 1.25 % (v/v) HEPES (1 M), 1 % (v/v) Glucose Solution; pH 7.2.

Mitotic Inhibitor Solution 0.33 mM 5-Fluoro-2'-deoxyuridine in distilled water, 0.33 mM Ara-C, 0.33 mM uridine.

Preparation Medium 98 % (v/v) GBSS, 1 % (v/v) Dissolved Kynurenic Acid, 1 % (v/v) Glucose Solution; pH 7.2.

Resin 100 mL glycidether + 89 mL MNA, 62 mL glycidether + 100 mL DDSA, 6.3 mL BDMA.

Roller Tube Culture Medium 48.5 % (v/v) BME, 25 % (v/v) HBSS, 25 % (v/v) horse serum, 1 % (v/v) Glucose Solution, 1 mM L-glutamine.

Thrombin Solution 0.5 g thrombin were dissolved in 50 mL distilled water and 50 mL GBSS (0.5 % (w/v) solution).

Thrombin Working Solution 742.5 µL GBSS, 7.5 µL Glucose Solution, 500 µL Thrombin Solution. Has to be made on the day of the preparation and stored at 4 °C.

B.2 Equipment

Electron Microscopy

EM UC6 Leica Microsystems, Wetzlar, Germany

JEM-1230 JEOL, Tokyo, Japan

SC1000 ORIUS Gatan, Pleasanton, US-CA

Ultrastainer Leica Microsystems, Wetzlar, Germany

Laser Scanning Microscope

500 DCXR Chroma, Rockingham, US-VT

525/50 BrightLine HC Semrock, Rochester, US-NY

536/40 BrightLine HC Semrock, Rochester, US-NY

561 LP Edge Basic Semrock, Rochester, US-NY

A 360 World Precision Instruments, Sarasota, US-FL

AG-M100N Newport, Irvine, US-CA

AHWP05M-600 Thorlabs, Newton, US-NJ
AQWP05M-600 Thorlabs, Newton, US-NJ
AxoClamp 2B Molecular Devices, Sunnyvale, US-CA
BNC-2090A National Instruments, Austin, US-TX
BP145B1 Thorlabs, Newton, US-NJ
CM1-PBS251 Thorlabs, Newton, US-NJ
DELAY MPI-BPC (home-built), Göttingen, Germany
DFG/USB2pro The Imaging Source Europe, Bremen, Germany
DMI6000 B Leica Microsystems, Wetzlar, Germany
GL5-A Thorlabs, Newton, US-NJ
HCX PL APO CS 63x/1.30 GLYC Leica Microsystems, Wetzlar, Germany
HM507 HAMEG Instruments, Mainhausen, Germany
Hum Bug Quest Scientific, North Vancouver, CA-BC
iXon DV885LC Andor Technology, Belfast, UK
Junior RE/LE System Luigs & Neumann, Ratingen, Germany
KP-M2RP Hitachi Kokusai Electric Europe, Erkrath, Germany
M350-80 ConOptics, Danbury, US-CT
MaiTai HP Spectra Physics, Mountain View, US-CA
MD-963 Excelitas Technologies, Waltham, US-MA
Model 410 Brownlee Precision, Palo Alto, US-CA
OCF-401 Becker & Hickl, Berlin, Germany
OPO Advanced APE, Berlin, Germany
PCIe-6363 National Instruments, Austin, US-TX
PDL 800-B Pico Quant, Berlin, Germany
Pico TA Pico Quant, Berlin, Germany
PIFOC P-721.LLQ Physik Instrumente, Karlsruhe, Germany
PMC-460Si-3.0-NA012-3-APC-200-P Schäfter+Kirchhoff, Hamburg, Germany
PMJ-3U3A-633-4/125-3-50-1-HP OZ Optics, Ottawa, CA-ON
Precision T7500 Dell, Round Rock, US-TX
RAC 3.2.15 B. Halle Nachfl., Berlin, Germany
SPCM-AQRH-13-FC Excelitas Technologies, Waltham, US-MA
ST Series Newport, Irvine, US-CA
UltraSharp 2001FP Dell, Round Rock, US-TX
V-Stim MPI-N (home built), Martinsried, Germany

VPP-1 RPC Photonics, Rochester, US-NY

Yanus IV Till Photonics, Gräfelfing, Germany

z 590 sprdc Chroma, Rockingham, US-VT

zt 514 RDC Chroma, Rockingham, US-VT

Organotypic Slice Cultures

Axioskop2 Carl Zeiss Microscopy, Jena, Germany

Axoporator 800A Molecular Devices, Sunnyvale, US-CA

Biopore Membranes Merck Millipore, Billerica, US-MA

GC150F-10 Harvard Apparatus, Edenbridge, UK

McIlwain Tissue Chopper Mickle Laboratory Engineering, Surrey, UK

Millicell Cell Culture Inserts Merck Millipore, Billerica, US-MA

Minipuls 3 Gilson, Middleton, US-WI

No. 1.5H Paul Marienfeld, Lauda-Königshofen, Germany

Nunc Cell Culture Tubes Thermo Fisher Scientific, Waltham, US-MA

P35GC-1.0-14-C MatTek, Ashland, US-MA

PC-10 Narishige, Tokyo, Japan

QIAGEN Plasmid Plus Midi Kit Qiagen, Venlo, Netherlands

QIAquick Gel Extraction Kit Qiagen, Venlo, Netherlands

SteREO LumarV.12 Carl Zeiss Microscopy, Jena, Germany

Tissue Culture Test Plate TPP Techno Plastic Products, Trasadingen, Switzerland

TooheySpritzer Toohey, Fairfield, US-NJ

TW150F-4 World Precision Instruments, Sarasota, US-FL

Unit MRE/MLE Mini-25 Luigs & Neumann, Ratingen, Germany

Software

DigitalMicrograph Gatan, Pleasanton, US-CA

ImageJ National Institute of Mental Health, Bethesda, US-MD

ImSpector MPI-BPC, Göttingen, Germany

LabVIEW National Instruments, Austin, US-TX

MATLAB The MathWorks, Natick, US-MA

MS Excel Microsoft, Redmond, US-WA

Python Python Software Foundation, US-DE

Reconstruct ©1996 - 2007, John C. Fiala

Uncaging Setup

LUMPlanFL, 60x/0.9 W Olympus Deutschland, Hamburg, Germany

Master-8-cp A.M.P.I, Jerusalem, Israel
Optem Zoom 70XL Qioptiq Photonics, Göttingen, Germany
OXX-405-100-LBX-ZIR Oxxius, Lannion, France

B.3 Chemicals

5-Fluoro-2'-deoxyuridine Sigma-Aldrich, Steinheim, Germany

Alexa Fluor 594 hydrazide Life Technologies, Darmstadt, Germany
Ampicillin Sigma-Aldrich, Steinheim, Germany
Ara-C Hydrochloride Sigma-Aldrich, Steinheim, Germany

BDMA (Benzyldimethylamine) Serva Electrophoresis, Heidelberg, Germany
BME (Basal medium eagle) Life Technologies, Darmstadt, Germany

Calcium chloride ($CaCl_2$) Sigma-Aldrich, Steinheim, Germany
Carbogen (95 % O_2, 5 % CO_2) Westfalen AG, Münster, Germany
CMNB-caged fluorescein Life Technologies, Darmstadt, Germany

D-Serine Biotrend Chemikalien, Köln, Germany
DDSA (2-Dodecenylsuccinic anhydride) Serva Electrophoresis, Heidelberg, Germany
Disodium hydrogen phosphate ($Na_2HPO_4 \cdot H_2O$) Merck, Darmstadt, Germany

Ethanol absolute Sigma-Aldrich, Steinheim, Germany

FluoSpheres, Carboxylate-Modified Microspheres, 0.04 um Life Technologies, Darmstadt, Germany

Glucose (α-**D(+)-glucose** $\cdot H_2O$) Carl Roth, Karlsruhe, Germany
Glutaraldehyde Electron Microscopy Sciences, Hatfield, US-PA
Glycidether 100 Serva Electrophoresis, Heidelberg, Germany

HBSS Life Technologies, Darmstadt, Germany
HEPES Carl Roth, Karlsruhe, Germany
Horse serum Life Technologies, Darmstadt, Germany

Kynurenic acid Sigma-Aldrich, Steinheim, Germany

L-Glutamine (200 mM) Life Technologies, Darmstadt, Germany

Lead citrate Leica Microsystems, Wetzlar, Germany

Magnesium chloride ($MgCl_2 \cdot 6H_2O$) Merck, Darmstadt, Germany
Magnesium sulfate ($MgSO_4 \cdot 7H_2O$) Merck, Darmstadt, Germany
MEM Life Technologies, Darmstadt, Germany
MNA (Methylnadic anhydride) Serva Electrophoresis, Heidelberg, Germany
MNI-caged-L-glutamate Tocris Bioscience, Bristol, UK
Monopotassium phosphate (KH_2PO_4) Merck, Darmstadt, Germany
Monosodium hydrogen phosphate ($NaH_2PO_4 \cdot H_2O$) Merck, Darmstadt, Germany

Paraformaldehyde Electron Microscopy Sciences, Hatfield, US-PA
Picodent Twinsil Picodent, Wipperfürth, Germany
Potassium chloride (KCl) Sigma-Aldrich, Steinheim, Germany
Propylen oxide Electron Microscopy Sciences, Hatfield, US-PA
PVP (Polyvinylpyrrolidon) Bio-Rad, München, Germany

Sodium bicarbonate ($NaHCO_3$) Merck, Darmstadt, Germany
Sodium cacodylate buffer (pH 7.4) Electron Microscopy Sciences, Hatfield, US-PA
Sodium chloride (NaCl) VWR International, Leuven, Belgium
Spermidine Sigma-Aldrich, Steinheim, Germany

TEA (Tetraethylammonium, Et_4N^+) Sigma-Aldrich, Steinheim, Germany
Thrombin Merck, Darmstadt, Germany
Trolox Sigma-Aldrich, Steinheim, Germany
TTX (Tetrodotoxin) Biotrend Chemikalien, Köln, Germany

Uranyl acetate Leica Microsystems, Wetzlar, Germany
Uridine Sigma-Aldrich, Steinheim, Germany

Appendix C

Sequences of Plasmid DNA

C.1 pCI-hSyn-tdimer2RFP

```
   1 ACGCGGCCTT TTACGGTTCC TGGCCTTTGC TGGCCTTTTG CTCACATGGC TCGACAGATC
  61 TAATCTGCAG AGGGCCCTGC GTATGAGTGC AAGTGGGTTT TAGGACCAGG ATGAGGCGGG
 121 GTGGGGGTGC CTACCTGACG ACCGACCCCG ACCCACTGGA CAAGCACCCA ACCCCCATTC
 181 CCCAAATTGC GCATCCCCTA TCAGAGAGGG GGAGGGGAAA CAGGATGCGG CGAGGCGCGT
 241 GCGCACTGCC AGCTTCAGCA CCGCGGACAG TGCCTTCGCC CCCGCCTGGC GGCGCGCGCC
 301 ACCGCCGCCT CAGCACTGAA GGCGCGCTGA CGTCACTCGC CGGTCCCCCG CAAACTCCCC
 361 TTCCCGGCCA CCTTGGTCGC GTCCGCGCCG CCGCCGGCCC AGCCGGACCG CACCACGCGA
 421 GGCGCGAGAT AGGGGGGCAC GGGCGCGACC ATCTGCGCTG CGGCGCCGGC GACTCAGCGC
 481 TGCCTCAGTC TGCGGTGGGC AGCGGAGGAG TCGTGTCGTG CCTGAGAGCG CAGCTGCAGC
 541 TAGGAAGTTG GTCGTGAGGC ACTGGGCAGG TAAGTATCAA GGTTACAAGA CAGGTTTAAG
 601 GAGACCAATA GAAACTGGGC TTGTCGAGAC AGAGAAGACT CTTGCGTTTC TGATAGGCAC
 661 CTATTGGTCT TACTGACATC CACTTTGCCT TTCTCTCCAC AGGTGTCCAC TCCCAGTTCA
 721 ATTACAGCTC TTAAGGCTAG AGTACTTAAT ACGACTCACT ATAGGCTAGC CTCGAGAATT
 781 CAAGCTGCTA GAAATAATTT TGTTTAACTT TAAGAAGGAG ATATACATAT GCGGGGTTCT
 841 CATCATCATC ATCATCATGG TATGGCTAGC ATGACTGGTG GACAGCAAAT GGGTCGGGAT
 901 CTGTACGACG ATGACGATAA GGATCCGATG GTGGCCTCCT CCGAGGACGT CATCAAAGAG
 961 TTCATGCGCT TCAAGGTGCG CATGGAGGGC TCCGTGAACG GCCACGAGTT CGAGATCGAG
1021 GGCGAGGGCG AGGGCCGCCC CTACGAGGGC ACCCAGACCG CCAAGCTGAA GGTGACCAAG
1081 GGCGGCCCCC TGCCCTTCGC CTGGGACATC CTGTCCCCCC AGTTCCAGTA CGGCTCCAAG
1141 GCGTACGTGA AGCACCCCGC CGACATCCCC GACTACAAGA AGCTGTCCTT CCCCGAGGGC
1201 TTCAAGTGGG AGCGCGTGAT GAACTTCGAG GACGGCGGCG TGGTGACCGT GACCCAGGAC
```

1261 TCCTCCCTGC AGGACGGCAC GCTGATCTAC AAGGTGAAGT TCCGCGGCAC CAACTTCCCC
1321 CCCGACGGCC CCGTAATGCA GAAGAAGACC ATGGGCTGGG AGGCCTCCAC CGAGCGCCTG
1381 TACCCCCGCG ACGGCGTGCT GAAGGGCGAG ATCCACCAGG CCCTGAAGCT GAAGGACGGC
1441 GGCCACTACC TGGTGGAGTT CAAGACCATC TACATGGCCA AGAAGCCCGT GCAGCTGCCC
1501 GGCTACTACT ACGTGGACAC CAAGCTGGAC ATCACCTCCC ACAACGAGGA CTACACCATC
1561 GTGGAACAGT ACGAGCGCTC CGAGGGCCGC CACCACCTGT TCCTGGGGCA TGGCACCGGC
1621 AGCACCGGCA GCGGCAGCTC CGGCACCGCC TCCTCCGAGG ACGTCATCAA AGAGTTCATG
1681 CGCTTCAAGG TGCGCATGGA GGGCTCCGTG AACGGCCACG AGTTCGAGAT CGAGGGCGAG
1741 GGCGAGGGCC GCCCCTACGA GGGCACCCAG ACCGCCAAGC TGAAGGTGAC CAAGGGCGGC
1801 CCCCTGCCCT TCGCCTGGGA CATCCTGTCC CCCCAGTTCC AGTACGGCTC CAAGGCGTAC
1861 GTGAAGCACC CCGCCGACAT CCCCGACTAC AAGAAGCTGT CCTTCCCCGA GGGCTTCAAG
1921 TGGGAGCGCG TGATGAACTT CGAGGACGGC GGCGTGGTGA CCGTGACCCA GGACTCCTCC
1981 CTGCAGGACG GCACGCTGAT CTACAAGGTG AAGTTCCGCG GCACCAACTT CCCCCCCGAC
2041 GGCCCCGTAA TGCAGAAGAA GACCATGGGC TGGGAGGCCT CCACCGAGCG CCTGTACCCC
2101 CGCGACGGCG TGCTGAAGGG CGAGATCCAC CAGGCCCTGA AGCTGAAGGA CGGCGGCCAC
2161 TACCTGGTGG AGTTCAAGAC CATCTACATG GCCAAGAAGC CCGTGCAGCT GCCCGGCTAC
2221 TACTACGTGG ACACCAAGCT GGACATCACC TCCCACAACG AGGACTACAC CATCGTGGAA
2281 CAGTACGAGC GCTCCGAGGG CCGCCACCAC CTGTTCCTGT AGGAATTCAC GCGTGGTACC
2341 TCTAGAGTCG ACCCGGGCGG CCGCTTCGAG CAGACATGAT AAGATACATT GATGAGTTTG
2401 GACAAACCAC AACTAGAATG CAGTGAAAAA AATGCTTTAT TTGTGAAATT TGTGATGCTA
2461 TTGCTTTATT TGTAACCATT ATAAGCTGCA ATAAACAAGT TAACAACAAC AATTGCATTC
2521 ATTTTATGTT TCAGGTTCAG GGGGAGATGT GGGAGGTTTT TTAAAGCAAG TAAAACCTCT
2581 ACAAATGTGG TAAAATCGAT AAGGATCCGG GCTGGCGTAA TAGCGAAGAG GCCCGCACCG
2641 ATCGCCCTTC CCAACAGTTG CGCAGCCTGA ATGGCGAATG GACGCGCCCT GTAGCGGCGC
2701 ATTAAGCGCG GCGGGTGTGG TGGTTACGCG CAGCGTGACC GCTACACTTG CCAGCGCCCT
2761 AGCGCCCGCT CCTTTCGCTT TCTTCCCTTC CTTTCTCGCC ACGTTCGCCG GCTTTCCCCG
2821 TCAAGCTCTA AATCGGGGGC TCCCTTTAGG GTTCCGATTT AGTGCTTTAC GGCACCTCGA
2881 CCCCAAAAAA CTTGATTAGG GTGATGGTTC ACGTAGTGGG CCATCGCCCT GATAGACGGT
2941 TTTTCGCCCT TTGACGTTGG AGTCCACGTT CTTTAATAGT GGACTCTTGT TCCAAACTGG
3001 AACAACACTC AACCCTATCT CGGTCTATTC TTTTGATTTA TAAGGGATTT TGCCGATTTC
3061 GGCCTATTGG TTAAAAAATG AGCTGATTTA ACAAAAATTT AACGCGAATT TTAACAAAAT
3121 ATTAACGCTT ACAATTTCCT GATGCGGTAT TTTCTCCTTA CGCATCTGTG CGGTATTTCA
3181 CACCGCATAT GGTGCACTCT CAGTACAATC TGCTCTGATG CCGCATAGTT AAGCCAGCCC
3241 CGACACCCGC CAACACCCGC TGACGCGCCC TGACGGGCTT GTCTGCTCCC GGCATCCGCT

3301 TACAGACAAG CTGTGACCGT CTCCGGGAGC TGCATGTGTC AGAGGTTTTC ACCGTCATCA
3361 CCGAAACGCG CGAGACGAAA GGGCCTCGTG ATACGCCTAT TTTTATAGGT TAATGTCATG
3421 ATAATAATGG TTTCTTAGAC GTCAGGTGGC ACTTTTCGGG GAAATGTGCG CGGAACCCCT
3481 ATTTGTTTAT TTTTCTAAAT ACATTCAAAT ATGTATCCGC TCATGAGACA ATAACCCTGA
3541 TAAATGCTTC AATAATATTG AAAAAGGAAG AGTATGAGTA TTCAACATTT CCGTGTCGCC
3601 CTTATTCCCT TTTTTGCGGC ATTTTGCCTT CCTGTTTTTG CTCACCCAGA AACGCTGGTG
3661 AAAGTAAAAG ATGCTGAAGA TCAGTTGGGT GCACGAGTGG GTTACATCGA ACTGGATCTC
3721 AACAGCGGTA AGATCCTTGA GAGTTTTCGC CCCGAAGAAC GTTTTCCAAT GATGAGCACT
3781 TTTAAAGTTC TGCTATGTGG CGCGGTATTA TCCCGTATTG ACGCCGGGCA AGAGCAACTC
3841 GGTCGCCGCA TACACTATTC TCAGAATGAC TTGGTTGAGT ACTCACCAGT CACAGAAAAG
3901 CATCTTACGG ATGGCATGAC AGTAAGAGAA TTATGCAGTG CTGCCATAAC CATGAGTGAT
3961 AACACTGCGG CCAACTTACT TCTGACAACG ATCGGAGGAC CGAAGGAGCT AACCGCTTTT
4021 TTGCACAACA TGGGGGATCA TGTAACTCGC CTTGATCGTT GGGAACCGGA GCTGAATGAA
4081 GCCATACCAA ACGACGAGCG TGACACCACG ATGCCTGTAG CAATGGCAAC AACGTTGCGC
4141 AAACTATTAA CTGGCGAACT ACTTACTCTA GCTTCCCGGC AACAATTAAT AGACTGGATG
4201 GAGGCGGATA AAGTTGCAGG ACCACTTCTG CGCTCGGCCC TTCCGGCTGG CTGGTTTATT
4261 GCTGATAAAT CTGGAGCCGG TGAGCGTGGG TCTCGCGGTA TCATTGCAGC ACTGGGGCCA
4321 GATGGTAAGC CCTCCCGTAT CGTAGTTATC TACACGACGG GGAGTCAGGC AACTATGGAT
4381 GAACGAAATA GACAGATCGC TGAGATAGGT GCCTCACTGA TTAAGCATTG GTAACTGTCA
4441 GACCAAGTTT ACTCATATAT ACTTTAGATT GATTTAAAAC TTCATTTTTA ATTTAAAAGG
4501 ATCTAGGTGA AGATCCTTTT TGATAATCTC ATGACCAAAA TCCCTTAACG TGAGTTTTCG
4561 TTCCACTGAG CGTCAGACCC CGTAGAAAAG ATCAAAGGAT CTTCTTGAGA TCCTTTTTTT
4621 CTGCGCGTAA TCTGCTGCTT GCAAACAAAA AAACCACCGC TACCAGCGGT GGTTTGTTTG
4681 CCGGATCAAG AGCTACCAAC TCTTTTTCCG AAGGTAACTG GCTTCAGCAG AGCGCAGATA
4741 CCAAATACTG TTCTTCTAGT GTAGCCGTAG TTAGGCCACC ACTTCAAGAA CTCTGTAGCA
4801 CCGCCTACAT ACCTCGCTCT GCTAATCCTG TTACCAGTGG CTGCTGCCAG TGGCGATAAG
4861 TCGTGTCTTA CCGGGTTGGA CTCAAGACGA TAGTTACCGG ATAAGGCGCA GCGGTCGGGC
4921 TGAACGGGGG GTTCGTGCAC ACAGCCCAGC TTGGAGCGAA CGACCTACAC CGAACTGAGA
4981 TACCTACAGC GTGAGCTATG AGAAAGCGCC ACGCTTCCCG AAGGGAGAAA GGCGGACAGG
5041 TATCCGGTAA GCGGCAGGGT CGGAACAGGA GAGCGCACGA GGGAGCTTCC AGGGGGAAAC
5101 GCCTGGTATC TTTATAGTCC TGTCGGGTTT CGCCACCTCT GACTTGAGCG TCGATTTTTG
5161 TGATGCTCGT CAGGGGGGCG GAGCCTATGG AAAAACGCCA GCA

C.2 pCI-Neo-PSD-95::EGFP

```
   1 TCAATATTGG CCATTAGCCA TATTATTCAT TGGTTATATA GCATAAATCA ATATTGGCTA
  61 TTGGCCATTG CATACGTTGT ATCTATATCA TAATATGTAC ATTTATATTG GCTCATGTCC
 121 AATATGACCG CCATGTTGGC ATTGATTATT GACTAGTTAT TAATAGTAAT CAATTACGGG
 181 GTCATTAGTT CATAGCCCAT ATATGGAGTT CCGCGTTACA TAACTTACGG TAAATGGCCC
 241 GCCTGGCTGA CCGCCCAACG ACCCCCGCCC ATTGACGTCA ATAATGACGT ATGTTCCCAT
 301 AGTAACGCCA ATAGGGACTT TCCATTGACG TCAATGGGTG GAGTATTTAC GGTAAACTGC
 361 CCACTTGGCA GTACATCAAG TGTATCATAT GCCAAGTCCG CCCCCTATTG ACGTCAATGA
 421 CGGTAAATGG CCCGCCTGGC ATTATGCCCA GTACATGACC TTACGGGACT TTCCTACTTG
 481 GCAGTACATC TACGTATTAG TCATCGCTAT TACCATGGTG ATGCGGTTTT GGCAGTACAC
 541 CAATGGGCGT GGATAGCGGT TTGACTCACG GGGATTTCCA AGTCTCCACC CCATTGACGT
 601 CAATGGGAGT TTGTTTTGGC ACCAAAATCA ACGGGACTTT CCAAAATGTC GTAACAACTG
 661 CGATCGCCCG CCCCGTTGAC GCAAATGGGC GGTAGGCGTG TACGGTGGGA GGTCTATATA
 721 AGCAGAGCTC GTTTAGTGAA CCGTCAGATC ACTAGAAGCT TTATTGCGGT AGTTTATCAC
 781 AGTTAAATTG CTAACGCAGT CAGTGCTTCT GACACAACAG TCTCGAACTT AAGCTGCAGT
 841 GACTCTCTTA AGGTAGCCTT GCAGAAGTTG GTCGTGAGGC ACTGGGCAGG TAAGTATCAA
 901 GGTTACAAGA CAGGTTTAAG GAGACCAATA GAAACTGGGC TTGTCGAGAC AGAGAAGACT
 961 CTTGCGTTTC TGATAGGCAC CTATTGGTCT TACTGACATC CACTTTGCCT TTCTCTCCAC
1021 AGGTGTCCAC TCCCAGTTCA ATTACAGCTC TTAAGGCTAG AGTACTTAAT ACGACTCACT
1081 ATAGGCTAGC CTCGAGACCA TGGACTGTCT CTGTATAGTG ACAACCAAGA AATACCGCTA
1141 CCAAGATGAA GACACGCCCC CTCTGGAACA CAGCCCGGCC CACCTCCCCA ACCAGGCCAA
1201 TTCTCCCCCT GTGATTGTCA ACACGGACAC CCTAGAAGCC CCAGGATATG AGTTGCAGGT
1261 GAATGGAACA GAGGGGGAGA TGGAGTATGA GGAGATCACA TTGGAAAGGG GTAACTCAGG
1321 TCTGGGCTTC AGCATCGCAG GTGGCACTGA CAACCCGCAC ATCGGTGACG ACCCGTCCAT
1381 TTTTATCACC AAGATCATTC CTGGTGGGGC TGCAGCCCAG GATGGCCGCC TCAGGGTCAA
1441 TGACAGCATC CTGTTTGTAA ATGAAGTGGA TGTTCGGGAG GTGACCCATT CAGCTGCGGT
1501 GGAGGCCCTC AAAGAGGCAG GTTCCATCGT TCGCCTCTAT GTCATGCGCC GGAAACCCCC
1561 AGCCGAAAAG GTCATGGAGA TCAAACTCAT CAAAGGGCCT AAAGGACTTG GCTTCAGCAT
1621 TGCGGGGGGC GTTGGGAACC AGCACATCCC TGGAGATAAC AGCATCTATG TAACGAAGAT
1681 CATCGAAGGA GGTGCTGCCC ACAAGGATGG CAGGTTGCAG ATTGGAGACA AGATCCTGGC
1741 GGTCAACAGT GTGGGGCTGG AGGACGTCAT GCACGAGGAT GCCGTGGCAG CCCTGAAGAA
1801 CACATATGAC GTTGTGTACC TAAAGGTGGC CAAGCCCAGC AATGCCTACC TGAGTGACAG
1861 CTATGCTCCC CCAGACATCA CAACCTCGTA TTCTCAGCAC CTGGACAATG AGATCAGTCA
1921 TAGCAGCTAC TTGGGCACTG ACTACCCCAC AGCCATGACC CCCACTTCCC CTCGGCGCTA
```

1981 CTCCCCTGTG GCCAAGGACC TGCTGGGGGA GGAAGACATT CCCCGGGAAC CAAGGCGGAT
2041 CGTGATCCAT CGGGGCTCCA CCGGCCTGGG CTTCAACATC GTGGGCGGCG AGGATGGTGA
2101 AGGCATCTTC ATCTCCTTCA TCCTTGCTGG GGGTCCAGCC GACCTCAGTG GGGAGCTACG
2161 GAAGGGGGAC CAGATCCTGT CGGTCAATGG TGTTGACCTC CGCAATGCCA GTCACGAACA
2221 GGCTGCCATT GCCCTGAAGA ATGCGGGTCA GACGGTCACG ATCATCGCTC AGTATAAACC
2281 AGAAGAGTAT AGTCGATTCG AGGCCAAGAT CCATGATCTT CGGGAACAGC TCATGAATAG
2341 TAGCCTAGGC TCAGGGACTG CATCCTTGCG AAGCAACCCC AAGAGGGGCT TCTACATTAG
2401 GGCCCTGTTT GATTACGACA AGACCAAGGA CTGCGGTTTC TTGAGCCAGG CCCTGAGCTT
2461 CCGCTTCGGG GATGTGCTTC ATGTCATTGA CGCTGGTGAC GAAGAGTGGT GGCAAGCACG
2521 GCGGGTCCAC TCCGACAGTG AGACCGACGA CATTGGCTTC ATTCCCAGCA AACGGCGGGT
2581 CGAGCGACGA GAGTGGTCAA GGTTAAAGGC CAAGGACTGG GGCTCCAGCT CTGGATCACA
2641 GGGTCGAGAA GACTCGGTTC TGAGCTATGA GACGGTGACC CAGATGGAAG TGCACTATGC
2701 TCGTCCCATC ATCATCCTTG GACCCACCAA AGACCGTGCC AACGATGATC TTCTCTCCGA
2761 GTTCCCCGAC AAGTTTGGAT CCTGTGTCCC TCATACGACA CGTCCTAAGC GGGAATATGA
2821 GATAGACGGC CGGGATTACC ACTTTGTCTC CTCCCGGGAG AAAATGGAGA AGGACATCCA
2881 GGCACACAAG TTCATTGAGG CTGGCCAGTA CAACAGCCAC CTCTATGGGA CCAGCGTCCA
2941 GTCTGTGCGA GAGGTAGCAG AGCAGGGGAA GCACTGCATC CTCGATGTCT CGGCCAATGC
3001 CGTGCGGCGG CTGCAGGCGG CCCACCTGCA CCCCATCGCC ATCTTCATCC GTCCCCGCTC
3061 CCTGGAGAAT GTGCTAGAGA TCAATAAGCG GATCACAGAG GAGCAAGCCC GGAAAGCCTT
3121 CGACAGAGCC ACGAAGCTGG AGCAGGAGTT CACAGAGTGC TTCTCAGCCA TCGTAGAGGG
3181 CGACAGCTTT GAAGAGATCT ATCACAAAGT GAAACGTGTC ATTGAAGACC TCTCAGGCCC
3241 CTACATCTGG GTCCCAGCCC GAGAGAGACT CGGAATTCGG ATGGTGAGCA AGGGCGAGGA
3301 GCTGTTCACC GGGGTGGTGC CCATCCTGGT CGAGCTGGAC GGCGACGTAA ACGGCCACAA
3361 GTTCAGCGTG TCCGGCGAGG GCGAGGGCGA TGCCACCTAC GGCAAGCTGA CCCTGAAGTT
3421 CATCTGCACC ACCGGCAAGC TGCCCGTGCC CTGGCCCACC CTCGTGACCA CCCTGACCTA
3481 CGGCGTGCAG TGCTTCAGCC GCTACCCCGA CCACATGAAG CAGCACGACT TCTTCAAGTC
3541 CGCCATGCCC GAAGGCTACG TCCAGGAGCG CACCATCTTC TTCAAGGACG ACGGCAACTA
3601 CAAGACCCGC GCCGAGGTGA AGTTCGAGGG CGACACCCTG GTGAACCGCA TCGAGCTGAA
3661 GGGCATCGAC TTCAAGGAGG ACGGCAACAT CCTGGGGCAC AAGCTGGAGT ACAACTACAA
3721 CAGCCACAAC GTCTATATCA TGGCCGACAA GCAGAAGAAC GGCATCAAGG TGAACTTCAA
3781 GATCCGCCAC AACATCGAGG ACGGCAGCGT GCAGCTCGCC GACCACTACC AGCAGAACAC
3841 CCCCATCGGC GACGGCCCCG TGCTGCTGCC CGACAACCAC TACCTGAGCA CCCAGTCCGC
3901 CCTGAGCAAA GACCCCAACG AGAAGCGCGA TCACATGGTC CTGCTGGAGT TCGTGACCGC
3961 CGCCGGGATC ACTCTCGGCA TGGACGAGCT GTACAAGTAA GCGGCCGCTT CCCTTTAGTG

4021 AGGGTTAATG CTTCGAGCAG ACATGATAAG ATACATTGAT GAGTTTGGAC AAACCACAAC
4081 TAGAATGCAG TGAAAAAAAT GCTTTATTTG TGAAATTTGT GATGCTATTG CTTTATTTGT
4141 AACCATTATA AGCTGCAATA AACAAGTTAA CAACAACAAT TGCATTCATT TTATGTTTCA
4201 GGTTCAGGGG GAGATGTGGG AGGTTTTTTA AAGCAAGTAA AACCTCTACA AATGTGGTAA
4261 AATCCGATAA GGATCGATCC GGGCTGGCGT AATAGCGAAG AGGCCCGCAC CGATCGCCCT
4321 TCCCAACAGT TGCGCAGCCT GAATGGCGAA TGGACGCGCC CTGTAGCGGC GCATTAAGCG
4381 CGGCGGGTGT GGTGGTTACG CGCAGCGTGA CCGCTACACT TGCCAGCGCC CTAGCGCCCG
4441 CTCCTTTCGC TTTCTTCCCT TCCTTTCTCG CCACGTTCGC CGGCTTTCCC CGTCAAGCTC
4501 TAAATCGGGG GCTCCCTTTA GGGTTCCGAT TTAGTGCTTT ACGGCACCTC GACCCCAAAA
4561 AACTTGATTA GGGTGATGGT TCACGTAGTG GGCCATCGCC CTGATAGACG GTTTTTCGCC
4621 CTTTGACGTT GGAGTCCACG TTCTTTAATA GTGGACTCTT GTTCCAAACT GGAACAACAC
4681 TCAACCCTAT CTCGGTCTAT TCTTTTGATT TATAAGGGAT TTTGCCGATT TCGGCCTATT
4741 GGTTAAAAAA TGAGCTGATT TAACAAAAAT TTAACGCGAA TTTTAACAAA ATATTAACGC
4801 TTACAATTTC CTGATGCGGT ATTTTCTCCT TACGCATCTG TGCGGTATTT CACACCGCAT
4861 ACGCGGATCT GCGCAGCACC ATGGCCTGAA ATAACCTCTG AAAGAGGAAC TTGGTTAGGT
4921 ACCTTCTGAG GCGGAAAGAA CCAGCTGTGG AATGTGTGTC AGTTAGGGTG TGGAAAGTCC
4981 CCAGGCTCCC CAGCAGGCAG AAGTATGCAA AGCATGCATC TCAATTAGTC AGCAACCAGG
5041 TGTGGAAAGT CCCCAGGCTC CCCAGCAGGC AGAAGTATGC AAAGCATGCA TCTCAATTAG
5101 TCAGCAACCA TAGTCCCGCC CCTAACTCCG CCCATCCCGC CCCTAACTCC GCCCAGTTCC
5161 GCCCATTCTC CGCCCCATGG CTGACTAATT TTTTTTATTT ATGCAGAGGC CGAGGCCGCC
5221 TCGGCCTCTG AGCTATTCCA GAAGTAGTGA GGAGGCTTTT TTGGAGGCCT AGGCTTTTGC
5281 AAAAAGCTTG ATTCTTCTGA CACAACAGTC TCGAACTTAA GGCTAGAGCC ACCATGATTG
5341 AACAAGATGG ATTGCACGCA GGTTCTCCGG CCGCTTGGGT GGAGAGGCTA TTCGGCTATG
5401 ACTGGGCACA ACAGACAATC GGCTGCTCTG ATGCCGCCGT GTTCCGGCTG TCAGCGCAGG
5461 GGCGCCCGGT TCTTTTTGTC AAGACCGACC TGTCCGGTGC CCTGAATGAA CTGCAGGACG
5521 AGGCAGCGCG GCTATCGTGG CTGGCCACGA CGGGCGTTCC TTGCGCAGCT GTGCTCGACG
5581 TTGTCACTGA AGCGGGAAGG GACTGGCTGC TATTGGGCGA AGTGCCGGGG CAGGATCTCC
5641 TGTCATCTCA CCTTGCTCCT GCCGAGAAAG TATCCATCAT GGCTGATGCA ATGCGGCGGC
5701 TGCATACGCT TGATCCGGCT ACCTGCCCAT TCGACCACCA AGCGAAACAT CGCATCGAGC
5761 GAGCACGTAC TCGGATGGAA GCCGGTCTTG TCGATCAGGA TGATCTGGAC GAAGAGCATC
5821 AGGGGCTCGC GCCAGCCGAA CTGTTCGCCA GGCTCAAGGC GCGCATGCCC GACGGCGAGG
5881 ATCTCGTCGT GACCCATGGC GATGCCTGCT TGCCGAATAT CATGGTGGAA AATGGCCGCT
5941 TTTCTGGATT CATCGACTGT GGCCGGCTGG GTGTGGCGGA CCGCTATCAG GACATAGCGT
6001 TGGCTACCCG TGATATTGCT GAAGAGCTTG GCGGCGAATG GGCTGACCGC TTCCTCGTGC

6061 TTTACGGTAT CGCCGCTCCC GATTCGCAGC GCATCGCCTT CTATCGCCTT CTTGACGAGT
6121 TCTTCTGAGC GGGACTCTGG GGTTCGAAAT GACCGACCAA GCGACGCCCA ACCTGCCATC
6181 ACGATGGCCG CAATAAAATA TCTTTATTTT CATTACATCT GTGTGTTGGT TTTTTGTGTG
6241 AATCGATAGC GATAAGGATC CGCGTATGGT GCACTCTCAG TACAATCTGC TCTGATGCCG
6301 CATAGTTAAG CCAGCCCCGA CACCCGCCAA CACCCGCTGA CGCGCCCTGA CGGGCTTGTC
6361 TGCTCCCGGC ATCCGCTTAC AGACAAGCTG TGACCGTCTC CGGGAGCTGC ATGTGTCAGA
6421 GGTTTTCACC GTCATCACCG AAACGCGCGA GACGAAAGGG CCTCGTGATA CGCCTATTTT
6481 TATAGGTTAA TGTCATGATA ATAATGGTTT CTTAGACGTC AGGTGGCACT TTTCGGGGAA
6541 ATGTGCGCGG AACCCCTATT TGTTTATTTT TCTAAATACA TTCAAATATG TATCCGCTCA
6601 TGAGACAATA ACCCTGATAA ATGCTTCAAT AATATTGAAA AAGGAAGAGT ATGAGTATTC
6661 AACATTTCCG TGTCGCCCTT ATTCCCTTTT TTGCGGCATT TTGCCTTCCT GTTTTTGCTC
6721 ACCCAGAAAC GCTGGTGAAA GTAAAAGATG CTGAAGATCA GTTGGGTGCA CGAGTGGGTT
6781 ACATCGAACT GGATCTCAAC AGCGGTAAGA TCCTTGAGAG TTTTCGCCCC GAAGAACGTT
6841 TTCCAATGAT GAGCACTTTT AAAGTTCTGC TATGTGGCGC GGTATTATCC CGTATTGACG
6901 CCGGGCAAGA GCAACTCGGT CGCCGCATAC ACTATTCTCA GAATGACTTG GTTGAGTACT
6961 CACCAGTCAC AGAAAAGCAT CTTACGGATG GCATGACAGT AAGAGAATTA TGCAGTGCTG
7021 CCATAACCAT GAGTGATAAC ACTGCGGCCA ACTTACTTCT GACAACGATC GGAGGACCGA
7081 AGGAGCTAAC CGCTTTTTTG CACAACATGG GGGATCATGT AACTCGCCTT GATCGTTGGG
7141 AACCGGAGCT GAATGAAGCC ATACCAAACG ACGAGCGTGA CACCACGATG CCTGTAGCAA
7201 TGGCAACAAC GTTGCGCAAA CTATTAACTG GCGAACTACT TACTCTAGCT TCCCGGCAAC
7261 AATTAATAGA CTGGATGGAG GCGGATAAAG TTGCAGGACC ACTTCTGCGC TCGGCCCTTC
7321 CGGCTGGCTG GTTTATTGCT GATAAATCTG GAGCCGGTGA GCGTGGGTCT CGCGGTATCA
7381 TTGCAGCACT GGGGCCAGAT GGTAAGCCCT CCCGTATCGT AGTTATCTAC ACGACGGGGA
7441 GTCAGGCAAC TATGGATGAA CGAAATAGAC AGATCGCTGA GATAGGTGCC TCACTGATTA
7501 AGCATTGGTA ACTGTCAGAC CAAGTTTACT CATATATACT TTAGATTGAT TTAAAACTTC
7561 ATTTTTAATT TAAAAGGATC TAGGTGAAGA TCCTTTTTGA TAATCTCATG ACCAAAATCC
7621 CTTAACGTGA GTTTTCGTTC CACTGAGCGT CAGACCCCGT AGAAAAGATC AAAGGATCTT
7681 CTTGAGATCC TTTTTTTCTG CGCGTAATCT GCTGCTTGCA AACAAAAAAA CCACCGCTAC
7741 CAGCGGTGGT TTGTTTGCCG GATCAAGAGC TACCAACTCT TTTTCCGAAG GTAACTGGCT
7801 TCAGCAGAGC GCAGATACCA AATACTGTTC TTCTAGTGTA GCCGTAGTTA GGCCACCACT
7861 TCAAGAACTC TGTAGCACCG CCTACATACC TCGCTCTGCT AATCCTGTTA CCAGTGGCTG
7921 CTGCCAGTGG CGATAAGTCG TGTCTTACCG GGTTGGACTC AAGACGATAG TTACCGGATA
7981 AGGCGCAGCG GTCGGGCTGA ACGGGGGGTT CGTGCACACA GCCCAGCTTG GAGCGAACGA
8041 CCTACACCGA ACTGAGATAC CTACAGCGTG AGCTATGAGA AAGCGCCACG CTTCCCGAAG

```
8101 GGAGAAAGGC GGACAGGTAT CCGGTAAGCG GCAGGGTCGG AACAGGAGAG CGCACGAGGG
8161 AGCTTCCAGG GGGAAACGCC TGGTATCTTT ATAGTCCTGT CGGGTTTCGC CACCTCTGAC
8221 TTGAGCGTCG ATTTTTGTGA TGCTCGTCAG GGGGGCGGAG CCTATGGAAA AACGCCAGCA
8281 ACGCGGCCTT TTTACGGTTC CTGGCCTTTT GCTGGCCTTT TGCTCACATG GCTCGACAGA
8341 TCT
```

C.3 pCI-hSyn-PSD-95::EGFP

```
   1 ACGCGGCCTT TTACGGTTCC TGGCCTTTGC TGGCCTTTTG CTCACATGGC TCGACAGATC
  61 TAATCTGCAG AGGGCCCTGC GTATGAGTGC AAGTGGGTTT TAGGACCAGG ATGAGGCGGG
 121 GTGGGGGTGC CTACCTGACG ACCGACCCCG ACCCACTGGA CAAGCACCCA ACCCCCATTC
 181 CCCAAATTGC GCATCCCCTA TCAGAGAGGG GGAGGGGAAA CAGGATGCGG CGAGGCGCGT
 241 GCGCACTGCC AGCTTCAGCA CCGCGGACAG TGCCTTCGCC CCCGCCTGGC GGCGCGCGCC
 301 ACCGCCGCCT CAGCACTGAA GGCGCGCTGA CGTCACTCGC CGGTCCCCCG CAAACTCCCC
 361 TTCCCGGCCA CCTTGGTCGC GTCCGCGCCG CCGCCGGCCC AGCCGGACCG CACCACGCGA
 421 GGCGCGAGAT AGGGGGGCAC GGGCGCGACC ATCTGCGCTG CGGCGCCGGC GACTCAGCGC
 481 TGCCTCAGTC TGCGGTGGGC AGCGGAGGAG TCGTGTCGTG CCTGAGAGCG CAGCTGCAGC
 541 TAGGAAGTTG GTCGTGAGGC ACTGGGCAGG TAAGTATCAA GGTTACAAGA CAGGTTTAAG
 601 GAGACCAATA GAAACTGGGC TTGTCGAGAC AGAGAAGACT CTTGCGTTTC TGATAGGCAC
 661 CTATTGGTCT TACTGACATC CACTTTGCCT TTCTCTCCAC AGGTGTCCAC TCCCAGTTCA
 721 ATTACAGCTC TTAAGGCTAG AGTACTTAAT ACGACTCACT ATAGGCTAGC CTCGAGACCA
 781 TGGACTGTCT CTGTATAGTG ACAACCAAGA AATACCGCTA CCAAGATGAA GACACGCCCC
 841 CTCTGGAACA CAGCCCGGCC CACCTCCCCA ACCAGGCCAA TTCTCCCCCT GTGATTGTCA
 901 ACACGGACAC CCTAGAAGCC CCAGGATATG AGTTGCAGGT GAATGGAACA GAGGGGGAGA
 961 TGGAGTATGA GGAGATCACA TTGGAAAGGG GTAACTCAGG TCTGGGCTTC AGCATCGCAG
1021 GTGGCACTGA CAACCCGCAC ATCGGTGACG ACCCGTCCAT TTTTATCACC AAGATCATTC
1081 CTGGTGGGGC TGCAGCCCAG GATGGCCGCC TCAGGGTCAA TGACAGCATC CTGTTTGTAA
1141 ATGAAGTGGA TGTTCGGGAG GTGACCCATT CAGCTGCGGT GGAGGCCCTC AAAGAGGCAG
1201 GTTCCATCGT TCGCCTCTAT GTCATGCGCC GGAAACCCCC AGCCGAAAAG GTCATGGAGA
1261 TCAAACTCAT CAAAGGGCCT AAAGGACTTG GCTTCAGCAT TGCGGGGGGC GTTGGGAACC
1321 AGCACATCCC TGGAGATAAC AGCATCTATG TAACGAAGAT CATCGAAGGA GGTGCTGCCC
1381 ACAAGGATGG CAGGTTGCAG ATTGGAGACA AGATCCTGGC GGTCAACAGT GTGGGGCTGG
1441 AGGACGTCAT GCACGAGGAT GCCGTGGCAG CCCTGAAGAA CACATATGAC GTTGTGTACC
1501 TAAAGGTGGC CAAGCCCAGC AATGCCTACC TGAGTGACAG CTATGCTCCC CCAGACATCA
```

1561 CAACCTCGTA TTCTCAGCAC CTGGACAATG AGATCAGTCA TAGCAGCTAC TTGGGCACTG
1621 ACTACCCCAC AGCCATGACC CCCACTTCCC CTCGGCGCTA CTCCCCTGTG GCCAAGGACC
1681 TGCTGGGGGA GGAAGACATT CCCCGGGAAC CAAGGCGGAT CGTGATCCAT CGGGGCTCCA
1741 CCGGCCTGGG CTTCAACATC GTGGGCGGCG AGGATGGTGA AGGCATCTTC ATCTCCTTCA
1801 TCCTTGCTGG GGGTCCAGCC GACCTCAGTG GGGAGCTACG GAAGGGGGAC CAGATCCTGT
1861 CGGTCAATGG TGTTGACCTC CGCAATGCCA GTCACGAACA GGCTGCCATT GCCCTGAAGA
1921 ATGCGGGTCA GACGGTCACG ATCATCGCTC AGTATAAACC AGAAGAGTAT AGTCGATTCG
1981 AGGCCAAGAT CCATGATCTT CGGGAACAGC TCATGAATAG TAGCCTAGGC TCAGGGACTG
2041 CATCCTTGCG AAGCAACCCC AAGAGGGGCT TCTACATTAG GGCCCTGTTT GATTACGACA
2101 AGACCAAGGA CTGCGGTTTC TTGAGCCAGG CCCTGAGCTT CCGCTTCGGG GATGTGCTTC
2161 ATGTCATTGA CGCTGGTGAC GAAGAGTGGT GGCAAGCACG GCGGGTCCAC TCCGACAGTG
2221 AGACCGACGA CATTGGCTTC ATTCCCAGCA AACGGCGGGT CGAGCGACGA GAGTGGTCAA
2281 GGTTAAAGGC CAAGGACTGG GGCTCCAGCT CTGGATCACA GGGTCGAGAA GACTCGGTTC
2341 TGAGCTATGA GACGGTGACC CAGATGGAAG TGCACTATGC TCGTCCCATC ATCATCCTTG
2401 GACCCACCAA AGACCGTGCC AACGATGATC TTCTCTCCGA GTTCCCCGAC AAGTTTGGAT
2461 CCTGTGTCCC TCATACGACA CGTCCTAAGC GGGAATATGA GATAGACGGC CGGGATTACC
2521 ACTTTGTCTC CTCCCGGGAG AAAATGGAGA AGGACATCCA GGCACACAAG TTCATTGAGG
2581 CTGGCCAGTA CAACAGCCAC CTCTATGGGA CCAGCGTCCA GTCTGTGCGA GAGGTAGCAG
2641 AGCAGGGGAA GCACTGCATC CTCGATGTCT CGGCCAATGC CGTGCGGCGG CTGCAGGCGG
2701 CCCACCTGCA CCCCATCGCC ATCTTCATCC GTCCCCGCTC CCTGGAGAAT GTGCTAGAGA
2761 TCAATAAGCG GATCACAGAG GAGCAAGCCC GGAAAGCCTT CGACAGAGCC ACGAAGCTGG
2821 AGCAGGAGTT CACAGAGTGC TTCTCAGCCA TCGTAGAGGG CGACAGCTTT GAAGAGATCT
2881 ATCACAAAGT GAAACGTGTC ATTGAAGACC TCTCAGGCCC CTACATCTGG GTCCCAGCCC
2941 GAGAGAGACT CGGAATTCGG ATGGTGAGCA AGGGCGAGGA GCTGTTCACC GGGGTGGTGC
3001 CCATCCTGGT CGAGCTGGAC GGCGACGTAA ACGGCCACAA GTTCAGCGTG TCCGGCGAGG
3061 GCGAGGGCGA TGCCACCTAC GGCAAGCTGA CCCTGAAGTT CATCTGCACC ACCGGCAAGC
3121 TGCCCGTGCC CTGGCCCACC CTCGTGACCA CCCTGACCTA CGGCGTGCAG TGCTTCAGCC
3181 GCTACCCCGA CCACATGAAG CAGCACGACT TCTTCAAGTC CGCCATGCCC GAAGGCTACG
3241 TCCAGGAGCG CACCATCTTC TTCAAGGACG ACGGCAACTA CAAGACCCGC GCCGAGGTGA
3301 AGTTCGAGGG CGACACCCTG GTGAACCGCA TCGAGCTGAA GGGCATCGAC TTCAAGGAGG
3361 ACGGCAACAT CCTGGGGCAC AAGCTGGAGT ACAACTACAA CAGCCACAAC GTCTATATCA
3421 TGGCCGACAA GCAGAAGAAC GGCATCAAGG TGAACTTCAA GATCCGCCAC AACATCGAGG
3481 ACGGCAGCGT GCAGCTCGCC GACCACTACC AGCAGAACAC CCCCATCGGC GACGGCCCCG
3541 TGCTGCTGCC CGACAACCAC TACCTGAGCA CCCAGTCCGC CCTGAGCAAA GACCCCAACG

3601 AGAAGCGCGA TCACATGGTC CTGCTGGAGT TCGTGACCGC CGCCGGGATC ACTCTCGGCA
3661 TGGACGAGCT GTACAAGTAA GCGGCCGCTT CGAGCAGACA TGATAAGATA CATTGATGAG
3721 TTTGGACAAA CCACAACTAG AATGCAGTGA AAAAAATGCT TTATTTGTGA AATTTGTGAT
3781 GCTATTGCTT TATTTGTAAC CATTATAAGC TGCAATAAAC AAGTTAACAA CAACAATTGC
3841 ATTCATTTTA TGTTTCAGGT TCAGGGGGAG ATGTGGGAGG TTTTTTAAAG CAAGTAAAAC
3901 CTCTACAAAT GTGGTAAAAT CGATAAGGAT CCGGGCTGGC GTAATAGCGA AGAGGCCCGC
3961 ACCGATCGCC CTTCCCAACA GTTGCGCAGC CTGAATGGCG AATGGACGCG CCCTGTAGCG
4021 GCGCATTAAG CGCGGCGGGT GTGGTGGTTA CGCGCAGCGT GACCGCTACA CTTGCCAGCG
4081 CCCTAGCGCC CGCTCCTTTC GCTTTCTTCC CTTCCTTTCT CGCCACGTTC GCCGGCTTTC
4141 CCCGTCAAGC TCTAAATCGG GGGCTCCCTT TAGGGTTCCG ATTTAGTGCT TTACGGCACC
4201 TCGACCCCAA AAAACTTGAT TAGGGTGATG GTTCACGTAG TGGGCCATCG CCCTGATAGA
4261 CGGTTTTTCG CCCTTTGACG TTGGAGTCCA CGTTCTTTAA TAGTGGACTC TTGTTCCAAA
4321 CTGGAACAAC ACTCAACCCT ATCTCGGTCT ATTCTTTTGA TTTATAAGGG ATTTTGCCGA
4381 TTTCGGCCTA TTGGTTAAAA AATGAGCTGA TTTAACAAAA ATTTAACGCG AATTTTAACA
4441 AAATATTAAC GCTTACAATT TCCTGATGCG GTATTTTCTC CTTACGCATC TGTGCGGTAT
4501 TTCACACCGC ATATGGTGCA CTCTCAGTAC AATCTGCTCT GATGCCGCAT AGTTAAGCCA
4561 GCCCCGACAC CCGCCAACAC CCGCTGACGC GCCCTGACGG GCTTGTCTGC TCCCGGCATC
4621 CGCTTACAGA CAAGCTGTGA CCGTCTCCGG GAGCTGCATG TGTCAGAGGT TTTCACCGTC
4681 ATCACCGAAA CGCGCGAGAC GAAAGGGCCT CGTGATACGC CTATTTTTAT AGGTTAATGT
4741 CATGATAATA ATGGTTTCTT AGACGTCAGG TGGCACTTTT CGGGGAAATG TGCGCGGAAC
4801 CCCTATTTGT TTATTTTTCT AAATACATTC AAATATGTAT CCGCTCATGA GACAATAACC
4861 CTGATAAATG CTTCAATAAT ATTGAAAAAG GAAGAGTATG AGTATTCAAC ATTTCCGTGT
4921 CGCCCTTATT CCCTTTTTTG CGGCATTTTG CCTTCCTGTT TTTGCTCACC CAGAAACGCT
4981 GGTGAAAGTA AAAGATGCTG AAGATCAGTT GGGTGCACGA GTGGGTTACA TCGAACTGGA
5041 TCTCAACAGC GGTAAGATCC TTGAGAGTTT TCGCCCCGAA GAACGTTTTC CAATGATGAG
5101 CACTTTTAAA GTTCTGCTAT GTGGCGCGGT ATTATCCCGT ATTGACGCCG GGCAAGAGCA
5161 ACTCGGTCGC CGCATACACT ATTCTCAGAA TGACTTGGTT GAGTACTCAC CAGTCACAGA
5221 AAAGCATCTT ACGGATGGCA TGACAGTAAG AGAATTATGC AGTGCTGCCA TAACCATGAG
5281 TGATAACACT GCGGCCAACT TACTTCTGAC AACGATCGGA GGACCGAAGG AGCTAACCGC
5341 TTTTTTGCAC AACATGGGGG ATCATGTAAC TCGCCTTGAT CGTTGGGAAC CGGAGCTGAA
5401 TGAAGCCATA CCAAACGACG AGCGTGACAC CACGATGCCT GTAGCAATGG CAACAACGTT
5461 GCGCAAACTA TTAACTGGCG AACTACTTAC TCTAGCTTCC CGGCAACAAT TAATAGACTG
5521 GATGGAGGCG GATAAAGTTG CAGGACCACT TCTGCGCTCG GCCCTTCCGG CTGGCTGGTT
5581 TATTGCTGAT AAATCTGGAG CCGGTGAGCG TGGGTCTCGC GGTATCATTG CAGCACTGGG

```
5641 GCCAGATGGT AAGCCCTCCC GTATCGTAGT TATCTACACG ACGGGGAGTC AGGCAACTAT
5701 GGATGAACGA AATAGACAGA TCGCTGAGAT AGGTGCCTCA CTGATTAAGC ATTGGTAACT
5761 GTCAGACCAA GTTTACTCAT ATATACTTTA GATTGATTTA AAACTTCATT TTTAATTTAA
5821 AAGGATCTAG GTGAAGATCC TTTTTGATAA TCTCATGACC AAAATCCCTT AACGTGAGTT
5881 TTCGTTCCAC TGAGCGTCAG ACCCCGTAGA AAAGATCAAA GGATCTTCTT GAGATCCTTT
5941 TTTTCTGCGC GTAATCTGCT GCTTGCAAAC AAAAAAACCA CCGCTACCAG CGGTGGTTTG
6001 TTTGCCGGAT CAAGAGCTAC CAACTCTTTT TCCGAAGGTA ACTGGCTTCA GCAGAGCGCA
6061 GATACCAAAT ACTGTTCTTC TAGTGTAGCC GTAGTTAGGC CACCACTTCA AGAACTCTGT
6121 AGCACCGCCT ACATACCTCG CTCTGCTAAT CCTGTTACCA GTGGCTGCTG CCAGTGGCGA
6181 TAAGTCGTGT CTTACCGGGT TGGACTCAAG ACGATAGTTA CCGGATAAGG CGCAGCGGTC
6241 GGGCTGAACG GGGGGTTCGT GCACACAGCC CAGCTTGGAG CGAACGACCT ACACCGAACT
6301 GAGATACCTA CAGCGTGAGC TATGAGAAAG CGCCACGCTT CCCGAAGGGA GAAAGGCGGA
6361 CAGGTATCCG GTAAGCGGCA GGGTCGGAAC AGGAGAGCGC ACGAGGGAGC TTCCAGGGGG
6421 AAACGCCTGG TATCTTTATA GTCCTGTCGG GTTTCGCCAC CTCTGACTTG AGCGTCGATT
6481 TTTGTGATGC TCGTCAGGGG GGCGGAGCCT ATGGAAAAAC GCCAGCA
```

C.4 pSCA-Lifeact::EYFP

```
   1 ATGGCGGATG TGTGACATAC ACGACGCCAA AAGATTTTGT TCCAGCTCCT GCCACCTCCG
  61 CTACGCGAGA GATTAACCAC CCACGATGGC CGCCAAAGTG CATGTTGATA TTGAGGCTGA
 121 CAGCCCATTC ATCAAGTCTT TGCAGAAGGC ATTTCCGTCG TTCGAGGTGG AGTCATTGCA
 181 GGTCACACCA AATGACCATG CAAATGCCAG AGCATTTTCG CACCTGGCTA CCAAATTGAT
 241 CGAGCAGGAG ACTGACAAAG ACACACTCAT CTTGGATATC GGCAGTGCGC CTTCCAGGAG
 301 AATGATGTCT ACGCACAAAT ACCACTGCGT ATGCCCTATG CGCAGCGCAG AAGACCCCGA
 361 AAGGCTCGAT AGCTACGCAA AGAAACTGGC AGCGGCCTCC GGGAAGGTGC TGGATAGAGA
 421 GATCGCAGGA AAAATCACCG ACCTGCAGAC CGTCATGGCT ACGCCAGACG CTGAATCTCC
 481 TACCTTTTGC CTGCATACAG ACGTCACGTG TCGTACGGCA GCCGAAGTGG CCGTATACCA
 541 GGACGTGTAT GCTGTACATG CACCAACATC GCTGTACCAT CAGGCGATGA AAGGTGTCAG
 601 AACGGCGTAT TGGATTGGGT TTGACACCAC CCCGTTTATG TTTGACGCGC TAGCAGGCGC
 661 GTATCCAACC TACGCCACAA ACTGGGCCGA CGAGCAGGTG TTACAGGCCA GGAACATAGG
 721 ACTGTGTGCA GCATCCTTGA CTGAGGGAAG ACTCGGCAAA CTGTCCATTC TCCGCAAGAA
 781 GCAATTGAAA CCTTGCGACA CAGTCATGTT CTCGGTAGGA TCTACATTGT ACACTGAGAG
 841 CAGAAAGCTA CTGAGGAGCT GGCACTTACC CTCCGTATTC CACCTGAAAG GTAAACAATC
 901 CTTTACCTGT AGGTGCGATA CCATCGTATC ATGTGAAGGG TACGTAGTTA AGAAAATCAC
```

```
 961 TATGTGCCCC GGCCTGTACG GTAAAACGGT AGGGTACGCC GTGACGTATC ACGCGGAGGG
1021 ATTCCTAGTG TGCAAGACCA CAGACACTGT CAAAGGAGAA AGAGTCTCAT TCCCTGTATG
1081 CACCTACGTC CCCTCAACCA TCTGTGATCA AATGACTGGC ATACTAGCGA CCGACGTCAC
1141 ACCGGAGGAC GCACAGAAGT TGTTAGTGGG ATTGAATCAG AGGATAGTTG TGAACGGAAG
1201 AACACAGCGA AACACTAACA CGATGAAGAA CTATCTGCTT CCGATTGTGG CCGTCGCATT
1261 TAGCAAGTGG GCGAGGGAAT ACAAGGCAGA CCTTGATGAT GAAAAACCTC TGGGTGTCCG
1321 AGAGAGGTCA CTTACTTGCT GCTGCTTGTG GGCATTTAAA ACGAGGAAGA TGCACACCAT
1381 GTACAAGAAA CCAGACACCC AGACAATAGT GAAGGTGCCT TCAGAGTTTA ACTCGTTCGT
1441 CATCCCGAGC CTATGGTCTA CAGGCCTCGC AATCCCAGTC AGATCACGCA TTAAGATGCT
1501 TTTGGCCAAG AAGACCAAGC GAGAGTTAAT ACCTGTTCTC GACGCGTCGT CAGCCAGGGA
1561 TGCTGAACAA GAGGAGAAGG AGAGGTTGGA GGCCGAGCTG ACTAGAGAAG CCTTACCACC
1621 CCTCGTCCCC ATCGCGCCGG CGGAGACGGG AGTCGTCGAC GTCGACGTTG AAGAACTAGA
1681 GTATCACGCA GGTGCAGGGG TCGTGGAAAC ACCTCGCAGC GCGTTGAAAG TCACCGCACA
1741 GCCGAACGAC GTACTACTAG GAAATTACGT AGTTCTGTCC CCGCAGACCG TGCTCAAGAG
1801 CTCCAAGTTG GCCCCCGTGC ACCCTCTAGC AGAGCAGGTG AAAATAATAA CACATAACGG
1861 GAGGGCCGGC GGTTACCAGG TCGACGGATA TGACGGCAGG GTCCTACTAC CATGTGGATC
1921 GGCCATTCCG GTCCCTGAGT TTCAAGCTTT GAGCGAGAGC GCCACTATGG TGTACAACGA
1981 AAGGGAGTTC GTCAACAGGA AACTATACCA TATTGCCGTT CACGGACCGT CGCTGAACAC
2041 CGACGAGGAG AACTACGAGA AAGTCAGAGC TGAAAGAACT GACGCCGAGT ACGTGTTCGA
2101 CGTAGATAAA AAATGCTGCG TCAAGAGAGA GGAAGCGTCG GGTTTGGTGT TGGTGGGAGA
2161 GCTAACCAAC CCCCCGTTCC ATGAATTCGC CTACGAAGGG CTGAAGATCA GGCCGTCGGC
2221 ACCATATAAG ACTACAGTAG TAGGAGTCTT TGGGGTTCCG GGATCAGGCA AGTCTGCTAT
2281 TATTAAGAGC CTCGTGACCA AACACGATCT GGTCACCAGC GGCAAGAAGG AGAACTGCCA
2341 GGAAATAGTT AACGACGTGA AGAAGCACCG CGGGAAGGGG ACAAGTAGGG AAAACAGTGA
2401 CTCCATCCTG CTAAACGGGT GTCGTCGTGC CGTGGACATC CTATATGTGG ACGAGGCTTT
2461 CGCTAGCCAT TCCGGTACTC TGCTGGCCCT AATTGCTCTT GTTAAACCTC GGAGCAAAGT
2521 GGTGTTATGC GGAGACCCCA AGCAATGCGG ATTCTTCAAT ATGATGCAGC TTAAGGTGAA
2581 CTTCAACCAC AACATCTGCA CTGAAGTATG TCATAAAAGT ATATCCAGAC GTTGCACGCG
2641 TCCAGTCACG GCCATCGTGT CTACGTTGCA CTACGGAGGC AAGATGCGCA CGACCAACCC
2701 GTGCAACAAA CCCATAATCA TAGACACCAC AGGACAGACC AAGCCCAAGC CAGGAGACAT
2761 CGTGTTAACA TGCTTCCGAG GCTGGGCAAA GCAGCTGCAG TTGGACTACC GTGGACACGA
2821 AGTCATGACA GCAGCAGCAT CTCAGGGCCT CACCCGCAAA GGGGTATACG CCGTAAGGCA
2881 GAAGGTGAAT GAAAATCCCT TGTATGCCCC TGCGTCGGAG CACGTGAATG TACTGCTGAC
2941 GCGCACTGAG GATAGGCTGG TGTGGAAAAC GCTGGCCGGC GATCCCTGGA TTAAGGTCCT
```

3001 ATCAAACATT CCACAGGGTA ACTTTACGGC CACATTGGAA GAATGGCAAG AAGAACACGA
3061 CAAAATAATG AAGGTGATTG AAGGACCGGC TGCGCCTGTG GACGCGTTCC AGAACAAAGC
3121 GAACGTGTGT TGGGCGAAAA GCCTGGTGCC TGTCCTGGAC ACTGCCGGAA TCAGATTGAC
3181 AGCAGAGGAG TGGAGCACCA TAATTACAGC ATTTAAGGAG GACAGAGCTT ACTCTCCAGT
3241 GGTGGCCTTG AATGAAATTT GCACCAAGTA CTATGGAGTT GACCTGGACA GTGGCCTGTT
3301 TTCTGCCCCG AAGGTGTCCC TGTATTACGA GAACAACCAC TGGGATAACA GACCTGGTGG
3361 AAGGATGTAT GGATTCAATG CCGCAACAGC TGCCAGGCTG GAAGCTAGAC ATACCTTCCT
3421 GAAGGGGCAG TGGCATACGG GCAAGCAGGC AGTTATCGCA GAAAGAAAAA TCCAACCGCT
3481 TTCTGTGCTG GACAATGTAA TTCCTATCAA CCGCAGGCTG CCGCACGCCC TGGTGGCTGA
3541 GTACAAGACG GTTAAAGGCA GTAGGGTTGA GTGGCTGGTC AATAAAGTAA GAGGGTACCA
3601 CGTCCTGCTG GTGAGTGAGT ACAACCTGGC TTTGCCTCGA CGCAGGGTCA CTTGGTTGTC
3661 ACCGCTGAAT GTCACAGGCG CCGATAGGTG CTACGACCTA AGTTTAGGAC TGCCGGCTGA
3721 CGCCGGCAGG TTCGACTTGG TCTTTGTGAA CATTCACACG GAATTCAGAA TCCACCACTA
3781 CCAGCAGTGT GTCGACCACG CCATGAAGCT GCAGATGCTT GGGGGAGATG CGCTACGACT
3841 GCTAAAACCC GGCGGCATCT TGATGAGAGC TTACGGATAC GCCGATAAAA TCAGCGAAGC
3901 CGTTGTTTCC TCCTTAAGCA GAAAGTTCTC GTCTGCAAGA GTGTTGCGCC CGGATTGTGT
3961 CACCAGCAAT ACAGAAGTGT TCTTGCTGTT CTCCAACTTT GACAACGGAA AGAGACCCTC
4021 TACGCTACAC CAGATGAATA CCAAGCTGAG TGCCGTGTAT GCCGGAGAAG CCATGCACAC
4081 GGCCGGGTGT GCACCATCCT ACAGAGTTAA GAGAGCAGAC ATAGCCACGT GCACAGAAGC
4141 GGCTGTGGTT AACGCAGCTA ACGCCCGTGG AACTGTAGGG GATGGCGTAT GCAGGGCCGT
4201 GGCGAAGAAA TGGCCGTCAG CCTTTAAGGG AGCAGCAACA CCAGTGGGCA CAATTAAAAC
4261 AGTCATGTGC GGCTCGTACC CCGTCATCCA CGCTGTAGCG CCTAATTTCT CTGCCACGAC
4321 TGAAGCGGAA GGGGACCGCG AATTGGCCGC TGTCTACCGG GCAGTGGCCG CCGAAGTAAA
4381 CAGACTGTCA CTGAGCAGCG TAGCCATCCC GCTGCTGTCC ACAGGAGTGT TCAGCGGCGG
4441 AAGAGATAGG CTGCAGCAAT CCCTCAACCA TCTATTCACA GCAATGGACG CCACGGACGC
4501 TGACGTGACC ATCTACTGCA GAGACAAAAG TTGGGAGAAG AAAATCCAGG AAGCCATTGA
4561 CATGAGGACG GCTGTGGAGT TGCTCAATGA TGACGTGGAG CTGACCACAG ACTTGGTGAG
4621 AGTGCACCCG GACAGCAGCC TGGTGGGTCG TAAGGGCTAC AGTACCACTG ACGGGTCGCT
4681 GTACTCGTAC TTTGAAGGTA CGAAATTCAA CCAGGCTGCT ATTGATATGG CAGAGATACT
4741 GACGTTGTGG CCCAGACTGC AAGAGGCAAA CGAACAGATA TGCCTATACG CGCTGGGCGA
4801 AACAATGGAC AACATCAGAT CCAAATGTCC GGTGAACGAT TCCGATTCAT CAACACCTCC
4861 CAGGACAGTG CCCTGCCTGT GCCGCTACGC AATGACAGCA GAACGGATCG CCCGCCTTAG
4921 GTCACACCAA GTTAAAAGCA TGGTGGTTTG CTCATCTTTT CCCCTCCCGA AATACCATGT
4981 AGATGGGGTG CAGAAGGTAA AGTGCGAGAA GGTTCTCCTG TTCGACCCGA CGGTACCTTC

5041 AGTGGTTAGT CCGCGGAAGT ATGCCGCATC TACGACGGAC CACTCAGATC GGTCGTTACG
5101 AGGGTTTGAC TTGGACTGGA CCACCGACTC GTCTTCCACT GCCAGCGATA CCATGTCGCT
5161 ACCCAGTTTG CAGTCGTGTG ACATCGACTC GATCTACGAG CCAATGGCTC CCATAGTAGT
5221 GACGGCTGAC GTACACCCTG AACCCGCAGG CATCGCGGAC CTGGCGGCAG ATGTGCATCC
5281 TGAACCCGCA GACCATGTGG ACCTGGAGAA CCCGATTCCT CCACCGCGCC CGAAGAGAGC
5341 TGCATACCTT GCCTCCCGCG CGGCGGAGCG ACCAGTGCCG GCGCCGAGAA AGCCGACGCC
5401 TGCCCCAAGG ACTGCGTTTA GGAACAAGCT GCCTTTGACG TTCGGCGACT TTGACGAGCA
5461 CGAGGTCGAT GCGTTGGCCT CCGGGATTAC TTTCGGAGAC TTCGACGACG TCCTGCGACT
5521 AGGCCGCGCG GGTGCATATA TTTTCTCCTC GGACACTGGC AGCGGACATT TACAACAAAA
5581 ATCCGTTAGG CAGCACAATC TCCAGTGCGC ACAACTGGAT GCGGTCGAGG AGGAGAAAAT
5641 GTACCCGCCA AAATTGGATA CTGAGAGGGA GAAGCTGTTG CTGCTGAAAA TGCAGATGCA
5701 CCCATCGGAG GCTAATAAGA GTCGATACCA GTCTCGCAAA GTGGAGAACA TGAAAGCCAC
5761 GGTGGTGGAC AGGCTCACAT CGGGGGCCAG ATTGTACACG GGAGCGGACG TAGGCCGCAT
5821 ACCAACATAC GCGGTTCGGT ACCCCCGCCC CGTGTACTCC CCTACCGTGA TCGAAAGATT
5881 CTCAAGCCCC GATGTAGCAA TCGCAGCGTG CAACGAATAC CTATCCAGAA ATTACCCAAC
5941 AGTGGCGTCG TACCAGATAA CAGATGAATA CGACGCATAC TTGGACATGG TTGACGGGTC
6001 GGATAGTTGC TTGGACAGAG CGACATTCTG CCCGGCGAAG CTCCGGTGCT ACCCGAAACA
6061 TCATGCGTAC CACCAGCCGA CTGTACGCAG TGCCGTCCCG TCACCCTTTC AGAACACACT
6121 ACAGAACGTG CTAGCAGCCG CCACCAAGAG AAACTGCAAC GTCACGCAAA TGCGAGAACT
6181 ACCCACCATG GACTCGGCAG TGTTCAACGT GGAGTGCTTC AAGCGCTATG CCTGCTCCGG
6241 AGAATATTGG GAAGAATATG CTAAACAACC TATCCGGATA ACCACTGAGA ACATCACTAC
6301 CTATGTGACC AAATTGAAAG GCCCGAAAGC TGCTGCCTTG TTCGCTAAGA CCCACAACTT
6361 GGTTCCGCTG CAGGAGGTTC CCATGGACAG ATTCACGGTC GACATGAAAC GAGATGTCAA
6421 AGTCACTCCA GGGACGAAAC ACACAGAGGA AAGACCCAAA GTCCAGGTAA TTCAAGCAGC
6481 GGAGCCATTG GCGACCGCTT ACCTGTGCGG CATCCACAGG GAATTAGTAA GGAGACTAAA
6541 TGCTGTGTTA CGCCCTAACG TGCACACATT GTTTGATATG TCGGCCGAAG ACTTTGACGC
6601 GATCATCGCC TCTCACTTCC ACCCAGGAGA CCCGGTACTA GAGACGGACA TTGCATCATT
6661 CGACAAAAGC CAGGACGACT CCTTGGCTCT TACAGGTTTA ATGATCCTCG AAGATCTAGG
6721 GGTGGATCAG TACCTGCTGG ACTTGATCGA GGCAGCCTTT GGGGAAATAT CCAGCTGTCA
6781 CCTACCAACT GGCACGCGCT TCAAGTTCGG AGCTATGATG AAATCGGGCA TGTTTCTGAC
6841 TTTGTTTATT AACACTGTTT TGAACATCAC CATAGCAAGC AGGGTACTGG AGCAGAGACT
6901 CACTGACTCC GCCTGTGCGG CCTTCATCGG CGACGACAAC ATCGTTCACG GAGTGATCTC
6961 CGACAAGCTG ATGGCGGAGA GGTGCGCGTC GTGGGTCAAC ATGGAGGTGA AGATCATTGA
7021 CGCTGTCATG GGCGAAAAAC CCCCATATTT TTGTGGGGGA TTCATAGTTT TTGACAGCGT

```
7081 CACACAGACC GCCTGCCGTG TTTCAGACCC ACTTAAGCGC CTGTTCAAGT TGGGTAAGCC
7141 GCTAACAGCT GAAGACAAGC AGGACGAAGA CAGGCGACGA GCACTGAGTG ACGAGGTTAG
7201 CAAGTGGTTC CGGACAGGCT TGGGGGCCGA ACTGGAGGTG GCACTAACAT CTAGGTATGA
7261 GGTAGAGGGC TGCAAAAGTA TCCTCATAGC CATGGCCACC TTGGCGAGGG ACATTAAGGC
7321 GTTTAAGAAA TTGAGAGGAC CTGTTATACA CCTCTACGGC GGTCCTAGAT TGGTGCGTTA
7381 ATACACAGAA TTCTGATTGG ATCCCGGGCT CGAGCTCAAG CTTCGAATTC ATGGGTGTCG
7441 CAGATTTGAT CAAGAAATTC GAAAGCATCT CAAAGGAAGA AGGGGATCCA CCGGTCGCCA
7501 CCATGGTGAG CAAGGGCGAG GAGCTGTTCA CCGGGGTGGT GCCCATCCTG GTCGAGCTGG
7561 ACGGCGACGT AAACGGCCAC AAGTTCAGCG TGTCCGGCGA GGGCGAGGGC GATGCCACCT
7621 ACGGCAAGCT GACCCTGAAG TTCATCTGCA CCACCGGCAA GCTGCCCGTG CCCTGGCCCA
7681 CCCTCGTGAC CACCTTCGGC TACGGCCTGC AGTGCTTCGC CCGCTACCCC GACCACATGA
7741 AGCAGCACGA CTTCTTCAAG TCCGCCATGC CCGAAGGCTA CGTCCAGGAG CGCACCATCT
7801 TCTTCAAGGA CGACGGCAAC TACAAGACCC GCGCCGAGGT GAAGTTCGAG GGCGACACCC
7861 TGGTGAACCG CATCGAGCTG AAGGGCATCG ACTTCAAGGA GGACGGCAAC ATCCTGGGGC
7921 ACAAGCTGGA GTACAACTAC AACAGCCACA ACGTCTATAT CATGGCCGAC AAGCAGAAGA
7981 ACGGCATCAA GGTGAACTTC AAGATCCGCC ACAACATCGA GGACGGCAGC GTGCAGCTCG
8041 CCGACCACTA CCAGCAGAAC ACCCCCATCG GCGACGGCCC CGTGCTGCTG CCCGACAACC
8101 ACTACCTGAG CTACCAGTCC GCCCTGAGCA AAGACCCCAA CGAGAAGCGC GATCACATGG
8161 TCCTGCTGGA GTTCGTGACC GCCGCCGGGA TCACTCTCGG CATGGACGAG CTGTACAAGT
8221 AAAGCGGCCG CAGGGTAATT AATTGAATTA CATCCCTACG CAAACGTTTT ACGGCCGCCG
8281 GTGGCGCCCG CGCCCGGCGG CCCGTCCTTG GCCGTTGCAG GCCACTCCGG TGGCTCCCGT
8341 CGTCCCCGAC TTCCAGGCCC AGCAGATGCA GCAACTCATC AGCGCCGTAA ATGCGCTGAC
8401 AATGAGACAG AACGCAATTG CTCCTGCTAG GCCTCCCAAA CCAAAGAAGA AGAAGACAAC
8461 CAAACCAAAG CCGAAAACGC AGCCCAAGAA GATCAACGGA AAAACGCAGC AGCAAAAGAA
8521 GAAAGACAAG CAAGCCGACA AGAAGAAGAA GAAACCCGGA AAAAGAGAAA GAATGTGCAT
8581 GAAGATTGAA AATGACTGTA TCTTCGTATG CGGCTAGCCA CAGTAACGTA GTGTTTCCAG
8641 ACATGTCGGG CACCGCACTA TCATGGGTGC AGAAAATCTC GGGTGGTCTG GGGGCCTTCG
8701 CAATCGGCGC TATCCTGGTG CTGGTTGTGG TCACTTGCAT TGGGCTCCGC AGATAAGTTA
8761 GGGTAGGCAA TGGCATTGAT ATAGCAAGAA AATTGAAAAC AGAAAAAGTT AGGGTAAGCA
8821 ATGGCATATA ACCATAACTG TATAACTTGT AACAAAGCGC AACAAGACCT GCGCAATTGG
8881 CCCCGTGGTC CGCCTCACGG AAACTCGGGG CAACTCATAT TGACACATTA ATTGGCAATA
8941 ATTGGAAGCT TACATAAGCT TAATTCGACG AATAATTGGA TTTTTATTTT ATTTTGCAAT
9001 TGGTTTTTAA TATTTCCAAA AAAAAAAAAA AAAAAAAAAA AAAAAAAAAA AAAAAAAAAA
9061 AAAAAAAAAA AAAAAAAAAA AAAAAAACTA GTGATCATAA TCAGCCATAC CACATTTGTA
```

```
 9121 GAGGTTTTAC TTGCTTTAAA AAACCTCCCA CACCTCCCCC TGAACCTGAA ACATAAAATG
 9181 AATGCAATTG TTGTTGTTAA CTTGTTTATT GCAGCTTATA ATGGTTACAA ATAAAGCAAT
 9241 AGCATCACAA ATTTCACAAA TAAAGCATTT TTTTCACTGC ATTCTAGTTG TGGTTTGTCC
 9301 AAACTCATCA ATGTATCTTA TCATGTCTGG ATCTAGTCTG CATTAATGAA TCGGCCAACG
 9361 CGCGGGGAGA GGCGGTTTGC GTATTGGGCG CTCTTCCGCT TCCTCGCTCA CTGACTCGCT
 9421 GCGCTCGGTC GTTCGGCTGC GGCGAGCGGT ATCAGCTCAC TCAAAGGCGG TAATACGGTT
 9481 ATCCACAGAA TCAGGGGATA ACGCAGGAAA GAACATGTGA GCAAAAGGCC AGCAAAAGGC
 9541 CAGGAACCGT AAAAAGGCCG CGTTGCTGGC GTTTTTCCAT AGGCTCCGCC CCCCTGACGA
 9601 GCATCACAAA AATCGACGCT CAAGTCAGAG GTGGCGAAAC CCGACAGGAC TATAAAGATA
 9661 CCAGGCGTTT CCCCCTGGAA GCTCCCTCGT GCGCTCTCCT GTTCCGACCC TGCCGCTTAC
 9721 CGGATACCTG TCCGCCTTTC TCCCTTCGGG AAGCGTGGCG CTTTCTCAAT GCTCGCGCTG
 9781 TAGGTATCTC AGTTCGGTGT AGGTCGTTCG CTCCAAGCTG GGCTGTGTGC ACGAACCCCC
 9841 CGTTCAGCCC GACCGCTGCG CCTTATCCGG TAACTATCGT CTTGAGTCCA ACCCGGTAAG
 9901 ACACGACTTA TCGCCACTGG CAGCAGCCAC TGGTAACAGG ATTAGCAGAG CGAGGTATGT
 9961 AGGCGGTGCT ACAGAGTTCT TGAAGTGGTG GCCTAACTAC GGCTACACTA GAAGGACAGT
10021 ATTTGGTATC TGCGCTCTGC TGAAGCCAGT TACCTTCGGA AAAAGAGTTG GTAGCTCTTG
10081 ATCCGGCAAA CAAACCACCG CTGGTAGCGG TGGTTTTTTT GTTTGCAAGC AGCAGATTAC
10141 GCGCAGAAAA AAAGGATCTC AAGAAGATCC TTTGATCTTT TCTACGGGGC ATTCTGACGC
10201 TCAGTGGAAC GAAAACTCAC GTTAAGGGAT TTTGGTCATG AGATTATCAA AAAGGATCTT
10261 CACCTAGATC CTTTTAAATT AAAAATGAAG TTTTAAATCA ATCTAAAGTA TATATGAGTA
10321 AACTTGGTCT GACAGTTACC AATGCTTAAT CAGTGAGGCA CCTATCTCAG CGATCTGTCT
10381 ATTTCGTTCA TCCATAGTTG CCTGACTCCC CGTCGTGTAG ATAACTACGA TACGGGAGGG
10441 CTTACCATCT GGCCCCAGTG CTGCAATGAT ACCGCGAGAC CCACGCTCAC CGGCTCCAGA
10501 TTTATCAGCA ATAAACCAGC CAGCCGGAAG GGCCGAGCGC AGAAGTGGTC CTGCAACTTT
10561 ATCCGCCTCC ATCCAGTCTA TTAATTGTTG CCGGGAAGCT AGAGTAAGTA GTTCGCCAGT
10621 TAATAGTTTG CGCAACGTTG TTGCCATTGC TACAGGCATC GTGGTGTCAC GCTCGTCGTT
10681 TGGTATGGCT TCATTCAGCT CCGGTTCCCA ACGATCAAGG CGAGTTACAT GATCCCCCAT
10741 GTTGTGCAAA AAAGCGGTTA GCTCCTTCGG TCCTCCGATC GTTGTCAGAA GTAAGTTGGC
10801 CGCAGTGTTA TCACTCATGG TTATGGCAGC ACTGCATAAT TCTCTTACTG TCATGCCATC
10861 CGTAAGATGC TTTTCTGTGA CTGGTGAGTA CTCAACCAAG TCATTCTGAG AATAGTGTAT
10921 GCGGCGACCG AGTTGCTCTT GCCCGGCGTC AATACGGGAT AATACCGCGC CACATAGCAG
10981 AACTTTAAAA GTGCTCATCA TTGGAAAACG TTCTTCGGGG CGAAAACTCT CAAGGATCTT
11041 ACCGCTGTTG AGATCCAGTT CGATGTAACC CACTCGTGCA CCCAACTGAT CTTCAGCATC
11101 TTTTACTTTC ACCAGCGTTT CTGGGTGAGC AAAAACAGGA AGGCAAAATG CCGCAAAAAA
```

```
11161 GGGAATAAGG GCGACACGGA AATGTTGAAT ACTCATACTC TTCCTTTTTC AATATTATTG
11221 AAGCATTTAT CAGGGTTATT GTCTCATGAG CGGATACATA TTTGAATGTA TTTAGAAAAA
11281 TAAACAAATA GGGGTTCCGC GCACATTTCC CCGAAAAGTG CCACCTGACG TCTAAGAAAC
11341 CATTATTATC ATGACATTAA CCTATAAAAA TAGGCGTATC ACGAGGCCCT TTCGTCTCGC
11401 GCGTTTCGGT GATGACGGTG AAAACCTCTG ACACATGCAG CTCCCGGAGA CGGTCACAGC
11461 TTCTGTCTAA GCGGATGCCG GGAGCAGACA AGCCCGTCAG GGCGCGTCAG CGGGTGTTGG
11521 CGGGTGTCGG GGCTGGCTTA ACTATGCGGC ATCAGAGCAG ATTGTACTGA GAGTGCACCA
11581 TATCGACGCT CTCCCTTATG CGACTCCTGC ATTAGGAAGC AGCCCAGTAC TAGGTTGAGG
11641 CCGTTGAGCA CCGCCGCCGC AAGGAATGGT GCATGCGTAA TCAATTACGG GGTCATTAGT
11701 TCATAGCCCA TATATGGAGT TCCGCGTTAC ATAACTTACG GTAAATGGCC CGCCTGGCTG
11761 ACCGCCCAAC GACCCCCGCC CATTGACGTC AATAATGACG TATGTTCCCA TAGTAACGCC
11821 AATAGGGACT TTCCATTGAC GTCAATGGGT GGAGTATTTA CGGTAAACTG CCCACTTGGC
11881 AGTACATCAA GTGTATCATA TGCCAAGTAC GCCCCCTATT GACGTCAATG ACGGTAAATG
11941 GCCCGCCTGG CATTATGCCC AGTACATGAC CTTATGGGAC TTTCCTACTT GGCAGTACAT
12001 CTACGTATTA GTCATCGCTA TTACCATGGT GATGCGGTTT TGGCAGTACA TCAATGGGCG
12061 TGGATAGCGG TTTGACTCAC GGGGATTTCC AAGTCTCCAC CCCATTGACG TCAATGGGAG
12121 TTTGTTTTGG CACCAAAATC AACGGGACTT TCCAAAATGT CGTAACAACT CCGCCCCATT
12181 GACGCAAATG GGCGGTAGGC GTGTACGGTG GGAGGTCTAT ATAAGCAGAG CTCTCTGGCT
12241 AACTAGAGAA CCCACTGCTT AACTGGCTTA TCGAAATTAA TACGACTCAC TATAGGGAGA
12301 CCGGAAGCTT GAATTC
```

Bibliography

Abbe, E. (1873). Beiträge zur Theorie des Mikroskops und der mikroskopischen Wahrnehmung. *Archiv für Mikroskopische Anatomie*, 9(1):413–418. Available from: http://link.springer.com/10.1007/BF02956173.

Abràmoff, M., Magalhães, P. J., and Ram, S. J. (2004). Image processing with ImageJ. *Biophotonics International*, 11(7):36–42. Available from: http://igitur-archive.library.uu.nl/med/2011-0512-200507/UUindex.html.

Albantakis, L. and Lohmann, C. (2009). A simple method for quantitative calcium imaging in unperturbed developing neurons. *Journal of Neuroscience Methods*, 184(2):206–12. Available from: http://dx.doi.org/10.1016/j.jneumeth.2009.08.004.

Alvarez, V. A. and Sabatini, B. L. (2007). Anatomical and physiological plasticity of dendritic spines. *Annual Review of Neuroscience*, 30:79–97. Available from: http://www.ncbi.nlm.nih.gov/pubmed/17280523.

Amaral, D. and Lavenex, P. (2006). Hippocampal Neuroanatomy. In Andersen, P., Morris, R., Amaral, D., Bliss, T., and OKeefe, J., editors, *The Hippocampus Book*. Oxford University Press, USA.

Andersen, P., Bliss, T., and Skrede, K. (1971). Lamellar organization of hippocampal excitatory pathways. *Experimental Brain Research*, 13(2):222–238. Available from: http://dx.doi.org/10.1007/BF00234087.

Andersen, P. and Soleng, A. F. (1998). Long-term potentiation and spatial training are both associated with the generation of new excitatory synapses. *Brain Research. Brain Research Reviews*, 26(2-3):353–9. Available from: http://www.ncbi.nlm.nih.gov/pubmed/9651551.

Aniksztejn, L. and Ben-Ari, Y. (1991). Novel form of long-term potentiation produced by a K+ channel blocker in the hippocampus. *Nature*, 349(6304):67–9. Available from: http://dx.doi.org/10.1038/349067a0.

Arellano, J. I., Benavides-Piccione, R., Defelipe, J., and Yuste, R. (2007). Ultrastructure of dendritic spines: correlation between synaptic and spine morphologies. *Frontiers in Neuroscience*, 1(1):131–43. Available from: http://www.pubmedcentral.nih.gov/articlerender.fcgi?artid=2518053&tool=pmcentrez&rendertype=abstract.

Auksorius, E., Boruah, B. R., Dunsby, C., Lanigan, P. M. P., Kennedy, G., Neil, M. A. A., and French, P. M. W. (2008). Stimulated emission depletion microscopy with a supercontinuum source and fluorescence lifetime imaging. *Optics Letters*, 33(2):113–5. Available from: http://www.ncbi.nlm.nih.gov/pubmed/18197209.

Baker, R. and Llinás, R. (1971). Electrotonic coupling between neurones in the rat mesencephalic nucleus. *The Journal of Physiology*, 212(1):45–63. Available from: http://www.pubmedcentral.nih.gov/articlerender.fcgi?artid=1395705&tool=pmcentrez&rendertype=abstract.

Bates, M., Huang, B., Dempsey, G. T., and Zhuang, X. (2007). Multicolor super-resolution imaging with photo-switchable fluorescent probes. *Science*, 317(5845):1749–53. Available from: http://www.sciencemag.org/content/317/5845/1749.

Berning, S., Willig, K. I., Steffens, H., Dibaj, P., and Hell, S. W. (2012). Nanoscopy in a Living Mouse Brain. *Science*, 335(6068):551–551. Available from: http://www.sciencemag.org/content/335/6068/551.abstract.

Bethge, P., Chéreau, R., Avignone, E., Marsicano, G., and Nägerl, U. V. (2013). Two-photon excitation STED microscopy in two colors in acute brain slices. *Biophysical Journal*, 104(4):778–85. Available from: http://www.ncbi.nlm.nih.gov/pubmed/23442956.

Betzig, E. (1995). Proposed method for molecular optical imaging. *Optics Letters*, 20(3):237–9. Available from: http://www.ncbi.nlm.nih.gov/pubmed/19859146.

Betzig, E., Patterson, G. H., Sougrat, R., Lindwasser, O. W., Olenych, S., Bonifacino, J. S., Davidson, M. W., Lippincott-Schwartz, J., and Hess, H. F. (2006). Imaging intracellular fluorescent proteins at nanometer resolution. *Science*, 313(5793):1642–5. Available from: http://www.sciencemag.org/content/313/5793/1642.abstract.

Bishop, D., Nikić, I., Brinkoetter, M., Knecht, S., Potz, S., Kerschensteiner, M., and Misgeld, T. (2011). Near-infrared branding efficiently correlates light and electron microscopy. *Nature Methods*, 8(7):568–70. Available from: http://dx.doi.org/10.1038/nmeth.1622.

Bliss, T. V. and Collingridge, G. L. (1993). A synaptic model of memory: long-term potentiation in the hippocampus. *Nature*, 361(6407):31–9. Available from: http://www.ncbi.nlm.nih.gov/pubmed/8421494.

Bliss, T. V. and Lomo, T. (1973). Long-lasting potentiation of synaptic transmission in the dentate area of the anaesthetized rabbit following stimulation of the perforant path. *The Journal of Physiology*, 232(2):331–56. Available from: http://www.pubmedcentral.nih.gov/articlerender.fcgi?artid=1350458&tool=pmcentrez&rendertype=abstract.

Bobroff, N. (1986). Position measurement with a resolution and noise-limited instrument. *Review of Scientific Instruments*, 57(6):1152. Available from: http://scitation.aip.org/content/aip/journal/rsi/57/6/10.1063/1.1138619.

Bonhoeffer, T. and Yuste, R. (2002). Spine motility. Phenomenology, mechanisms, and function. *Neuron*, 35(6):1019–27. Available from: http://www.ncbi.nlm.nih.gov/pubmed/12354393.

Bosch, M. and Hayashi, Y. (2011). Structural plasticity of dendritic spines. *Current Opinion in Neurobiology*, 22(3):383–8. Available from: http://www.ncbi.nlm.nih.gov/pubmed/21963169.

Bourne, J. and Harris, K. M. (2007). Do thin spines learn to be mushroom spines that remember? *Current Opinion in Neurobiology*, 17(3):381–6. Available from: http://dx.doi.org/10.1016/j.conb.2007.04.009.

Bourne, J. N. and Harris, K. M. K. (2001). Dendritic Spines. In *eLS*, pages 1–7. John Wiley & Sons, Ltd. Available from: http://dx.doi.org/10.1002/9780470015902.a0000093.pub2.

Bozdagi, O., Shan, W., Tanaka, H., Benson, D. L., and Huntley, G. W. (2000). Increasing numbers of synaptic puncta during late-phase LTP: N-cadherin is synthesized, recruited to synaptic sites, and required for potentiation. *Neuron*, 28(1):245–59. Available from: http://www.ncbi.nlm.nih.gov/pubmed/11086998.

Bozdagi, O., Wang, X.-b., Nikitczuk, J. S., Anderson, T. R., Bloss, E. B., Radice, G. L., Zhou, Q., Benson, D. L., and Huntley, G. W. (2010). Persistence of coordinated long-term potentiation and dendritic spine enlargement at mature hippocampal CA1 synapses requires N-cadherin. *The Journal of Neuroscience*, 30(30):9984–9. Available from: http://www.pubmedcentral.nih.gov/articlerender.fcgi?artid=2921177&tool=pmcentrez&rendertype=abstract.

Braitenberg, V. (2007). Brain. *Scholarpedia*, 2(11):2918. Available from: http://www.scholarpedia.org/article/Brain.

Bretschneider, S., Eggeling, C., and Hell, S. W. (2007). Breaking the diffraction barrier in fluorescence microscopy by optical shelving. *Physical Review Letters*, 98(21):218103. Available from: http://www.ncbi.nlm.nih.gov/pubmed/17677813.

Brightman, M. W. and Reese, T. S. (1969). Junctions between intimately apposed cell membranes in the vertebrate brain. *The Journal of Cell Biology*, 40(3):648–77. Available from: http://www.pubmedcentral.nih.gov/articlerender.fcgi?artid=2107650&tool=pmcentrez&rendertype=abstract.

Buckby, L. E., Mummery, R., Crompton, M. R., Beesley, P. W., and Empson, R. M. (2004). Comparison of neuroplastin and synaptic marker protein expression in acute and cultured organotypic hippocampal slices from rat. *Brain Research. Developmental Brain Research*, 150(1):1–7. Available from: http://www.ncbi.nlm.nih.gov/pubmed/15126032.

Bückers, J., Wildanger, D., Vicidomini, G., Kastrup, L., and Hell, S. W. (2011). Simultaneous multi-lifetime multi-color STED imaging for colocalization analyses. *Optics Express*, 19(4):3130. Available from: http://www.opticsexpress.org/abstract.cfm?URI=oe-19-4-3130.

Burns, D. H., Callis, J. B., Christian, G. D., and Davidson, E. R. (1985). Strategies for attaining superresolution using spectroscopic data as constraints. *Applied Optics*, 24(2):154. Available from: http://ao.osa.org/abstract.cfm?URI=ao-24-2-154.

Buzsaki, G. (2011). Hippocampus. *Scholarpedia*, 6(1):1468. Available from: http://www.scholarpedia.org/article/Hippocampus.

Cagnet, M., Françon, M., and Thrierr, J. C. (1962). *Atlas optischer Erscheinungen / Atlas de phénomènes doptique / Atlas of optical phenomena*. Springer Berlin Heidelberg. Available from: http://link.springer.com/10.1007/978-3-642-47385-2.

Cajal, S. R. y. (1899). *Textura del sistema nervioso del hombre y de los vertebrados: Estudios sobre el plan estructural y composicíon histológica de los centros nerviosos adicionados de consideraciones fisiológicas fundadas en los nuevos descubrimientos*. Madrid, Moya, primera edition.

Cajal, S. R. y. (1952). *Histologie du Systeme Nerveux de l'homme et des Vertebres*. Madrid, Instituto Ramon y Cajal.

Callaway, E. M. and Katz, L. C. (1993). Photostimulation using caged glutamate reveals functional circuitry in living brain slices. *Proceedings of the National Academy of Sciences of the United States of America*, 90(16):7661–5. Available from: http://www.pubmedcentral.nih.gov/articlerender.fcgi?artid=47202&tool=pmcentrez&rendertype=abstract.

Calverley, R. K. and Jones, D. G. (1990). Contributions of dendritic spines and perforated synapses to synaptic plasticity. *Brain Research. Brain Research Reviews*, 15(3):215–49. Available from: http://www.ncbi.nlm.nih.gov/pubmed/2289086.

Castillo, P. E. (2012). Presynaptic LTP and LTD of excitatory and inhibitory synapses. *Cold Spring Harbor Perspectives in Biology*, 4(2):a005728. Available from: http://cshperspectives.cshlp.org/content/4/2/a005728.abstract.

Chang, F. L. and Greenough, W. T. (1984). Transient and enduring morphological correlates of synaptic activity and efficacy change in the rat hippocampal slice. *Brain Research*, 309(1):35–46. Available from: http://www.ncbi.nlm.nih.gov/pubmed/6488013.

Chen, S. Y., Bagley, J., and Marasco, W. A. (1994). Intracellular antibodies as a new class of therapeutic molecules for gene therapy. *Human Gene Therapy*, 5(5):595–601. Available from: http://www.ncbi.nlm.nih.gov/pubmed/7914435.

Chmyrov, A., Keller, J., Grotjohann, T., Ratz, M., D'Este, E., Jakobs, S., Eggeling, C., and Hell, S. W. (2013). Nanoscopy with more than 100,000 'doughnuts'. *Nature Methods*, 10(8):737–740. Available from: http://www.nature.com/doifinder/10.1038/nmeth.2556.

Collingridge, G. L., Herron, C. E., and Lester, R. A. (1988). Synaptic activation of n-methyl-d-aspartate receptors in the schaffer collateral-commissural pathway of rat hippocampus. *The Journal of Physiology*, 399(1):283–300. Available from: http://jp.physoc.org/content/399/1/283.abstract.

Collins, T. J. (2007). ImageJ for microscopy. *BioTechniques*, 43(1 Suppl):25–30. Available from: http://www.ncbi.nlm.nih.gov/pubmed/17936939.

Colonnier, M. (1968). Synaptic patterns on different cell types in the different laminae of the cat visual cortex. An electron microscope study. *Brain Research*, 9(2):268–287. Available from: http://www.sciencedirect.com/science/article/pii/0006899368902345.

Connors, B. W. and Long, M. A. (2004). Electrical synapses in the mammalian brain. *Annual Review of Neuroscience*, 27:393–418. Available from: http://www.ncbi.nlm.nih.gov/pubmed/15217338.

Cremer, C. and Cremer, T. (1978). Considerations on a laser-scanning-microscope with high resolution and depth of field. *Microscopica Acta*, 81(1):31–44. Available from: http://www.ncbi.nlm.nih.gov/pubmed/713859.

Cremer, C., Kaufmann, R., Gunkel, M., Pres, S., Weiland, Y., Müller, P., Ruckelshausen, T., Lemmer, P., Geiger, F., Degenhard, S., Wege, C., Lemmermann, N. A. W., Holtappels, R., Strickfaden, H., and Hausmann, M. (2011). Superresolution imaging of biological nanostructures by spectral precision distance microscopy. *Biotechnology Journal*, 6(9):1037–51. Available from: http://www.ncbi.nlm.nih.gov/pubmed/21910256.

Dan, Y. and Poo, M.-M. (2006). Spike timing-dependent plasticity: from synapse to perception. *Physiol Rev*, 86(3):1033–1048. Available from: http://dx.doi.org/10.1152/physrev.00030.2005.

Dani, A., Huang, B., Bergan, J., Dulac, C., and Zhuang, X. (2010). Superresolution imaging of chemical synapses in the brain. *Neuron*, 68(5):843–56. Available from: http://www.cell.com/neuron/fulltext/S0896-6273(10)00937-2.

De Simoni, A., Griesinger, C. B., and Edwards, F. A. (2003). Development of rat CA1 neurones in acute versus organotypic slices: role of experience in synaptic morphology and activity. *The Journal of Physiology*, 550(Pt 1):135–47. Available from: http://www.pubmedcentral.nih.gov/articlerender.fcgi?artid=2343027&tool=pmcentrez&rendertype=abstract.

Dean, C., Liu, H., Staudt, T., Stahlberg, M. a., Vingill, S., Bückers, J., Kamin, D., Engelhardt, J., Jackson, M. B., Hell, S. W., and Chapman, E. R. (2012). Distinct subsets of Syt-IV/BDNF vesicles are sorted to axons versus dendrites and recruited to synapses by activity. *The Journal of Neuroscience*, 32(16):5398–413. Available from: http://www.pubmedcentral.nih.gov/articlerender.fcgi?artid=3352930&tool=pmcentrez&rendertype=abstract.

Deng, S., Liu, L., Cheng, Y., Li, R., and Xu, Z. (2010). Effects of primary aberrations on the fluorescence depletion patterns of STED microscopy. *Optics Express*, 18(2):1657. Available from: http://www.opticsexpress.org/abstract.cfm?URI=oe-18-2-1657.

Denk, W. (1994). Two-photon scanning photochemical microscopy: Mapping ligand-gated ion. 91(July):6629–6633.

Denk, W. and Horstmann, H. (2004). Serial block-face scanning electron microscopy to reconstruct three-dimensional tissue nanostructure. *PLoS Biology*, 2(11):e329. Available from: http://dx.plos.org/10.1371/journal.pbio.0020329.

Dertinger, T., Colyer, R., Iyer, G., Weiss, S., and Enderlein, J. (2009). Fast, background-free, 3D super-resolution optical fluctuation imaging (SOFI). *Proceedings of the National Academy of Sciences of the United States of America*, 106(52):22287–22292. Available from: http://www.ncbi.nlm.nih.gov/pubmed/20018714.

Desmond, N. L. and Levy, W. B. (1983). Synaptic correlates of associative potentiation/depression: an ultrastructural study in the hippocampus. *Brain Research*, 265(1):21–30. Available from: http://www.ncbi.nlm.nih.gov/pubmed/6850319.

Desmond, N. L. and Levy, W. B. (1986a). Changes in the numerical density of synaptic contacts with long-term potentiation in the hippocampal dentate gyrus. *The Journal of Comparative Neurology*, 253(4):466–75. Available from: http://www.ncbi.nlm.nih.gov/pubmed/3025272.

Desmond, N. L. and Levy, W. B. (1986b). Changes in the postsynaptic density with long-term potentiation in the dentate gyrus. *The Journal of Comparative Neurology*, 253(4):476–82. Available from: http://www.ncbi.nlm.nih.gov/pubmed/3025273.

Desmond, N. L. and Levy, W. B. (1988). Synaptic interface surface area increases with long-term potentiation in the hippocampal dentate gyrus. *Brain Research*, 453(1-2):308–14. Available from: http://www.ncbi.nlm.nih.gov/pubmed/3401768.

Diaspro, A., Bianchini, P., Vicidomini, G., Faretta, M., Ramoino, P., and Usai, C. (2006). Multi-photon excitation microscopy. *Biomedical Engineering Online*, 5:36. Available from: http://www.pubmedcentral.nih.gov/articlerender.fcgi?artid=1550243&tool=pmcentrez&rendertype=abstract.

Ding, J. B., Takasaki, K. T., and Sabatini, B. L. (2009). Supraresolution imaging in brain slices using stimulated-emission depletion two-photon laser scanning microscopy. *Neuron*, 63(4):429–37. Available from: http://www.pubmedcentral.nih.gov/articlerender.fcgi?artid=2756148&tool=pmcentrez&rendertype=abstract.

Dityatev, A., Schachner, M., and Sonderegger, P. (2010). The dual role of the extracellular matrix in synaptic plasticity and homeostasis. *Nature Reviews. Neuroscience*, 11(11):735–46. Available from: http://www.ncbi.nlm.nih.gov/pubmed/20944663.

Dunaevsky, A., Tashiro, A., Majewska, A., Mason, C., and Yuste, R. (1999). Developmental regulation of spine motility in the mammalian central nervous system. *Proceedings of the National Academy of Sciences of the United States of America*, 96(23):13438–43. Available from: http://www.pubmedcentral.nih.gov/articlerender.fcgi?artid=23966&tool=pmcentrez&rendertype=abstract.

Dyba, M. (2004). *STED-4Pi Microscopy*. PhD thesis, Ruperto-Carola University of Heidelberg. Available from: http://archiv.ub.uni-heidelberg.de/volltextserver/4438/1/Dissertation_Marcus_Dyba.pdf.

Dyba, M. and Hell, S. W. (2003). Photostability of a fluorescent marker under pulsed excited-state depletion through stimulated emission. *Applied Optics*, 42(25):5123–9. Available from: http://www.ncbi.nlm.nih.gov/pubmed/12962391.

Eggeling, C., Ringemann, C., Medda, R., Schwarzmann, G., Sandhoff, K., Polyakova, S., Belov, V. N., Hein, B., von Middendorff, C., Schönle, A., and Hell, S. W. (2009). Direct observation of the nanoscale dynamics of membrane lipids in a living cell. *Nature*, 457(7233):1159–62. Available from: http://www.ncbi.nlm.nih.gov/pubmed/19098897.

Ehrengruber, M. U., Lundstrom, K., Schweitzer, C., Heuss, C., Schlesinger, S., Gähwiler, B. H., and Gahwiler, B. H. (1999). Recombinant Semliki Forest virus and Sindbis virus efficiently infect neurons in hippocampal slice cultures. *Proceedings of the National Academy of Sciences of the United States of America*, 96(12):7041–6. Available from: http://www.pnas.org.emedien.ub.uni-muenchen.de/content/96/12/7041.

Ehrlich, I., Klein, M., Rumpel, S., and Malinow, R. (2007). PSD-95 is required for activity-driven synapse stabilization. *Proceedings of the National Academy of Sciences of the United States of America*, 104(10):4176–81. Available from: http://www.pubmedcentral.nih.gov/articlerender.fcgi?artid=1820728&tool=pmcentrez&rendertype=abstract.

Engert, F. and Bonhoeffer, T. (1999). Dendritic spine changes associated with hippocampal long-term synaptic plasticity. *Nature*, 399(6731):66–70. Available from: http://www.scopus.com/inward/record.url?eid=2-s2.0-0033529082&partnerID=tZOtx3y1.

Feng, G., Mellor, R. H., Bernstein, M., Keller-Peck, C., Nguyen, Q. T., Wallace, M., Nerbonne, J. M., Lichtman, J. W., and Sanes, J. R. (2000). Imaging Neuronal Subsets in Transgenic Mice Expressing Multiple Spectral Variants of GFP. *Neuron*, 28(1):41–51. Available from: http://www.ncbi.nlm.nih.gov/pubmed/11086982.

Fiala, J. (2005). Reconstruct: a free editor for serial section microscopy. *Journal of Microscopy*, 218(April):52–61. Available from: http://onlinelibrary.wiley.com/doi/10.1111/j.1365-2818.2005.01466.x/full.

Fiala, J. C., Allwardt, B., and Harris, K. M. (2002). Dendritic spines do not split during hippocampal LTP or maturation. *Nature Neuroscience*, 5(4):297–8. Available from: http://dx.doi.org/10.1038/nn830.

Fiala, J. C., Feinberg, M., Popov, V., and Harris, K. M. (1998). Synaptogenesis via dendritic filopodia in developing hippocampal area CA1. *The Journal of Neuroscience*, 18(21):8900–11. Available from: http://www.ncbi.nlm.nih.gov/pubmed/9786995.

Fifková, E. (1985). Actin in the nervous system. *Brain Research Reviews*, 9(2):187–215. Available from: http://www.sciencedirect.com/science/article/pii/0165017385900128.

Fifková, E. and Anderson, C. L. (1981). Stimulation-induced changes in dimensions of stalks of dendritic spines in the dentate molecular layer. *Experimental Neurology*, 74(2):621–7. Available from: http://www.ncbi.nlm.nih.gov/pubmed/7297640.

Fifková, E. and Van Harreveld, A. (1977). Long-lasting morphological changes in dendritic spines of dentate granular cells following stimulation of the entorhinal area. *Journal of Neurocytology*, 6(2):211–30. Available from: http://www.ncbi.nlm.nih.gov/pubmed/856951.

Fire, A., Xu, S., Montgomery, M. K., Kostas, S. A., Driver, S. E., and Mello, C. C. (1998). Potent and specific genetic interference by double-stranded RNA in Caenorhabditis elegans. *Nature*, 391(6669):806–11. Available from: http://www.ncbi.nlm.nih.gov/pubmed/9486653.

Fischer, M., Kaech, S., Knutti, D., and Matus, A. (1998). Rapid actin-based plasticity in dendritic spines. *Neuron*, 20(5):847–54. Available from: http://www.ncbi.nlm.nih.gov/pubmed/9620690.

Fischer, M., Kaech, S., Wagner, U., Brinkhaus, H., and Matus, A. (2000). Glutamate receptors regulate actin-based plasticity in dendritic spines. *Nature Neuroscience*, 3(9):887–94. Available from: http://www.ncbi.nlm.nih.gov/pubmed/10966619.

Fölling, J., Bossi, M., Bock, H., Medda, R., Wurm, C. A., Hein, B., Jakobs, S., Eggeling, C., and Hell, S. W. (2008). Fluorescence nanoscopy by ground-state depletion and single-molecule return. *Nature Methods*, 5(11):943–5. Available from: http://dx.doi.org/10.1038/nmeth.1257.

Frost, N. A., Shroff, H., Kong, H., Betzig, E., and Blanpied, T. A. (2010). Single-molecule discrimination of discrete perisynaptic and distributed sites of actin filament assembly within dendritic spines. *Neuron*, 67(1):86–99. Available from: http://www.sciencedirect.com/science/article/pii/S0896627310004228.

Fujii, S., Sasaki, H., Mikoshiba, K., Kuroda, Y., Yamazaki, Y., Mostafa Taufiq, A., and Kato, H. (2004). A chemical LTP induced by co-activation of metabotropic and N-methyl-D-aspartate glutamate receptors in hippocampal CA1 neurons. *Brain Research*, 999(1):20–8. Available from: http://www.ncbi.nlm.nih.gov/pubmed/14746918.

Gähwiler, B. (1981). Organotypic monolayer cultures of nervous tissue. *Journal of Neuroscience Methods*, 4:329–342. Available from: http://www.sciencedirect.com/science/article/pii/0165027081900030.

Gähwiler, B. H. (1988). Organotypic cultures of neural tissue. *Trends in Neurosciences*, 11(11):484–9. Available from: http://www.ncbi.nlm.nih.gov/pubmed/2469173.

Gähwiler, B. H., Thompson, S. M., and Muller, D. (2001). Preparation and maintenance of organotypic slice cultures of CNS tissue. *Current Protocols in Neuroscience*, Chapter 6:Unit 6.11. Available from: http://www.ncbi.nlm.nih.gov/pubmed/18428510.

Geinisman, Y., DeToledo-Morrell, L., and Morrell, F. (1991). Induction of long-term potentiation is associated with an increase in the number of axospinous synapses with segmented postsynaptic densities. *Brain Research*, 566(1-2):77–88. Available from: http://www.ncbi.nlm.nih.gov/pubmed/1814558.

Gökçe, O. (2013). *Channelrhodopsin Assisted Synapse Identity Mapping Reveals Clustering of Layer 5 Intralaminar Inputs*. Phd thesis, Ludwig Maximilians University Munich.

Gordon, M., Ha, T., and Selvin, P. (2004). Single-molecule high-resolution imaging with photobleaching. *Proceedings of the National Academy of Sciences of the United States of America*, 101(17):6462–6465. Available from: http://www.pnas.org/content/101/17/6462.short.

Gray, E. G. (1959). Electron Microscopy of Synaptic Contacts on Dendrite Spines of the Cerebral Cortex. *Nature*, 183(4675):1592–1593. Available from: http://www.nature.com/nature/journal/v183/n4675/pdf/1831592a0.pdf.

Gray, N. W., Weimer, R. M., Bureau, I., and Svoboda, K. (2006). Rapid redistribution of synaptic PSD-95 in the neocortex in vivo. *PLoS Biology*, 4(11):e370. Available from: http://www.pubmedcentral.nih.gov/articlerender.fcgi?artid=1634879&tool=pmcentrez&rendertype=abstract.

Grunditz, A., Holbro, N., Tian, L., Zuo, Y., and Oertner, T. G. (2008). Spine neck plasticity controls postsynaptic calcium signals through electrical compartmentalization. *The Journal of Neuroscience*, 28(50):13457–66. Available from: http://www.ncbi.nlm.nih.gov/pubmed/19074019.

Gu, J., Lee, C. W., Fan, Y., Komlos, D., Tang, X., Sun, C., Yu, K., Hartzell, H. C., Chen, G., Bamburg, J. R., and Zheng, J. Q. (2010). ADF/cofilin-mediated actin dynamics regulate AMPA receptor trafficking during synaptic plasticity. *Nature Neuroscience*, 13(10):1208–15. Available from: http://www.nature.com/neuro/journal/v13/n10/full/nn.2634.html.

Gulley, R. L. and Reese, T. S. (1981). Cytoskeletal organization at the postsynaptic complex. *The Journal of Cell Biology*, 91(1):298–302. Available from: http://www.pubmedcentral.nih.gov/articlerender.fcgi?artid=2111925&tool=pmcentrez&rendertype=abstract.

Gunkel, M., Erdel, F., Rippe, K., Lemmer, P., Kaufmann, R., Hörmann, C., Amberger, R., and Cremer, C. (2009). Dual color localization microscopy of cellular nanostructures. *Biotechnology Journal*, 4(6):927–938. Available from: http://www.ncbi.nlm.nih.gov/pubmed/19548231.

Gustafsson, M. G. L. (2005). Nonlinear structured-illumination microscopy: wide-field fluorescence imaging with theoretically unlimited resolution. *Proceedings of the National Academy of Sciences of the United States of America*, 102(37):13081–6. Available from: http://www.pubmedcentral.nih.gov/articlerender.fcgi?artid=1201569&tool=pmcentrez&rendertype=abstract.

Haas, K., Sin, W. C., Javaherian, A., Li, Z., and Cline, H. T. (2001). Single-cell electroporation for gene transfer in vivo. *Neuron*, 29(3):583–91. Available from: http://www.ncbi.nlm.nih.gov/pubmed/11301019.

Harke, B., Keller, J., Ullal, C., and Westphal, V. (2008). Resolution scaling in STED microscopy. *Opt. Express*, 16(6):1347–1355. Available from: http://www3.mpibpc.mpg.de/groups/hell/publications/pdf/Opt._Exp._16_4154-4162.pdf.

Harms, K. J. and Dunaevsky, A. (2007). Dendritic spine plasticity: looking beyond development. *Brain Research*, 1184:65–71. Available from: http://www.ncbi.nlm.nih.gov/pubmed/16600191.

Harris, K. M., Jensen, F. E., and Tsao, B. (1992). Three-dimensional structure of dendritic spines and synapses in rat hippocampus (CA1) at postnatal day 15 and adult ages: implications for the maturation of synaptic physiology and long-term potentiation. *The Journal of Neuroscience*, 12(7):2685–705. Available from: http://www.ncbi.nlm.nih.gov/pubmed/1613552.

Harris, K. M. and Stevens, J. K. (1988). Dendritic spines of rat cerebellar Purkinje cells: serial electron microscopy with reference to their biophysical characteristics. *The Journal of Neuroscience*, 8(12):4455–69. Available from: http://www.ncbi.nlm.nih.gov/pubmed/3199186.

Harris, K. M. and Stevens, J. K. (1989). Dendritic spines of CA 1 pyramidal cells in the rat hippocampus: serial electron microscopy with reference to their biophysical characteristics. *The Journal of Neuroscience*, 9(8):2982–97. Available from: http://www.ncbi.nlm.nih.gov/pubmed/2769375.

Harris, K. M. and Sultan, P. (1995). Variation in the number, location and size of synaptic vesicles provides an anatomical basis for the nonuniform probability of release at hippocampal CA1 synapses. *Neuropharmacology*, 34(11):1387–95. Available from: http://www.ncbi.nlm.nih.gov/pubmed/8606788.

Harris, K. M. and Weinberg, R. J. (2012). Ultrastructure of synapses in the mammalian brain. *Cold Spring Harbor Perspectives in Biology*, 4(5). Available from: http://www.ncbi.nlm.nih.gov/pubmed/22357909.

Hebb, D. (1949). *The Organization of Behavior: A Neuropsychological Theory*. Psychology Press.

Hedde, P. N., Dörlich, R. M., Blomley, R., Gradl, D., Oppong, E., Cato, A. C. B., and Nienhaus, G. U. (2013). Stimulated emission depletion-based raster image correlation spectroscopy reveals biomolecular dynamics in live cells. *Nature Communications*, 4(May):2093. Available from: http://www.ncbi.nlm.nih.gov/pubmed/23803641.

Heilemann, M., van de Linde, S., Schüttpelz, M., Kasper, R., Seefeldt, B., Mukherjee, A., Tinnefeld, P., and Sauer, M. (2008). Subdiffraction-resolution fluorescence imaging with conventional fluorescent probes. *Angewandte Chemie Int. Ed. Engl.*, 47(33):6172–6176. Available from: http://dx.doi.org/10.1002/anie.200802376.

Hein, B., Willig, K. I., and Hell, S. W. (2008). Stimulated emission depletion (STED) nanoscopy of a fluorescent protein-labeled organelle inside a living cell. *Proceedings of the National Academy of Sciences of the United States of America*, 105(38):14271–6. Available from: http://www.pubmedcentral.nih.gov/articlerender.fcgi?artid=2538451&tool=pmcentrez&rendertype=abstract.

Heintzmann, R., Jovin, T. M., and Cremer, C. (2002). Saturated patterned excitation microscopy–a concept for optical resolution improvement. *Journal of the Optical Society of America. A, Optics, Image Science, and Vision*, 19(8):1599–609. Available from: http://www.ncbi.nlm.nih.gov/pubmed/12152701.

Hell, S. W. (2002). Increasing the resolution of far-field fluorescence light microscopy by point-spread-function engineering. In Lakowicz, J., editor, *Topics in fluorescence spectroscopy, Volume 5: Nonlinear and Two-Photon-Induced Fluorescence*, volume 5, pages 361–426. Springer US. Available from: http://www.springerlink.com/index/NUP058J8V1215085.pdf.

Hell, S. W. (2003). Toward fluorescence nanoscopy. *Nature Biotechnology*, 21(11):1347–55. Available from: http://www.ncbi.nlm.nih.gov/pubmed/14595362.

Hell, S. W. (2004). Strategy for far-field optical imaging and writing without diffraction limit. *Physics Letters A*, 326(1-2):140–145. Available from: http://linkinghub.elsevier.com/retrieve/pii/S0375960104004918.

Hell, S. W. (2009). Microscopy and its focal switch. *Nature Methods*, 6(1):24–32. Available from: http://dx.doi.org/10.1038/nmeth.1291.

Hell, S. W., Dyba, M., and Jakobs, S. (2004). Concepts for nanoscale resolution in fluorescence microscopy. *Current Opinion in Neurobiology*, 14(5):599–609. Available from: http://www.ncbi.nlm.nih.gov/pubmed/15464894.

Hell, S. W., Jakobs, S., and Kastrup, L. (2003). Imaging and writing at the nanoscale with focused visible light through saturable optical transitions. *Applied Physics A: Materials Science & Processing*, 77(7):859–860. Available from: http://link.springer.com/10.1007/s00339-003-2292-4.

Hell, S. W. and Kroug, M. (1995). Ground-state-depletion fluorscence microscopy: A concept for breaking the diffraction resolution limit. *Applied Physics B Lasers and Optics*, 60(5):495–497. Available from: http://link.springer.com/10.1007/BF01081333.

Hell, S. W., Soukka, J., and Hänninen, P. E. (1995). Two- and multiphoton detection as an imaging mode and means of increasing the resolution in far field light microscopy: A study based on photon optics. *Bioimaging*, 3(2):64–69. Available from: http://onlinelibrary.wiley.com/doi/10.1002/1361-6374(199506)3:2<64::AID-BIO2>3.0.CO;2-O/abstract.

Hell, S. W., Stelzer, E. H. K., Lindek, S., and Cremer, C. (1994). Confocal microscopy with an increased detection aperture: type-B 4Pi confocal microscopy. *Optics Letters*, 19(3):222. Available from: http://ol.osa.org/abstract.cfm?URI=ol-19-3-222.

Hell, S. W. and Wichmann, J. (1994). Breaking the diffraction resolution limit by stimulated emission: stimulated-emission-depletion fluorescence microscopy. *Optics Letters*, 19(11):780. Available from: http://www.opticsinfobase.org/abstract.cfm?URI=ol-19-11-780.

Hell, S. W., Willig, K. I., Dyba, M., Jakobs, S., Kastrup, L., and Westphal, V. (2006). Nanoscale Resolution with Focused Light: STED and Other RESOLFT Microscopy Concepts. In Pawley, J. B., editor, *Handbook of biological confocal microscopy*, pages 571–579. Springer US. Available from: http://link.springer.com/chapter/10.1007/978-0-387-45524-2_31.

Helmstaedter, M. (2013). Cellular-resolution connectomics: challenges of dense neural circuit reconstruction. *Nature Methods*, 10(6):501–7. Available from: http://dx.doi.org/10.1038/nmeth.2476.

Hering, H. and Sheng, M. (2001). Dendritic spines: structure, dynamics and regulation. *Nature Reviews. Neuroscience*, 2(12):880–8. Available from: http://www.ncbi.nlm.nih.gov/pubmed/11733795.

Hess, S. T., Girirajan, T. P. K., and Mason, M. D. (2006). Ultra-high resolution imaging by fluorescence photoactivation localization microscopy. *Biophysical Journal*, 91(11):4258–72. Available from: http://www.pubmedcentral.nih.gov/articlerender.fcgi?artid=1635685&tool=pmcentrez&rendertype=abstract.

Hille, B. (1967). The selective inhibition of delayed potassium currents in nerve by tetraethylammonium ion. *The Journal of General Physiology*, 50(5):1287–302. Available from: http://www.pubmedcentral.nih.gov/articlerender.fcgi?artid=2225709&tool=pmcentrez&rendertype=abstract.

Hinrichsen, C. F. (1970). Coupling between cells of the trigeminal mesencephalic nucleus. *Journal of Dental Research*, 49(6):Suppl:1369–73. Available from: http://www.ncbi.nlm.nih.gov/pubmed/5274363.

Holderith, N., Lorincz, A., Katona, G., Rózsa, B., Kulik, A., Watanabe, M., and Nusser, Z. (2012). Release probability of hippocampal glutamatergic terminals scales with the size of the active zone. *Nature Neuroscience*, 15(7):988–97. Available from: http://www.pubmedcentral.nih.gov/articlerender.fcgi?artid=3386897&tool=pmcentrez&rendertype=abstract.

Holtmaat, A. and Svoboda, K. (2009). Experience-dependent structural synaptic plasticity in the mammalian brain. *Nature Reviews. Neuroscience*, 10(9):647–58. Available from: http://www.ncbi.nlm.nih.gov/pubmed/19693029.

Holtmaat, A. J. G. D., Trachtenberg, J. T., Wilbrecht, L., Shepherd, G. M., Zhang, X., Knott, G. W., and Svoboda, K. (2005). Transient and persistent dendritic spines in the neocortex in vivo. *Neuron*, 45(2):279–91. Available from: http://www.ncbi.nlm.nih.gov/pubmed/15664179.

Honkura, N., Matsuzaki, M., Noguchi, J., Ellis-Davies, G. C. R., and Kasai, H. (2008). The subspine organization of actin fibers regulates the structure and plasticity of dendritic spines. *Neuron*, 57(5):719–29. Available from: http://www.ncbi.nlm.nih.gov/pubmed/18341992.

Hoopmann, P., Punge, A., Barysch, S. V., Westphal, V., Bückers, J., Opazo, F., Bethani, I., Lauterbach, M. a., Hell, S. W., and Rizzoli, S. O. (2010). Endosomal sorting of readily releasable synaptic vesicles. *Proceedings of the National Academy of Sciences of the United States of America*, 107(44):19055–60. Available from: http://www.pnas.org/content/early/2010/10/15/1007037107.

Hosokawa, T., Rusakov, D. A., Bliss, T. V., and Fine, A. (1995). Repeated confocal imaging of individual dendritic spines in the living hippocampal slice: evidence for changes in length and orientation associated with chemically induced LTP. *The Journal of Neuroscience*, 15(8):5560–73. Available from: http://www.ncbi.nlm.nih.gov/pubmed/7643201.

Hoze, N., Nair, D., Hosy, E., Sieben, C., Manley, S., Herrmann, A., Sibarita, J.-B., Choquet, D., and Holcman, D. (2012). Heterogeneity of AMPA receptor trafficking and molecular interactions revealed by superresolution analysis of live cell imaging. *Proceedings of the National Academy of Sciences of the United States of America*, 109(42):17052–17057. Available from: http://www.pubmedcentral.nih.gov/articlerender.fcgi?artid=3479500&tool=pmcentrez&rendertype=abstract.

Hu, B. R., Park, M., Martone, M. E., Fischer, W. H., Ellisman, M. H., and Zivin, J. A. (1998). Assembly of proteins to postsynaptic densities after transient cerebral ischemia. *The Journal of Neuroscience*, 18(2):625–33. Available from: http://www.ncbi.nlm.nih.gov/pubmed/9425004.

Huang, B., Wang, W., Bates, M., and Zhuang, X. (2008). Three-dimensional super-resolution imaging by stochastic optical reconstruction microscopy. *Science*, 319(5864):810–3. Available from: http://www.sciencemag.org/content/319/5864/810.

Huber, K. M., Mauk, M. D., and Kelly, P. T. (1995). Distinct LTP induction mechanisms: contribution of NMDA receptors and voltage-dependent calcium channels. *Journal of Neurophysiology*, 73(1):270–9. Available from: http://www.ncbi.nlm.nih.gov/pubmed/7714571.

Izeddin, I., Specht, C. G., Lelek, M., Darzacq, X., Triller, A., Zimmer, C., and Dahan, M. (2011). Super-Resolution Dynamic Imaging of Dendritic Spines Using a Low-Affinity Photoconvertible Actin Probe. *PLoS ONE*, 6(1):e15611. Available from: http://dx.plos.org/10.1371/journal.pone.0015611.

Jones, E. G. (1994). The Neuron Doctrine 1891. *Journal of the History of the Neurosciences*, 3(1):3–20. Available from: http://www.ncbi.nlm.nih.gov/pubmed/11618804.

Jones, E. G. and Powell, T. P. (1969). Morphological variations in the dendritic spines of the neocortex. *Journal of Cell Science*, 5(2):509–29. Available from: http://www.ncbi.nlm.nih.gov/pubmed/5362339.

Judkewitz, B., Rizzi, M., Kitamura, K., and Häusser, M. (2009). Targeted single-cell electroporation of mammalian neurons in vivo. *Nature Protocols*, 4(6):862–9. Available from: http://www.ncbi.nlm.nih.gov/pubmed/19444243.

Juette, M. F., Gould, T. J., Lessard, M. D., Mlodzianoski, M. J., Nagpure, B. S., Bennett, B. T., Hess, S. T., and Bewersdorf, J. (2008). Three-dimensional sub-100 nm resolution fluorescence microscopy of thick samples. *Nature Methods*, 5(6):527–9. Available from: http://www.ncbi.nlm.nih.gov/pubmed/18469823.

Kamin, D., Lauterbach, M. a., Westphal, V., Keller, J., Schönle, A., Hell, S. W., and Rizzoli, S. O. (2010). High- and low-mobility stages in the synaptic vesicle cycle. *Biophysical Journal*, 99(2):675–84. Available from: http://dx.doi.org/10.1016/j.bpj.2010.04.054.

Kandler, K., Katz, L. C., and Kauer, J. a. (1998). Focal photolysis of caged glutamate produces long-term depression of hippocampal glutamate receptors. *Nature Neuroscience*, 1(2):119–23. Available from: http://www.ncbi.nlm.nih.gov/pubmed/10195126.

Kasai, H., Hayama, T., Ishikawa, M., Watanabe, S., Yagishita, S., and Noguchi, J. (2010). Learning rules and persistence of dendritic spines. *The European Journal of Neuroscience*, 32(2):241–9. Available from: http://www.ncbi.nlm.nih.gov/pubmed/20646057.

Kastrup, L. and Hell, S. W. (2004). Absolute optical cross section of individual fluorescent molecules. *Angewandte Chemie (International ed. in English)*, 43(48):6646–9. Available from: http://www.ncbi.nlm.nih.gov/pubmed/15558641.

Keller, J. (2006). *Optimal de-excitation patterns for RESOLFT-Microscopy*. PhD thesis, Ruperto-Carola University of Heidelberg. Available from: http://archiv.ub.uni-heidelberg.de/volltextserver/7163/1/Thesis_Jan_Keller_Heidok.pdf.

Kennedy, M. B. (2000). Signal-Processing Machines at the Postsynaptic Density. *Science*, 290(5492):750–754. Available from: http://www.sciencemag.org/content/290/5492/750.

Kerr, J. M. and Blanpied, T. a. (2012). Subsynaptic AMPA receptor distribution is acutely regulated by actin-driven reorganization of the postsynaptic density. *The Journal of Neuroscience*, 32(2):658–73. Available from: http://www.pubmedcentral.nih.gov/articlerender.fcgi?artid=3596168&tool=pmcentrez&rendertype=abstract.

Kim, C. H. and Lisman, J. E. (1999). A role of actin filament in synaptic transmission and long-term potentiation. *The Journal of Neuroscience*, 19(11):4314–24. Available from: http://www.ncbi.nlm.nih.gov/pubmed/10341235.

Kim, E. and Sheng, M. (2009). The postsynaptic density. *Current Biology*, 19(17):R723–4. Available from: http://www.sciencedirect.com/science/article/pii/S0960982209014730.

Kittel, R. J., Wichmann, C., Rasse, T. M., Fouquet, W., Schmidt, M., Schmid, A., Wagh, D. A., Pawlu, C., Kellner, R. R., Willig, K. I., Hell, S. W., Buchner, E., Heckmann, M., and Sigrist, S. J. (2006). Bruchpilot promotes active zone assembly, Ca2+ channel clustering, and vesicle release. *Science*, 312(5776):1051–4. Available from: http://www.sciencemag.org/content/312/5776/1051.abstract.

Klar, T. (2001). *Progress in Stimulated Emission Depletion Microscopy (Berichte Aus Der Physik)*. Shaker Verlag GmbH, Germany.

Klar, T., Engel, E., and Hell, S. (2001). Breaking Abbes diffraction resolution limit in fluorescence microscopy with stimulated emission depletion beams of various shapes. *Physical Review E*, 64(6):066613. Available from: http://link.aps.org/doi/10.1103/PhysRevE.64.066613.

Klar, T. a. and Hell, S. W. (1999). Subdiffraction resolution in far-field fluorescence microscopy. *Optics Letters*, 24(14):954–6. Available from: http://www.ncbi.nlm.nih.gov/pubmed/18073907.

Klar, T. A., Jakobs, S., Dyba, M., Egner, A., and Hell, S. W. (2000). Fluorescence microscopy with diffraction resolution barrier broken by stimulated emission. *Proceedings of the National Academy of Sciences of the United States of America*, 97(15):8206–10. Available from: http://www.pubmedcentral.nih.gov/articlerender.fcgi?artid=26924&tool=pmcentrez&rendertype=abstract.

Knott, G. W., Holtmaat, A., Trachtenberg, J. T., Svoboda, K., and Welker, E. (2009). A protocol for preparing GFP-labeled neurons previously imaged in vivo and in slice preparations for light and electron microscopic analysis. *Nature Protocols*, 4(8):1145–56. Available from: http://www.ncbi.nlm.nih.gov/pubmed/19617886.

Kopec, C. D., Li, B., Wei, W., Boehm, J., and Malinow, R. (2006). Glutamate receptor exocytosis and spine enlargement during chemically induced long-term potentiation. *The Journal of Neuroscience*, 26(7):2000–9. Available from: http://www.ncbi.nlm.nih.gov/pubmed/16481433.

Kopec, C. D., Real, E., Kessels, H. W., and Malinow, R. (2007). GluR1 links structural and functional plasticity at excitatory synapses. *The Journal of Neuroscience*, 27(50):13706–18. Available from: http://www.ncbi.nlm.nih.gov/pubmed/18077682.

Korobova, F. and Svitkina, T. (2010). Molecular architecture of synaptic actin cytoskeleton in hippocampal neurons reveals a mechanism of dendritic spine morphogenesis. *Molecular Biology of the Cell*, 21(1):165–76. Available from: http://www.molbiolcell.org/content/21/1/165.

Krucker, T., Siggins, G. R., and Halpain, S. (2000). Dynamic actin filaments are required for stable long-term potentiation (LTP) in area CA1 of the hippocampus. *Proceedings of the National Academy of Sciences of the United States of America*, 97(12):6856–61. Available from: http://www.pnas.org/content/97/12/6856.full.

Kwon, H.-B. and Sabatini, B. L. (2011). Glutamate induces de novo growth of functional spines in developing cortex. *Nature*, 474(7349):100–4. Available from: http://www.nature.com/nature/journal/v474/n7349/full/nature09986.html.

Lakowicz, J. R., editor (2006). *Principles of Fluorescence Spectroscopy*. Springer US, Boston, MA. Available from: http://www.springerlink.com/index/10.1007/978-0-387-46312-4.

Landis, D. M. and Reese, T. S. (1983). Cytoplasmic organization in cerebellar dendritic spines. *The Journal of Cell Biology*, 97(4):1169–78. Available from: http://www.pubmedcentral.nih.gov/articlerender.fcgi?artid=2112605&tool=pmcentrez&rendertype=abstract.

Lang, C., Barco, A., Zablow, L., Kandel, E. R., Siegelbaum, S. a., and Zakharenko, S. S. (2004). Transient expansion of synaptically connected dendritic spines upon induction of hippocampal long-term potentiation. *Proceedings of the National Academy of Sciences of the United States of America*, 101(47):16665–70. Available from: http://www.pubmedcentral.nih.gov/articlerender.fcgi?artid=534531&tool=pmcentrez&rendertype=abstract.

Lang, S. B., Bonhoeffer, T., and Lohmann, C. (2006). Simultaneous imaging of morphological plasticity and calcium dynamics in dendrites. *Nature Protocols*, 1(4):1859–64. Available from: http://dx.doi.org/10.1038/nprot.2006.267.

Lauterbach, M. a., Guillon, M., Soltani, A., and Emiliani, V. (2013). STED microscope with spiral phase contrast. *Scientific Reports*, 3:2050. Available from: http://www.pubmedcentral.nih.gov/articlerender.fcgi?artid=3689173&tool=pmcentrez&rendertype=abstract.

Lee, K., Oliver, M., Schottler, F., Creager, R., and Lynch, G. (1979). Ultrastructural effects of repetitive synaptic stimulation in the hippocampal slice preparation: a preliminary report. *Experimental Neurology*, 65(2):478–80. Available from: http://www.ncbi.nlm.nih.gov/pubmed/477800.

Lee, K. S., Schottler, F., Oliver, M., and Lynch, G. (1980). Brief bursts of high-frequency stimulation produce two types of structural change in rat hippocampus. *Journal of Neurophysiology*, 44(2):247–58. Available from: http://www.ncbi.nlm.nih.gov/pubmed/7411185.

Lemmer, P., Gunkel, M., Baddeley, D., Kaufmann, R., Urich, A., Weiland, Y., Reymann, J., Müller, P., Hausmann, M., and Cremer, C. (2008). SPDM: light microscopy with single-molecule resolution at the nanoscale. *Applied Physics B*, 93(1):1–12. Available from: http://link.springer.com/10.1007/s00340-008-3152-x.

Lendvai, B., Stern, E. A., Chen, B., and Svoboda, K. (2000). Experience-dependent plasticity of dendritic spines in the developing rat barrel cortex in vivo. *Nature*, 404(6780):876–81. Available from: http://www.ncbi.nlm.nih.gov/pubmed/10786794.

Levy, W. B. and Steward, O. (1979). Synapses as associative memory elements in the hippocampal formation. *Brain Research*, 175(2):233–45. Available from: http://www.ncbi.nlm.nih.gov/pubmed/487154.

Lisman, J. E. and Harris, K. M. (1993). Quantal analysis and synaptic anatomy–integrating two views of hippocampal plasticity. *Trends in Neurosciences*, 16(4):141–7. Available from: http://www.ncbi.nlm.nih.gov/pubmed/7682347.

Livet, J., Weissman, T. A., Kang, H., Draft, R. W., Lu, J., Bennis, R. A., Sanes, J. R., and Lichtman, J. W. (2007). Transgenic strategies for combinatorial expression of fluorescent proteins in the nervous system. *Nature*, 450(7166):56–62. Available from: http://dx.doi.org/10.1038/nature06293.

Llinas, R. (2008). Neuron. *Scholarpedia*, 3(8):1490. Available from: http://www.scholarpedia.org/article/Neuron.

Lohmann, C. and Bonhoeffer, T. (2008). A role for local calcium signaling in rapid synaptic partner selection by dendritic filopodia. *Neuron*, 59(2):253–60. Available from: http://www.ncbi.nlm.nih.gov/pubmed/18667153.

Lohmann, C., Finski, A., and Bonhoeffer, T. (2005). Local calcium transients regulate the spontaneous motility of dendritic filopodia. *Nature Neuroscience*, 8(3):305–12. Available from: http://dx.doi.org/10.1038/nn1406.

Lucić, V., Yang, T., Schweikert, G., Förster, F., and Baumeister, W. (2005). Morphological characterization of molecular complexes present in the synaptic cleft. *Structure*, 13(3):423–34. Available from: http://www.ncbi.nlm.nih.gov/pubmed/15766544.

Lüscher, C. and Malenka, R. C. (2012). NMDA receptor-dependent long-term potentiation and long-term depression (LTP/LTD). *Cold Spring Harbor Perspectives in Biology*, 4(6):a005710. Available from: http://www.ncbi.nlm.nih.gov/pubmed/22510460.

Mahajan, V. N. (2011). *Optical Imaging and Aberrations, Part II. Wave Diffraction Optics (SPIE Press Monograph Vol. PM209)*. SPIE Press.

Majewska, A., Brown, E., Ross, J., and Yuste, R. (2000a). Mechanisms of calcium decay kinetics in hippocampal spines: role of spine calcium pumps and calcium diffusion through the spine neck in biochemical compartmentalization. *The Journal of Neuroscience*, 20(5):1722–34. Available from: http://www.ncbi.nlm.nih.gov/pubmed/10684874.

Majewska, A., Tashiro, A., and Yuste, R. (2000b). Regulation of spine calcium dynamics by rapid spine motility. *The Journal of Neuroscience*, 20(22):8262–8. Available from: http://www.ncbi.nlm.nih.gov/pubmed/11069932.

Malenka, R. C. and Bear, M. F. (2004). LTP and LTD: an embarrassment of riches. *Neuron*, 44(1):5–21. Available from: http://www.ncbi.nlm.nih.gov/pubmed/15450156.

Malenka, R. C. and Nicoll, R. A. (1993). NMDA-receptor-dependent synaptic plasticity: multiple forms and mechanisms. *Trends in Neurosciences*, 16(12):521–527. Available from: http://www.sciencedirect.com/science/article/pii/016622369390197T.

Maletic-Savatic, M., Malinow, R., and Svoboda, K. (1999). Rapid Dendritic Morphogenesis in CA1 Hippocampal Dendrites Induced by Synaptic Activity. *Science*, 283(5409):1923–1927. Available from: http://www.sciencemag.org/content/283/5409/1923.

Matsuzaki, M., Ellis-Davies, G. C., Nemoto, T., Miyashita, Y., Iino, M., and Kasai, H. (2001). Dendritic spine geometry is critical for AMPA receptor expression in hippocampal CA1 pyramidal neurons. *Nature Neuroscience*, 4(11):1086–92. Available from: http://www.ncbi.nlm.nih.gov/pubmed/11687814.

Matsuzaki, M., Honkura, N., Ellis-Davies, G. G. C. R., and Kasai, H. (2004). Structural basis of long-term potentiation in single dendritic spines. *Nature*, 429(June):761–6. Available from: http://www.nature.com/nature/journal/v429/n6993/abs/nature02617.html.

Matus, A. (2000). Actin-Based Plasticity in Dendritic Spines. *Science*, 290(5492):754–758. Available from: http://www.sciencemag.org/cgi/doi/10.1126/science.290.5492.754.

McAllister, a. K. (2000). Biolistic transfection of neurons. *Science's STKE: Signal Transduction Knowledge Environment*, 2000(51):pl1. Available from: http://www.ncbi.nlm.nih.gov/pubmed/11752611.

McKinney, R. A., Capogna, M., Dürr, R., Gähwiler, B. H., and Thompson, S. M. (1999). Miniature synaptic events maintain dendritic spines via AMPA receptor activation. *Nature Neuroscience*, 2(1):44–9. Available from: http://www.nature.com.emedien.ub.uni-muenchen.de/neuro/journal/v2/n1/full/nn0199_44.html.

Mendez, P., De Roo, M., Poglia, L., Klauser, P., and Muller, D. (2010). N-cadherin mediates plasticity-induced long-term spine stabilization. *The Journal of Cell Biology*, 189(3):589–600. Available from: http://jcb.rupress.org/content/189/3/589.

Meyer, D. (2013). *Correlated plasticity of synaptic structures and its relationship to the stabilization of synaptic enlargement*. PhD thesis, Ludwig Maximilians University Munich. Available from: http://nbn-resolving.de/urn:nbn:de:bvb:19-155516.

Meyer, D., Bonhoeffer, T., and Scheuss, V. (2014). Balance and stability of synaptic structures during synaptic plasticity. *Neuron*, in press.

Micheva, K. D. and Smith, S. J. (2007). Array tomography: a new tool for imaging the molecular architecture and ultrastructure of neural circuits. *Neuron*, 55(1):25–36. Available from: http://www.pubmedcentral.nih.gov/articlerender.fcgi?artid=2080672&tool=pmcentrez&rendertype=abstract.

Moffitt, J. R., Osseforth, C., and Michaelis, J. (2011). Time-gating improves the spatial resolution of STED microscopy. *Optics Express*, 19(5):4242. Available from: http://www.opticsexpress.org/abstract.cfm?URI=oe-19-5-4242.

Moser, M.-B. and Moser, E. I. (1998). Functional differentiation in the hippocampus. *Hippocampus*, 8(6):608–619. Available from: http://doi.wiley.com/10.1002/(SICI)1098-1063(1998)8:6<608::AID-HIPO3>3.0.CO;2-7.

Muller, D., Buchs, P. A., and Stoppini, L. (1993). Time course of synaptic development in hippocampal organotypic cultures. *Brain Research. Developmental Brain Research*, 71(1):93–100. Available from: http://www.ncbi.nlm.nih.gov/pubmed/8432004.

Muller, D., Toni, N., and Buchs, P. (2001). Interface organotypic hippocampal slice cultures. In Fedoroff, S. and Richardson, A., editors, *Protocols for Neural Cell Culture*, pages 13–27. Humana Press, Inc., Totowa, NJ, 3rd edition. Available from: http://link.springer.com/protocol/10.1385/1-59259-207-4:13.

Müller, T., Schumann, C., and Kraegeloh, A. (2012). STED microscopy and its applications: new insights into cellular processes on the nanoscale. *ChemPhysChem: a European journal of chemical physics and physical chemistry*, 13(8):1986–2000. Available from: http://www.ncbi.nlm.nih.gov/pubmed/22374829.

Munck, S., Miskiewicz, K., Sannerud, R., Menchon, S. a., Jose, L., Heintzmann, R., Verstreken, P., and Annaert, W. (2012). Sub-diffraction imaging on standard microscopes through photobleaching microscopy with non-linear processing. *Journal of Cell Science*, 125(Pt 9):2257–66. Available from: http://www.ncbi.nlm.nih.gov/pubmed/22357945.

Nagel, G., Szellas, T., Huhn, W., Kateriya, S., Adeishvili, N., Berthold, P., Ollig, D., Hegemann, P., and Bamberg, E. (2003). Channelrhodopsin-2, a directly light-gated cation-selective membrane channel. *Proceedings of the National Academy of Sciences of the United States of America*, 100(24):13940–5. Available from: http://www.pnas.org/content/100/24/13940.long.

Nägerl, U. V. and Bonhoeffer, T. (2010). Imaging living synapses at the nanoscale by STED microscopy. *The Journal of Neuroscience*, 30(28):9341–6. Available from: http://www.ncbi.nlm.nih.gov/pubmed/20631162.

Nägerl, U. V., Willig, K. I., Hein, B., Hell, S. W., and Bonhoeffer, T. (2008). Live-cell imaging of dendritic spines by STED microscopy. *Proceedings of the National Academy of Sciences of the United States of America*, 105(48):18982–7. Available from: http://www.pnas.org/content/105/48/18982.

Naredi-Rainer, N. (2014). *Advanced Confocal Microscopy: From Setups To Applications*. Phd thesis, Ludwig Maximilians University Munich.

Nelson, S. B. and Turrigiano, G. G. (2008). Strength through diversity. *Neuron*, 60(3):477–82. Available from: http://www.cell.com/neuron/fulltext/S0896-6273(08)00893-3.

Neuhoff, H., Roeper, J., and Schweizer, M. (1999). Activity-dependent formation of perforated synapses in cultured hippocampal neurons. *The European Journal of Neuroscience*, 11(12):4241–50. Available from: http://www.ncbi.nlm.nih.gov/pubmed/10594650.

Nevian, T. and Helmchen, F. (2007). Calcium indicator loading of neurons using single-cell electroporation. *Pflügers Archiv: European Journal of Physiology*, 454(4):675–88. Available from: http://www.ncbi.nlm.nih.gov/pubmed/17334778.

Nicoll, R. A., Oliet, S. H., and Malenka, R. C. (1998). NMDA receptor-dependent and metabotropic glutamate receptor-dependent forms of long-term depression coexist in CA1 hippocampal pyramidal cells. *Neurobiology of Learning and Memory*, 70(1-2):62–72. Available from: http://www.ncbi.nlm.nih.gov/pubmed/9753587.

Nimchinsky, E. A., Sabatini, B. L., and Svoboda, K. (2002). Structure and function of dendritic spines. *Annual Review of Physiology*, 64:313–53. Available from: http://www.annualreviews.org/doi/pdf/10.1146/annurev.physiol.64.081501.160008.

Nobel Media AB (2013). The Nobel Prize in Physiology or Medicine 1906. Available from: http://www.nobelprize.org/nobel_prizes/medicine/laureates/1906/.

Novotny, L. (2007). The history of near-field optics. *Progress in Optics*, 184:137–183. Available from: http://www.sciencedirect.com/science/article/pii/S0079663807500053.

Nusser, Z., Lujan, R., Laube, G., Roberts, J. D., Molnar, E., and Somogyi, P. (1998). Cell type and pathway dependence of synaptic AMPA receptor number and variability in the hippocampus. *Neuron*, 21(3):545–59. Available from: http://www.ncbi.nlm.nih.gov/pubmed/9768841.

Nusser, Z. and Somogyi, P. (1997). Compartmentalised distribution of GABAA and glutamate receptors in relation to transmitter release sites on the surface of cerebellar neurones. *Progress in Brain Research*, 114:109–27. Available from: http://www.ncbi.nlm.nih.gov/pubmed/9193141.

Oe, Y., Tominaga-Yoshino, K., Hasegawa, S., and Ogura, A. (2013). Dendritic spine dynamics in synaptogenesis after repeated LTP inductions: dependence on pre-existing spine density. *Scientific Reports*, 3:1957. Available from: http://www.nature.com/srep/2013/130606/srep01957/full/srep01957.html.

Okabe, S., Kim, H. D., Miwa, A., Kuriu, T., and Okado, H. (1999). Continual remodeling of postsynaptic density and its regulation by synaptic activity. *Nature Neuroscience*, 2(9):804–11. Available from: http://www.ncbi.nlm.nih.gov/pubmed/10461219.

Okamoto, K.-I., Nagai, T., Miyawaki, A., and Hayashi, Y. (2004). Rapid and persistent modulation of actin dynamics regulates postsynaptic reorganization underlying bidirectional plasticity. *Nature Neuroscience*, 7(10):1104–12. Available from: http://www.ncbi.nlm.nih.gov/pubmed/15361876.

O'Keefe, J. and Dostrovsky, J. (1971). The hippocampus as a spatial map. Preliminary evidence from unit activity in the freely-moving rat. *Brain Research*, 34(1):171–5. Available from: http://www.ncbi.nlm.nih.gov/pubmed/5124915.

Opazo, F., Punge, A., Bückers, J., Hoopmann, P., Kastrup, L., Hell, S. W., and Rizzoli, S. O. (2010). Limited intermixing of synaptic vesicle components upon vesicle recycling. *Traffic*, 11(6):800–12. Available from: http://www.ncbi.nlm.nih.gov/pubmed/20230528.

Orlando, C., Ster, J., Gerber, U., Fawcett, J. W., and Raineteau, O. (2012). Perisynaptic chondroitin sulfate proteoglycans restrict structural plasticity in an integrin-dependent manner. *The Journal of Neuroscience*, 32(50):18009–17, 18017a. Available from: http://www.ncbi.nlm.nih.gov/pubmed/23238717.

Ostroff, L. E., Fiala, J. C., Allwardt, B., and Harris, K. M. (2002). Polyribosomes Redistribute from Dendritic Shafts into Spines with Enlarged Synapses during LTP in Developing Rat Hippocampal Slices. *Neuron*, 35(3):535–545. Available from: http://www.sciencedirect.com/science/article/pii/S0896627302007857.

Otmakhov, N., Khibnik, L., Otmakhova, N., Carpenter, S., Riahi, S., Asrican, B., and Lisman, J. (2004a). Forskolin-induced LTP in the CA1 hippocampal region is NMDA receptor dependent. *Journal of Neurophysiology*, 91(5):1955–62. Available from: http://jn.physiology.org/content/91/5/1955.full.

Otmakhov, N., Tao-Cheng, J.-H., Carpenter, S., Asrican, B., Dosemeci, A., Reese, T. S., and Lisman, J. (2004b). Persistent accumulation of calcium/calmodulin-dependent protein kinase II in dendritic spines after induction of NMDA receptor-dependent chemical long-term potentiation. *The Journal of Neuroscience*, 24(42):9324–31. Available from: http://www.ncbi.nlm.nih.gov/pubmed/15496668.

Palmer, M. J., Irving, A. J., Seabrook, G. R., Jane, D. E., and Collingridge, G. L. (1997). The group I mGlu receptor agonist DHPG induces a novel form of LTD in the CA1 region of the hippocampus. *Neuropharmacology*, 36(11-12):1517–32. Available from: http://www.ncbi.nlm.nih.gov/pubmed/9517422.

Parnass, Z., Tashiro, A., and Yuste, R. (2000). Analysis of spine morphological plasticity in developing hippocampal pyramidal neurons. *Hippocampus*, 10(5):561–8. Available from: http://www.ncbi.nlm.nih.gov/pubmed/11075826.

Pascual-Leone, A., Amedi, A., Fregni, F., and Merabet, L. B. (2005). The plastic human brain cortex. *Annual Review of Neuroscience*, 28:377–401. Available from: http://www.annualreviews.org/doi/full/10.1146/annurev.neuro.27.070203.144216.

Patterson, G., Davidson, M., Manley, S., and Lippincott-Schwartz, J. (2010). Superresolution imaging using single-molecule localization. *Annual Review of Physical Chemistry*, 61:345–67. Available from: http://www.pubmedcentral.nih.gov/articlerender.fcgi?artid=3658623&tool=pmcentrez&rendertype=abstract.

Peters, A. and Kaiserman-Abramof, I. R. (1970). The small pyramidal neuron of the rat cerebral cortex. The perikaryon, dendrites and spines. *The American Journal of Anatomy*, 127(4):321–55. Available from: http://www.ncbi.nlm.nih.gov/pubmed/4985058.

Pohl, D. W., Denk, W., and Lanz, M. (1984). Optical stethoscopy: Image recording with resolution $\lambda/20$. *Applied Physics Letters*, 44(7):651. Available from: http://scitation.aip.org/content/aip/journal/apl/44/7/10.1063/1.94865.

Popov, V. I., Davies, H. A., Rogachevsky, V. V., Patrushev, I. V., Errington, M. L., Gabbott, P. L. A., Bliss, T. V. P., and Stewart, M. G. (2004). Remodelling of synaptic morphology but unchanged synaptic density during late phase long-term potentiation (LTP): a serial section electron micrograph study in the dentate gyrus in the anaesthetised rat. *Neuroscience*, 128(2):251–62. Available from: http://www.sciencedirect.com/science/article/pii/S030645220400497X.

Rae, J. L. and Levis, R. A. (2002). Single-cell electroporation. *Pflügers Archiv: European Journal of Physiology*, 443(4):664–70. Available from: http://www.ncbi.nlm.nih.gov/pubmed/11907835.

Rathenberg, J., Nevian, T., and Witzemann, V. (2003). High-efficiency transfection of individual neurons using modified electrophysiology techniques. *Journal of Neuroscience Methods*, 126(1):91–8. Available from: http://www.ncbi.nlm.nih.gov/pubmed/12788505.

Rayleigh, L. (1903). On the Theory of Optical Images, with special reference to the Microscope. *Journal of the Royal Microscopical Society*, 23(4):474–482. Available from: http://doi.wiley.com/10.1111/j.1365-2818.1903.tb04831.x.

Redondo, R. L. and Morris, R. G. M. (2011). Making memories last: the synaptic tagging and capture hypothesis. *Nature Reviews. Neuroscience*, 12(1):17–30. Available from: http://www.ncbi.nlm.nih.gov/pubmed/21170072.

Requejo-Isidro, J. (2013). Fluorescence nanoscopy. Methods and applications. *Journal of Chemical Biology*, 6(3):97–120. Available from: http://www.ncbi.nlm.nih.gov/pubmed/24432127.

Reuss, M., Engelhardt, J., and Hell, S. W. (2010). Birefringent device converts a standard scanning microscope into a STED microscope that also maps molecular orientation. *Optics Express*, 18(2):1049. Available from: http://www.opticsexpress.org/abstract.cfm?URI=oe-18-2-1049.

Richards, D. A., Mateos, J. M., Hugel, S., de Paola, V., Caroni, P., Gähwiler, B. H., and McKinney, R. A. (2005). Glutamate induces the rapid formation of spine head protrusions in hippocampal slice cultures. *Proceedings of the National Academy of Sciences of the United States of America*, 102(17):6166–71. Available from: http://www.pnas.org/cgi/content/abstract/102/17/6166.

Riedl, J., Crevenna, A. H., Kessenbrock, K., Yu, J. H., Neukirchen, D., Bradke, F., Jenne, D., Holak, T. A., Werb, Z., Sixt, M., and Wedlich-soldner, R. (2008). Lifeact : a versatile marker to visualize F-actin. 5(7):605–607. Available from: http://www.pubmedcentral.nih.gov/articlerender.fcgi?artid=2814344&tool=pmcentrez&rendertype=abstract.

Roberts, E. (2007). Gamma-aminobutyric acid. *Scholarpedia*, 2(10):3356. Available from: http://www.scholarpedia.org/article/Gamma-aminobutyric_acid.

Rodriguez, A., Ehlenberger, D. B., Dickstein, D. L., Hof, P. R., and Wearne, S. L. (2008). Automated three-dimensional detection and shape classification of dendritic spines from fluorescence microscopy images. *PloS ONE*, 3(4):e1997. Available from: http://www.plosone.org/article/info:doi/10.1371/journal.pone.0001997#s4.

Roelandse, M., Welman, A., Wagner, U., Hagmann, J., and Matus, A. (2003). Focal motility determines the geometry of dendritic spines. *Neuroscience*, 121(1):39–49. Available from: http://www.ncbi.nlm.nih.gov/pubmed/12946698.

Ronzitti, E., Harke, B., and Diaspro, A. (2013). Frequency dependent detection in a STED microscope using modulated excitation light. *Optics Express*, 21(1):210–9. Available from: http://www.ncbi.nlm.nih.gov/pubmed/23388913.

Rusakov, D. A., Stewart, M. G., and Korogod, S. M. (1996). Branching of active dendritic spines as a mechanism for controlling synaptic efficacy. *Neuroscience*, 75(1):315–23. Available from: http://www.ncbi.nlm.nih.gov/pubmed/8923544.

Rust, M. J., Bates, M., and Zhuang, X. (2006). Sub-diffraction-limit imaging by stochastic optical reconstruction microscopy (STORM). *Nature Methods*, 3(10):793–5. Available from: http://dx.doi.org/10.1038/nmeth929.

Santschi, L., Reyes-Harde, M., and Stanton, P. K. (1999). Chemically induced, activity-independent LTD elicited by simultaneous activation of PKG and inhibition of PKA. *Journal of Neurophysiology*, 82(3):1577–89. Available from: http://www.ncbi.nlm.nih.gov/pubmed/10482771.

Schätzle, P., Ster, J., Verbich, D., McKinney, R. A., Gerber, U., Sonderegger, P., Mateos, J. M., and María Mateos, J. (2011). Rapid and reversible formation of spine head filopodia in response to muscarinic receptor activation in CA1 pyramidal cells. *The Journal of Physiology*, 589(Pt 17):4353–64. Available from: http://jp.physoc.org/cgi/content/abstract/589/17/4353.

Schikorski, T. and Stevens, C. F. (2001). Morphological correlates of functionally defined synaptic vesicle populations. *Nature Neuroscience*, 4(4):391–5. Available from: http://www.ncbi.nlm.nih.gov/pubmed/11276229.

Schindelin, J., Arganda-Carreras, I., Frise, E., Kaynig, V., Longair, M., Pietzsch, T., Preibisch, S., Rueden, C., Saalfeld, S., Schmid, B., Tinevez, J.-Y., White, D. J., Hartenstein, V., Eliceiri, K., Tomancak, P., and Cardona, A. (2012). Fiji: an open-source platform for biological-image analysis. *Nature Methods*, 9(7):676–82. Available from: http://www.pubmedcentral.nih.gov/articlerender.fcgi?artid=3855844&tool=pmcentrez&rendertype=abstract.

Schmidt, R., Wurm, C. A., Jakobs, S., Engelhardt, J., Egner, A., and Hell, S. W. (2008). Spherical nanosized focal spot unravels the interior of cells. *Nature Methods*, 5(6):539–44. Available from: http://www.ncbi.nlm.nih.gov/pubmed/18488034.

Schönle, A. (2006). Imspector Image Acquisition & Analysis Software, v0.10. Available from: http://www.imspector.de.

Schönle, A., Hell, S. W., and Van den Bos, A. (2007). Nanoscale Resolution in Far-Field Fluorescence Microscopy. In Hawkes, P. W. and Spence, J. C. H., editors, *Sciene of microscopy. Vol. 2, 790-834 (2007)*, pages 790 – 834. Springer New York, New York, NY. Available from: http://www.springerlink.com/index/10.1007/978-0-387-49762-4.

Scoville, W. B. and Milner, B. (1957). Loss of recent memory after bilateral hippocampal lesions. *Journal of Neurology, Neurosurgery, and Psychiatry*, 20(1):11–21. Available from: http://www.pubmedcentral.nih.gov/articlerender.fcgi?artid=497229&tool=pmcentrez&rendertype=abstract.

Shepherd, G. M. and Harris, K. M. (1998). Three-dimensional structure and composition of CA3→CA1 axons in rat hippocampal slices: implications for presynaptic connectivity and compartmentalization. *The Journal of Neuroscience*, 18(20):8300–10. Available from: http://www.ncbi.nlm.nih.gov/pubmed/9763474.

Shroff, H., Galbraith, C. G., Galbraith, J. A., and Betzig, E. (2008). Live-cell photoactivated localization microscopy of nanoscale adhesion dynamics. *Nature Methods*, 5(5):417–23. Available from: http://dx.doi.org/10.1038/nmeth.1202.

Shroff, H., Galbraith, C. G., Galbraith, J. A., White, H., Gillette, J., Olenych, S., Davidson, M. W., and Betzig, E. (2007). Dual-color superresolution imaging of genetically expressed probes within individual adhesion complexes. *Proceedings of the National Academy of Sciences of the United States of America*, 104(51):20308–13. Available from: http://www.pnas.org/content/104/51/20308.long.

Sorra, K. E., Fiala, J. C., and Harris, K. M. (1998). Critical assessment of the involvement of perforations, spinules, and spine branching in hippocampal synapse formation. *The Journal of Comparative Neurology*, 398(2):225–40. Available from: http://www.ncbi.nlm.nih.gov/pubmed/9700568.

Sorra, K. E., Mishra, A., Kirov, S. A., and Harris, K. M. (2006). Dense core vesicles resemble active-zone transport vesicles and are diminished following synaptogenesis in mature hippocampal slices. *Neuroscience*, 141(4):2097–106. Available from: http://www.ncbi.nlm.nih.gov/pubmed/16797135.

Star, E. N., Kwiatkowski, D. J., and Murthy, V. N. (2002). Rapid turnover of actin in dendritic spines and its regulation by activity. *Nature Neuroscience*, 5(3):239–46. Available from: http://www.ncbi.nlm.nih.gov/pubmed/11850630.

Steinhauer, C., Forthmann, C., Vogelsang, J., and Tinnefeld, P. (2008). Superresolution microscopy on the basis of engineered dark states. *Journal of the American Chemical Society*, 130(50):16840–1. Available from: http://dx.doi.org/10.1021/ja806590m.

Stewart, M. G., Medvedev, N. I., Popov, V. I., Schoepfer, R., Davies, H. A., Murphy, K., Dallérac, G. M., Kraev, I. V., and Rodríguez, J. J. (2005). Chemically induced long-term potentiation

increases the number of perforated and complex postsynaptic densities but does not alter dendritic spine volume in CA1 of adult mouse hippocampal slices. *The European Journal of Neuroscience*, 21(12):3368–78. Available from: http://www.ncbi.nlm.nih.gov/pubmed/16026474.

Stoppini, L., Buchs, P. a., and Muller, D. (1991). A simple method for organotypic cultures of nervous tissue. *Journal of Neuroscience Methods*, 37(2):173–82. Available from: http://www.ncbi.nlm.nih.gov/pubmed/1715499.

Südhof, T. C. (2004). The synaptic vesicle cycle. *Annual Review of Neuroscience*, 27:509–47. Available from: http://www.ncbi.nlm.nih.gov/pubmed/15217342.

Südhof, T. C. and Rizo, J. (2011). Synaptic vesicle exocytosis. *Cold Spring Harbor Perspectives in Biology*, 3(12):a005637. Available from: http://cshperspectives.cshlp.org/content/3/12/a005637.full.

Swanger, S. a., Yao, X., Gross, C., and Bassell, G. J. (2011). Automated 4D analysis of dendritic spine morphology: applications to stimulus-induced spine remodeling and pharmacological rescue in a disease model. *Molecular Brain*, 4(1):38. Available from: http://www.pubmedcentral.nih.gov/articlerender.fcgi?artid=3213078&tool=pmcentrez&rendertype=abstract.

Takasaki, K. T., Ding, J. B., and Sabatini, B. L. (2013). Live-cell superresolution imaging by pulsed STED two-photon excitation microscopy. *Biophysical Journal*, 104(4):770–7. Available from: http://www.ncbi.nlm.nih.gov/pubmed/23442955.

Tao-Cheng, J.-H. (2007). Ultrastructural localization of active zone and synaptic vesicle proteins in a preassembled multi-vesicle transport aggregate. *Neuroscience*, 150(3):575–84. Available from: http://www.pubmedcentral.nih.gov/articlerender.fcgi?artid=2190624&tool=pmcentrez&rendertype=abstract.

Tao-Cheng, J.-H., Dosemeci, A., Gallant, P. E., Miller, S., Galbraith, J. A., Winters, C. A., Azzam, R., and Reese, T. S. (2009). Rapid turnover of spinules at synaptic terminals. *Neuroscience*, 160(1):42–50. Available from: http://www.pubmedcentral.nih.gov/articlerender.fcgi?artid=2673145&tool=pmcentrez&rendertype=abstract.

Tashiro, A. and Yuste, R. (2003). Structure and molecular organization of dendritic spines. *Histology and Histopathology*, 18(2):617–34. Available from: http://www.ncbi.nlm.nih.gov/pubmed/12647812.

Tatavarty, V., Das, S., and Yu, J. (2012). Polarization of actin cytoskeleton is reduced in dendritic protrusions during early spine development in hippocampal neuron. *Molecular Biology of the Cell*, 23(16):3167–77. Available from: http://www.molbiolcell.org/content/23/16/3167.full.

Tatavarty, V., Kim, E.-J., Rodionov, V., and Yu, J. (2009). Investigating sub-spine actin dynamics in rat hippocampal neurons with super-resolution optical imaging. *PloS ONE*, 4(11):e7724. Available from: http://dx.plos.org/10.1371/journal.pone.0007724.

Testa, I., Urban, N. T., Jakobs, S., Eggeling, C., Willig, K. I., and Hell, S. W. (2012). Nanoscopy of living brain slices with low light levels. *Neuron*, 75(6):992–1000. Available from: http://www.ncbi.nlm.nih.gov/pubmed/22998868.

Toni, N., Buchs, P. A., Nikonenko, I., Bron, C. R., and Muller, D. (1999). LTP promotes formation of multiple spine synapses between a single axon terminal and a dendrite. *Nature*, 402(6760):421–5. Available from: http://www.ncbi.nlm.nih.gov/pubmed/10586883.

Toni, N., Buchs, P. A., Nikonenko, I., Povilaitite, P., Parisi, L., and Muller, D. (2001). Remodeling of synaptic membranes after induction of long-term potentiation. *The Journal of Neuroscience*, 21(16):6245–51. Available from: http://www.ncbi.nlm.nih.gov/pubmed/11487647.

Tønnesen, J., Nadrigny, F., Willig, K. I., Wedlich-Söldner, R., and Nägerl, U. V. (2011). Two-color STED microscopy of living synapses using a single laser-beam pair. *Biophysical Journal*, 101(10):2545–52. Available from: http://www.pubmedcentral.nih.gov/articlerender.fcgi?artid=3218326&tool=pmcentrez&rendertype=abstract.

Tønnesen, J. and Nägerl, U. V. (2012). Superresolution imaging for neuroscience. *Experimental Neurology*, null(null). Available from: http://dx.doi.org/10.1016/j.expneurol.2012.10.004.

Toomre, D. and Bewersdorf, J. (2010). A new wave of cellular imaging. *Annual Review of Cell and Developmental Biology*, 26:285–314. Available from: http://www.ncbi.nlm.nih.gov/pubmed/20929313.

Trigo, F. F., Corrie, J. E. T., and Ogden, D. (2009). Laser photolysis of caged compounds at 405 nm: photochemical advantages, localisation, phototoxicity and methods for calibration. *Journal of Neuroscience Methods*, 180(1):9–21. Available from: http://www.ncbi.nlm.nih.gov/pubmed/19427524.

Trommald, M., Hulleberg, G., and Andersen, P. (1996). Long-term potentiation is associated with new excitatory spine synapses on rat dentate granule cells. *Learning & Memory*, 3(2-3):218–28. Available from: http://www.ncbi.nlm.nih.gov/pubmed/10456092.

Urban, N. T., Willig, K. I., Hell, S. W., and Nägerl, U. V. (2011). STED Nanoscopy of Actin Dynamics in Synapses Deep Inside Living Brain Slices. *Biophysical Journal*, 101(5):1277–84. Available from: http://www.pubmedcentral.nih.gov/articlerender.fcgi?artid=3164186&tool=pmcentrez&rendertype=abstract.

Van Harreveld, A. and Fifkova, E. (1975). Swelling of dendritic spines in the fascia dentata after stimulation of the perforant fibers as a mechanism of post-tetanic potentiation. *Experimental Neurology*, 49(3):736–49. Available from: http://www.ncbi.nlm.nih.gov/pubmed/173566.

Verdet, E. (1869). *Leçons d'optique physique, Tome 1 (Google eBook)*. Available from: http://books.google.de/books/about/Le\unhbox\voidb@x\setbox\z@\hbox{c}\accent24cons_d_optique_physique.html?id=SgVe3ZRubgkC&pgis=1.

Verzi, D. W. and Noris, O. Y. (2009). A compartmental model for activity-dependent dendritic spine branching. *Bulletin of Mathematical Biology*, 71(5):1048–72. Available from: http://www.ncbi.nlm.nih.gov/pubmed/19172359.

Vicidomini, G., Moneron, G., Eggeling, C., Rittweger, E., and Hell, S. W. (2012). STED with wavelengths closer to the emission maximum. *Optics Express*, 20(5):5225–36. Available from: http://www.ncbi.nlm.nih.gov/pubmed/22418329.

Vicidomini, G., Moneron, G., Han, K. Y., Westphal, V., Ta, H., Reuss, M., Engelhardt, J., Eggeling, C., and Hell, S. W. (2011). Sharper low-power STED nanoscopy by time gating. *Nature Methods*, 8(7):571–3. Available from: http://dx.doi.org/10.1038/nmeth.1624.

Vicidomini, G., Schönle, A., Ta, H., Han, K. Y., Moneron, G., Eggeling, C., and Hell, S. W. (2013). STED nanoscopy with time-gated detection: theoretical and experimental aspects. *PloS ONE*, 8(1):e54421. Available from: http://www.pubmedcentral.nih.gov/articlerender.fcgi?artid=3548795&tool=pmcentrez&rendertype=abstract.

Waldeyer, W. (1891). Ueber einige neuere Forschungen im Gebiete der Anatomie des Centralnervensystems. *DMW - Deutsche Medizinische Wochenschrift*, 17(49):1213–1218, 1244–1246, 1267–1269, 1287–1289, 1331–1. Available from: https://www.thieme-connect.de/ejournals/abstract/10.1055/s-0029-1206824.

Wang, M., Orwar, O., Olofsson, J., and Weber, S. G. (2010). Single-cell electroporation. *Analytical and Bioanalytical Chemistry*, 397(8):3235–48. Available from: http://www.ncbi.nlm.nih.gov/pubmed/20496058.

Westphal, V., Blanca, C. M., Dyba, M., Kastrup, L., and Hell, S. W. (2003). Laser-diode-stimulated emission depletion microscopy. *Applied Physics Letters*, 82(18):3125. Available from: http://scitation.aip.org/content/aip/journal/apl/82/18/10.1063/1.1571656.

Westphal, V. and Hell, S. W. (2005). Nanoscale resolution in the focal plane of an optical microscope. *Physical Review Letters*, 143903(April):1–4. Available from: http://prl.aps.org/abstract/PRL/v94/i14/e143903.

Westphal, V., Rizzoli, S. O., Lauterbach, M. a., Kamin, D., Jahn, R., and Hell, S. W. (2008). Video-rate far-field optical nanoscopy dissects synaptic vesicle movement. *Science*, 320(5873):246–9. Available from: http://www.ncbi.nlm.nih.gov/pubmed/18292304.

Wildanger, D., Medda, R., Kastrup, L., and Hell, S. W. (2009). A compact STED microscope providing 3D nanoscale resolution. *Journal of Microscopy*, 236(1):35–43. Available from: http://www.ncbi.nlm.nih.gov/pubmed/19772534.

Willig, K. I., Harke, B., Medda, R., and Hell, S. W. (2007). STED microscopy with continuous wave beams. *Nature Methods*, 4(11):915–918. Available from: http://dx.doi.org/10.1038/nmeth1108.

Willig, K. I. and Nägerl, U. V. (2012). Stimulated emission depletion (STED) imaging of dendritic spines in living hippocampal slices. *Cold Spring Harbor Protocols*,

2012(5):pdb.prot069260–pdb.prot069260. Available from: http://cshprotocols.cshlp.org/cgi/content/abstract/2012/5/pdb.prot069260.

Willig, K. I., Rizzoli, S. O., Westphal, V., Jahn, R., and Hell, S. W. (2006). STED microscopy reveals that synaptotagmin remains clustered after synaptic vesicle exocytosis. *Nature*, 440(7086):935–9. Available from: http://www.ncbi.nlm.nih.gov/pubmed/16612384.

Willig, K. I., Steffens, H., Gregor, C., Herholt, A., Rossner, M. J., and Hell, S. W. (2014). Nanoscopy of filamentous actin in cortical dendrites of a living mouse. *Biophysical Journal*, 106(1):L01–3. Available from: http://www.ncbi.nlm.nih.gov/pubmed/24411266.

Wurm, C. A., Neumann, D., Schmidt, R., Egner, A., and Jakobs, S. (2010). Sample Preparation for STED Microscopy. *Methods in Molecular Biology*, 591:185–99. Available from: http://www.ncbi.nlm.nih.gov/pubmed/19957131.

Yang, Y., Wang, X.-b., Frerking, M., and Zhou, Q. (2008). Spine expansion and stabilization associated with long-term potentiation. *The Journal of Neuroscience*, 28(22):5740–51. Available from: http://www.jneurosci.org/content/28/22/5740.

Yuste, R. (2002). The discovery of dendritic spines. *IBRO History of Neuroscience*, pages 2–7. Available from: http://www.ibro.info/Pub/Pub_Main_Display.asp?LC_Docs_ID=3532.

Yuste, R. (2010). *Dendritic Spines*. The MIT Press.

Yuste, R. and Bonhoeffer, T. (2001). Morphological changes in dendritic spines associated with long-term synaptic plasticity. *Annual Review of Neuroscience*, 24:1071–89. Available from: http://www.ncbi.nlm.nih.gov/pubmed/11520928.

Yuste, R. and Denk, W. (1995). Dendritic spines as basic functional units of neuronal integration. *Nature*, 375(6533):682–4. Available from: http://www.ncbi.nlm.nih.gov/pubmed/7791901.

Zhang, Y.-P., Holbro, N., and Oertner, T. G. (2008). Optical induction of plasticity at single synapses reveals input-specific accumulation of alphaCaMKII. *Proceedings of the National Academy of Sciences of the United States of America*, 105(33):12039–44. Available from: http://www.pnas.org/content/105/33/12039.

Zhou, Q., Homma, K. J., and Poo, M.-m. (2004). Shrinkage of dendritic spines associated with long-term depression of hippocampal synapses. *Neuron*, 44(5):749–57. Available from: http://www.sciencedirect.com/science/article/pii/S0896627304007226.

Ziff, E. (1997). Enlightening the postsynaptic density. *Neuron*, 19:1163–1174. Available from: http://scholar.google.com/scholar?hl=en&btnG=Search&q=intitle:Enlightening+the+Postsynaptic+Density#0.

Zimmermann, T., Rietdorf, J., and Pepperkok, R. (2003). Spectral imaging and its applications in live cell microscopy. *FEBS Letters*, 546(1):87–92. Available from: http://linkinghub.elsevier.com/retrieve/pii/S0014579303005210.

Zuber, B., Nikonenko, I., Klauser, P., Muller, D., and Dubochet, J. (2005). The mammalian central nervous synaptic cleft contains a high density of periodically organized complexes. *Proceedings of the National Academy of Sciences of the United States of America*, 102(52):19192–7. Available from: http://www.pubmedcentral.nih.gov/articlerender.fcgi?artid=1323199&tool=pmcentrez&rendertype=abstract.

Zuo, Y., Lin, A., Chang, P., and Gan, W.-B. (2005). Development of long-term dendritic spine stability in diverse regions of cerebral cortex. *Neuron*, 46(2):181–9. Available from: http://www.sciencedirect.com/science/article/pii/S0896627305003090.

Acknowledgements

I thank my thesis advisors: Tobias Bonhoeffer, who supervised the project and gave me the freedom to pursue it rather independently, Hans Lüscher, who spent his last sabbatical together with me in the lab to built up the nanoscope and who set a role model of a polymath, Katrin Willig who designed the optical layout and helped exceedingly with troubleshooting, and Oliver Griesbeck, who not only introduced me to a variety of cool fluorescent tags, but also always had a few encouraging words here and there.

I'd like to thank the jury of my thesis, Rainer Uhl, Martin Heß, Christian Leibold, Wolfgang Enard and Veronica Egger, for taking their time to judge my work. I hope you could enjoy it at least a bit.

I owe the workshops at the Max Planck campus a debt of gratitude. All the people there do a really great job and without them I would probably still be busy with the build-up of the optical system.

Many thanks to Max Sperling, Claudia Huber and Frank Voss for their technical assistance, as well as to Ursula Weber and Marianne Braun for processing brain slices for EM and taking the respective images.

Volker Scheuss and Daniel Meyer introduced me to their synaptic stimulation paradigm and kindly shared their chemicals and imaging setup, Cvetalina Coneva taught me how to transfect tissue slices by means of single-cell electroporation and Adam Urness installed the multi-color option at the detection pathway of the STED-LSM. Thank you all for your support.

I thank those fellows, who had to share the office with me – alongside diverse interns Juliane Jaepel-Schael, Onur Gökçe and Volker Staiger – for their forbearingness with a moody choleric. Moreover, Volker has been one of the greatest colleagues I have met by now. He taught me basically everything practically relevant to perform a proper experiment. Many thanks for that, I will miss the times we spent tinkering. Onur helped me quite a bit with the analysis of my data and gave inspiring comments on the manuskript, on science and life in general. Thanks for calling me a friend.

To all the other folks in the Bonhoeffer lab: thank you for your company, discussions, lunch- and coffee-breaks, which made my time as a PhD student much more than just bearable.

Arnab Chakrabarty proof read the thesis and more than once nurtured my intercultural competence. Thanks for becoming the personification of my bad conscience.

Finally, I'd like to thank those, who are closest to me: my parents, Martina and Dietmar, my brother, Andreas, his wife, Mirjam, and my mother-in-law, Dorothea, for their exceptional backing by word and deed at all times. The biggest thanks by far go to Julia for her unconditional support, unfortunately, far too often to her own detriment. Without her it would have been impossible to start this wonderful family by now. Last but not least, I thank Paula for her patience with a far too busy dad. I promise to improve and am looking forward to spending a lifetime with this cute little lady.

By the way

Unlike Santiago Ramón y Cajal, I used to have a rather static idea of synaptic connections, before I had started my investigation[1]. Therefore, most astonishing to me was the simple understanding that they move at all — which reminds me of Heraklit: *Pánta chorei kaì oudèn ménei.*

[1] This probably undoubtedly proves, that I am not a great mind – a painful personal deficit I have learned, deeply ashamed, to admit.

Eidesstattliche Versicherung

Ich versichere hiermit an Eides statt, dass ich die vorliegende Dissertation mit dem Titel „Analysis of Spine Plasticity in CA1 Hippocampal Pyramidal Neurons employing Live Cell Nanoscopic Imaging“ selbständig und ohne unerlaubte Hilfe angefertigt habe.

Erklärung

Hiermit erkläre ich, dass ich mich nicht anderweitig einer Doktorprüfung ohne Erfolg unterzogen habe. Die Dissertation wurde in ihrer jetzigen oder ähnlichen Form bei keiner anderen Hochschule eingereicht und hat noch keinen sonstigen Prüfungszwecken gedient.

Martinsried, 25. März 2014

Marcus Knopp